UNIVERSITÀ
DEGLI STUDI
FIRENZE

DOTTORATO DI RICERCA IN
SCIENZE BIOMEDICHE

CICLO XXVII

COORDINATORE Prof.re Persio Dello Sbarba

IN VIVO AND IN VITRO ASSESSMENT OF PREVENTIVE EFFECTS OF RANOLAZINE ON PATHOLOGICAL PHENOTYPE IN TRANSGENIC MOUSE MODELS OF HYPERTROPHIC CARDIOMYOPATHY

Settore Scientifico Disciplinare BIO/10

Dottorando
Dott. Luca Mazzoni

_____
(firma)

Tutore
Prof.ssa Paola Chiarugi

_____
(firma)

Co-Tutore
Dott. Raffaele Coppini

_____
(firma)

Coordinatore
Prof. re Persio Dello Sbarba

_____
(firma)

Anni 2012/2014

INDEX

Chapter 1: Hypertrophic cardiomyopathy: state of the art

1.1.1 Hypertrophic cardiomyopathy: general features

Hypertrophic cardiomyopathy (HCM) is the most common inherited disease of the heart, involving 1:500 people (Maron, 2002). HCM is a dominant disease of the cardiac sarcomere and it is characterized by the presence of left ventricular hypertrophy (LVH), left ventricular wall and septal hypertrophy, in the absence of other cardiac or systemic disease, such as pressure overload (systemic hypertension, aortic stenosis) or other multisystem illness (storage or infiltrative diseases). The hallmark of HCM, left ventricular (LV) hypertrophy usually develops at puberty or early adulthood, but can be present at birth, or develop as late as the 6th decade (Maron BJ, 2002). The distribution of LV hypertrophy in HCM is typically regional and asymmetric, develops in virtually all imaginable patterns within the ventricle (Klues et al, 1995), and may involve the right ventricle and papillary muscles. The transition from hypertrophied to non-hypertrophied regions may be characteristically abrupt, giving rise to a "lumpy" appearance of the LV wall profile. For reasons that remain unknown, the basal anterior septum and anterolateral free wall are almost always involved, and generally represent the site of maximum wall thickness values (Maron MS et al, 2009). These range from very mild (13-15 mm) to extreme hypertrophy (30 mm or more), with an average of 21 to 23 mm in large HCM cohorts (Nistri et al 2006; Olivotto et al, 2003b). Obstruction of the left ventricular outflow tract is present at rest in approximately 25% of patients and in a higher proportion during exercise. Although HCM is a very heterogeneous disease, the diagnosis is based on the two-dimensional echography identification of an otherwise unexplained LVH (Olivotto & Cecchi, 2003), however, it is important to treat HCM not solely as a hypertrophic disease but as a progressive cardiac pathology that leads to complex changes in ventricular geometry and function.

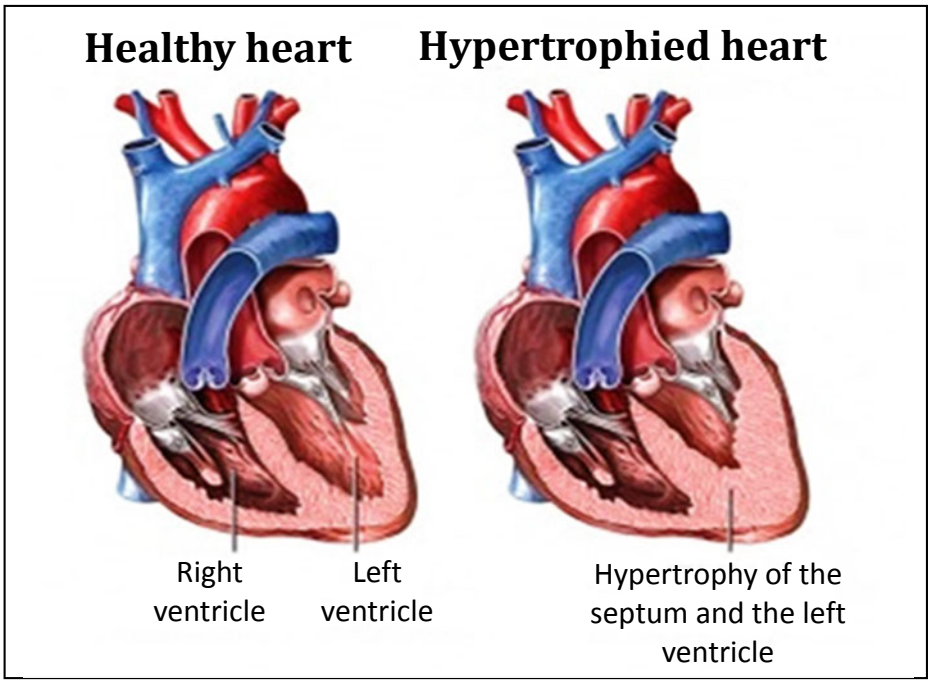

Figure 1: anatomical changes in hypertrophic cardiomyopathy. Figure shows the evolution of the disease, hypertrophied heart results in a thickening of the septum and left ventricle wall.

Histologically, myocyte disarray and interstitial fibrosis are characteristic of the disease. Myocyte disarray is defined as a profound derangement of myocyte alignment, with loss of the physiological, parallel orientation of the cells, arranged in a chaotic pattern and forming a typical disorganized architecture (Basso et al, 2000; Maron, 2002). The functional consequences of disarray may affect LV mechanics by interfering with the physiological homogeneity of contraction and relaxation (Ho et al, 2002) and represent a potential substrate for ventricular arrhythmias (Basso et al, 2000).

Variable and sometimes striking patterns of intra-myocardial fibrosis have been described in HCM hearts based on pathological studies (Basso et al, 2000) and, more recently, by cardiac magnetic resonance (CMR) techniques allowing in vivo visualization of areas of late gadolinium enhancement (LGE) (Maron et al, 2009; Olivotto et al, 2008). CMR late gadolinium enhancement is present in about two-thirds of HCM patients, varying from very limited to large, confluent, infarct-like patches occupying significant proportions of the LV (Olivotto et al, 2008). LGE localizes preferentially to the most hypertrophied regions of the ventricle, often represented by the basal and mid-septum, and are more often found in patients with diffuse and severe hypertrophy. Preliminary evidences points to LGE areas as a potential substrate of ventricular arrhythmias (Adabag et al, 2008).

Another pathophysiological hallmark of HCM is microvascular dysfunction. In the past decade, a number of studies have demonstrated that in HCM patients the coronary vasodilator reserve is markedly impaired not only in the hypertrophied septum, but also in the least hypertrophied LV free wall (Camici & Crea, 2007; Olivotto et al, 2006). In the absence of epicardial coronary stenoses, this finding is indicative of diffuse microvascular dysfunction, in line with pathologic evidence of marked and widespread remodeling of the intramural coronary arterioles (Basso et al, 2000), which show smooth muscle hyperplasia and disorganized elastic fibres, causing deformation and irregular narrowing of the vessel lumen. Microvascular dysfunction is the most important substrate for recurrent ischemia in HCM, and has been shown to represent an important predictor of long-term prognosis and adverse LV remodeling (Camici & Crea, 2007; Olivotto et al, 2006). Although systolic contractility is preserved and features of hypercontractility are observed at the whole heart level, outflow obstruction and impaired relaxation can cause progressive forward and backward heart failure and an increased incidence of ventricular arrhythmia can lead to sudden cardiac death.

A notable feature of HCM is that the underlying molecular defect (present from birth) can apparently be compensated in nearly all patients until adolescence and indeed, as indicated by the finding of incomplete penetrance, in some individuals for all of their life. Some mutations have been reported with very high penetrance (close to 100%) whereas the penetrance of other mutations appears to be incomplete. For example with mutations in TNNI3 (which encodes cardiac troponin I), it was reported that a single mutation (ΔLys183) had a high penetrance with evidence of cardiomyopathy present in 88% by echocardiography and 96% by ECG (Kokado et al., 2000). However, a report of 100 TNNI3 mutation carriers identified in 23 families (13 different mutations) found that disease penetrance was only 48% and that penetrance was complete in only one family (Mogensen et al., 2004). Further, there is evidence that some HCM mutation carriers can make an abrupt transition from having a structurally normal heart to one showing overt hypertrophy in later adult life (Maron B et al. 2004). These are important points, in that they give rise to the suggestion that there may be a “tipping point”, beyond which pathways are activated to stimulate disease progression. The physiological and metabolic conditions that define this point may be manipulated to prevent downstream consequences and specific interventions aimed at this may modify (and potentially halt) the disease process resulting in substantial therapeutic benefit**.** However, no specific drug or other therapeutic

measure has been shown able to prevent the development of overt disease in carrier patients, making it still a great medical need.

It will be made clear through this introduction that, although great recent advances in the understanding of the pathophysiogy of HCM brought new light into the field, no totally effective therapy is yet available that is able to substantially reduce the clinical burden of this disease.

Recently, a simple framework for systematic clinical staging of the disease has been proposed. Four clinical stages have been identified, with special emphasis on diagnosis, potential mechanisms, challenges for management, and targets for future investigation: these are defined as *nonhypertrophic HCM*, *classic* phenotype, *adverse remodeling*, and *overt dysfunction* (Olivotto et al, 2012).

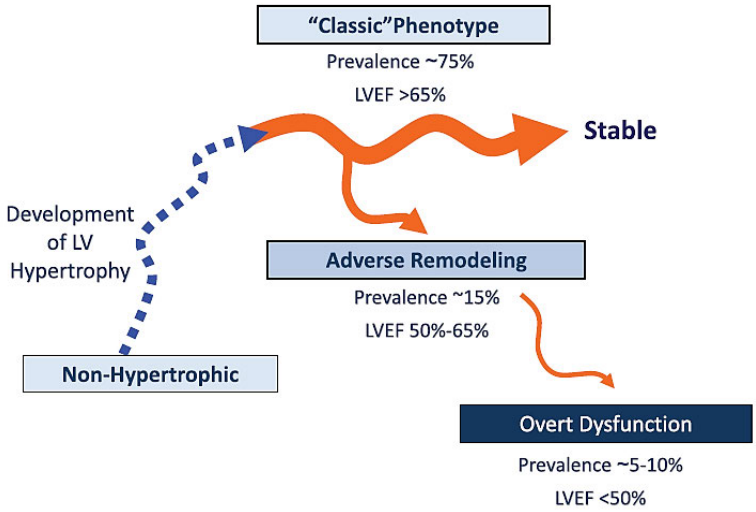

Figure 2: Stages of hypertrophic cardiomyopathy. Thickness of the orange lines reflects prevalence of each stage in HCM cohorts. Prevalence of nonhypertrophic HCM is unknown. LVEF indicates left ventricular ejection fraction.

Nonhypertrophic HCM is a state characterized by the absence of LV hypertrophy in individuals harboring HCM-causing mutations, investigated in the course of systematic family screenings. Subtle echocardiographic abnormalities may be found, such as impaired LV relaxation, mitral valve or subvalvar abnormalities, and mild degrees of left atrial (LA) dilatation, all of which are not diagnostic per se but may be instrumental to suspecting HCM in a familial context. Furthermore, elevated levels of type I collagen precursors has been found and coronary microvascular function may be altered in genotype-positive individuals. The whole spectrum of abnormalities may be present in individuals with nonhypertrophic HCM.

Classic HCM phenotype is defined as the phase in which the hypertrophic phenotype is fully expressed and the LV is hyperdynamic (as defined by an ejection fraction [EF] >65%), in the absence of extensive fibrotic changes suggesting unfavorable progression. The majority of HCM patients in cross-sectional studies belong to this stage.

Adverse remodeling is defined by the presence of unfavorable structural modifications, superimposed to the "classic" HCM phenotype, translating into increasing LV fibrosis and worsening function (i.e. an LVEF in the low-normal range of 50% to 65%), with relatively preserved clinical and hemodynamic balance. Rather than being an "average" process, this seems to represent a selective pathway followed by about 15% to 20% of HCM patients, a smaller proportion of whom will ultimately progress to overt dysfunction and heart failure.

Overt dysfunction is an uncommon clinical evolution of HCM and represents about 5% of patients in most cohorts. It is characterized by severe functional deterioration of the LV (defined by an LVEF <50%), subtended by extreme degrees of fibrosis and remodeling and generally associated with hemodynamic decompensation and adverse. This subset coincides with so-called "end-stage" HCM.

1.1.2 HCM genetic features

In 1990, the first missense mutation in a sarcomeric protein, R403Q in the β-cardiac myosin heavy chain (β-MyHC), was shown to be responsible for HCM (Geisterfer-Lowrance et al. 1990). Since then, molecular genetics has revealed that HCM is a complex molecular disease, exhibiting both gene and allele heterogeneity (multiple disease genes and multiple mutations), with as many as 10 sarcomere related genes and more than 400, predominantly missense, mutations described.
The HCM-causing mutant genes encode: β-MyHC, cardiac myosin binding protein-C (cMyBP-C) both regulatory (RLC) and essential (ELC) myosin light chains, α-tropomyosin (α-Tm), cardiac troponin I (cTnI) cardiac troponin T (cTnT), cardiac troponin C (cTnC), cardiac actin and the giant structural protein titin.
Disease-causing mutations in sarcomere proteins are detected in 60-70% of HCM affected individuals and the most commonly affected genes are MYBPC3 (cMyBP-C) and MYH7 (β-MyHC).
The prevalence of mutations in sarcomeric proteins has led to the designation of HCM as primarily a "*disease of the sarcomere*" (Thierfelder et al. 1994; Seidman et al. 2001; Marian and Roberts 2001; Belus A et al, 2008). This raises the question of how molecular defects in sarcomeric proteins can lead to the heterogeneous phenotypic expression that characterizes HCM. In fact asymmetric left ventricular hypertrophy, diastolic dysfunction and sudden death are only the three well known hallmarks of HCM, but the disease has a much wider spectrum of clinical faces, including the so called "pre-hypertrophic phenotype". Healthy carriers of sarcomeric mutations during the pre-hypertrophic phase often have subtle echocardiographic abnormalities but will not necessarily develop an overt hypertrophy and/or symptoms. Atrial remodeling (e.g. increase size) and abnormalities of the mitral valve apparatus (including disproportionate mitral leaflet elongation, anomalous chordae and/or papillary muscle insertions, and papillary muscles alterations in terms of size and number) are common in HCM patients, and have been described also in patients with very mild or no hypertrophy. No treatments are now in use during the pre-hypertrophic phase to prevent the development of hypertrophy: with the wider availability of genetic screening for HCM-related mutations, the number of detected *genotype-positive* mutation carriers without cardiac hypertrophy is increasing. A treatment to prevent the development of hypertrophy could therefore be applicable to such patients and the lack of an effective drug is a great unmet medical need.

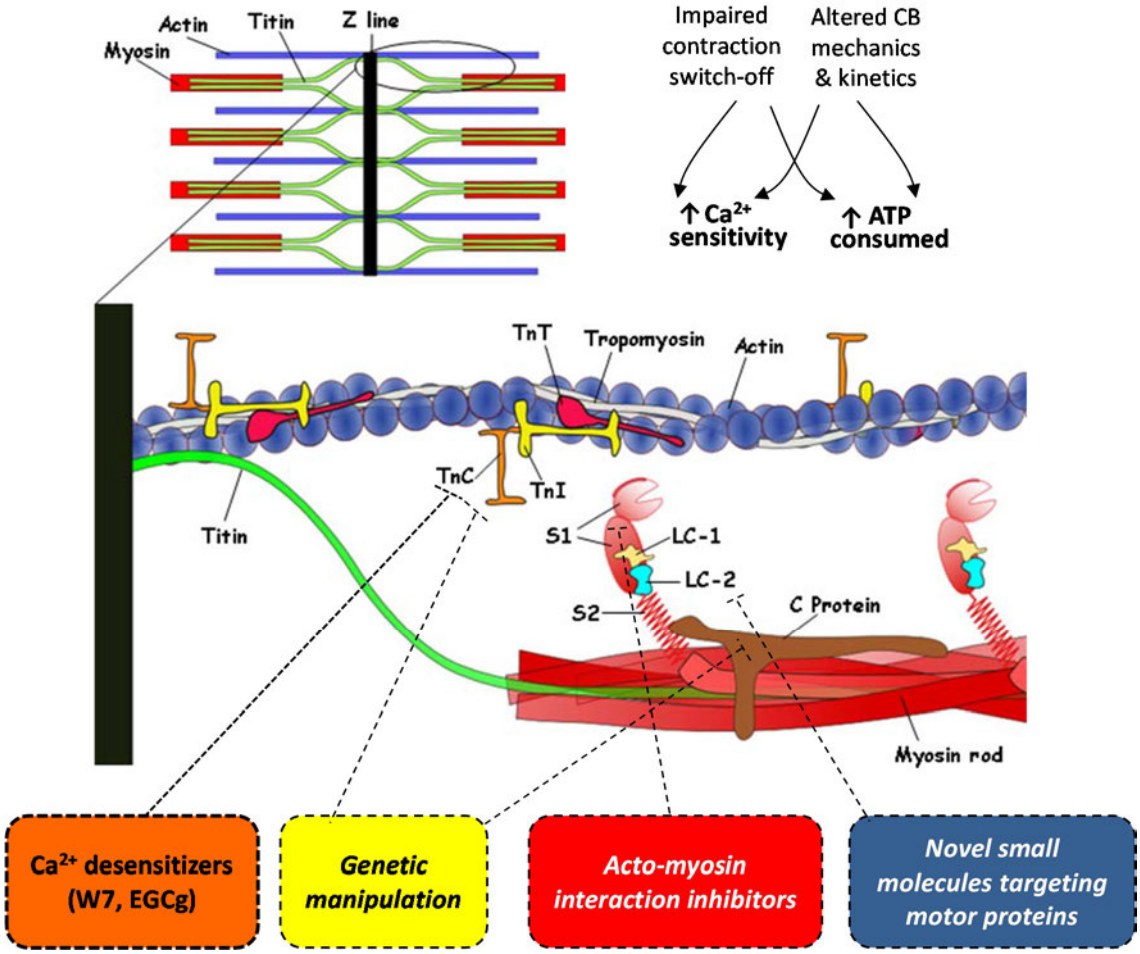

Figure 3: Targeting primary changes in HCM. Figure depicting the schematic structure of cardiac sarcomere. Panel above shows the general structure of cardiac myofilaments where different regions are indicated. Panel below shows a magnified half-sarcomere with detailed structure of all proteins and their localization within the sarcomeric framework. Abbreviations: TnT= troponin T; TnC= troponin C; TnI= troponin I; S, S2= S1 and S2 portions of myosin head; LC-1 and 2= Myosin light chain 1, 2. C protein= myosin binding protein C. (Tardiff et al. 2015, Cardiovascular Research, manuscript in press)

1.1.3 HCM and diastolic dysfunction

Diastolic dysfunction with an impaired LV filling seems to be the first change in myocardial function in HCM mutation carriers without hypertrophy, both in animal models and in patients (Ho et al, 2002; Nagueh et al, 2003). The origin of diastolic dysfunction in HCM is multifactorial and complex, with changes at the cellular level (e.g. impaired sarcomeric function and Ca^{2+} handling) and also abnormalities at the tissue level (myocyte disarray, interstitial fibrosis, microvascular dysfunction). Diastolic dysfunction is the main determinant of symptoms in HCM patients: reduced exercise capacity, chest pain and discomfort, dyspnea episodes, are all associated with impaired myocardial relaxation, which leads to increased ventricular filling pressure and increased atrial pressure (Olivotto & Cecchi, 2003).

Even though the possible causes of diastolic dysfunction in HCM are, at least partially, understood, no specific therapy exists that is able to improve myocardial relaxation in these patients. Recent PET studies in HCM patients have clearly demonstrated the occurrence of microvascular abnormalities (e.g. fibrosis), that lead to reduced myocardial blood flow (e.g. hyperemic myocardial blood flow < 1.2 mg/ml/min) and are a predictor of unfavorable outcome

and LV failure. Other than microvascular fibrosis, also an impaired myocardial relaxation and the subsequent increased LV tissue pressure during diastole can contribute to myocardial blood flow impairment.
Loss of systolic function is relatively rare in HCM (prevalence of LV failure and "end-stage" progression<1%) and generally occurs at later stages of disease development; however it represents an important cause of mortality in this cohort, second only to Sudden Death.
Alterations of diastolic function are now considered the first signs of HCM even before the development of overt hypertrophy, the so called preclinical HCM. Doppler imaging (TDI) and echocardiographic strain analysis, allow characterization of the pathophysiology of the preclinical state in greater detail. TDI measures myocardial velocities in systole (S′), early diastole (E′), and with atrial contraction (A′). E′ velocities reflect diastolic function with reduced velocities indicating impaired relaxation. By measuring TDI velocities in a genotyped patient population, impaired relaxation can be detected prior to the onset of LVH in preclinical disease. This finding has been consistently demonstrated in preclinical HCM. Individuals with preclinical HCM have a significant 13–20% decrease in E′ velocity compared with normal controls [Ho et al, 2002, Nagueh et al, 2000]. Those with overt disease have an even more profound decrease in diastolic function. These findings indicate that subtle myocardial dysfunction is present prior to the development of cardiac hypertrophy in preclinical HCM.

1.1.4 HCM, Sudden Death and arrhythmias

Sudden Death occurs in 1-2 % of HCM patients and identifying high-risk patients remains a very challenging task. SD in HCM is arrhythmia-based due to primary ventricular tachycardia/fibrillation (VT/VF) (Maron B et al.2007) with a relationship to patient age (Maron, 2002). SD may occur at a wide range of ages with the highest rate during adolescence and young adulthood, most commonly less than about 25 to 30 years of age. Indeed, HCM is now recognized as the most common cause of SD in young people (Maron, 2003). However, SD risk continues into midlife (and even beyond), although at a lower rate, and absolute immunity to SD is not achieved in HCM solely by achieving a particular age (Maron B, 2000). However, over the age of 60 years, SD due to HCM (in the absence of atherosclerotic coronary artery disease) appears to be uncommon (see Table 1).
The predisposition of HCM patients to arrhythmias is well established, and may include virtually all known rhythm disturbances. Sustained ventricular arrhythmias bear the greatest prognostic relevance, as the most frequent cause of sudden death in this population (McLeod CJ et al.2009).
Conversely, nonsustained ventricular tachycardia is very common, particularly in adult and elderly patients, so that their predictive value seems largely confined to younger individuals (Elliot P et al 2004). Atrial fibrillation occurs in 20%-30% of consecutive HCM cohorts, often presents in young patients, and represents an important predictor of disease progression and heart-failure-related complications (Olivotto I et al. 2001). Finally, bradyarrhythmias and conduction blocks may occur in HCM patients, occasionally at a young age, possibly due to early involvement of conduction system by the disease process.
A major goal in treatment of HCM is to limit the life-threatening consequences of arrhythmia. The greatest limitation to this however is the relative lack of knowledge about the molecular and cellular mechanisms determining HCM-related pro-arrhythmic substrate. While tissue fibrosis and microvascular dysfunction might provide a substrate for the maintenance of ventricular automaticity by favoring establishment of reentry circuits, to date no knowledge of the cellular

triggers for arrhythmias initiation in HCM is present. In spite of considerable advances in understanding HCM genetics and pathophysiology, current pharmacological treatment of patients with HCM has remained largely empiric and unchanged over the past two decades.

Table 1: Risk Factors for Sudden Death in HCM (Maron BJ et al.2003)

Major	Possible in Individual Patients
Cardiac arrest (ventricular fibrillation)	Atrial fibrillation
Spontaneous sustained ventricular tachycardia	Myocardial ischemia
Family history of premature sudden death	LV outflow obstruction
Unexplained syncope	High-risk mutation
LV thickness greater than or equal to 30 mm	Intense (competitive) physical exertion
Abnormal exercise blood pressure	
Nonsustained ventricular tachycardia (Holter)	

1.1.5 HCM caused by mutation in the thin filament regulatory proteins of the sarcomere

Thin filament mutations occur in only 6-8% of patients with hypertrophic cardiomyopathy, making thin-filament HCM a relatively rare condition. However, several clinical and preclinical studies pointed out that HCM associated with thin-filament mutations is in many ways a disease on its own, since both the clinical course and the molecular pathophysiology are different from the much more common thick-filament HCM. To date, a wide array of nearly 100 independent mutations in all components of the cardiac thin filament have been identified (Tardiff, 2011). Although the clinical heterogeneity observed in this group of patients, compared with patients carrying thick filament mutations, thin-filament patients appear to suffer from a higher risk of sudden cardiac death, even in the absence of the "classical" risk factors such as the presence of massive hypertrophy. Moreover, these patients are more likely to develop severe diastolic dysfunction, systolic abnormalities and refractory heart failure. Thin-filament HCM has been much less studied due to its rarity and no specific preventive therapeutic option exists to address the increase risk of arrhythmias and clinical progression.

In 1994, mutations in cardiac α-tropomyosin (Tm) and troponin TnT (cTnT) were shown to cause familial hypertrophic cardiomyopathy (HCM) (Thierfelder et al, 1994). In a considerable subgroup of patients, HCM is determined by mutations of the sarcomere thin-filament regulatory protein genes, including cTnT, cTnI and Tm (Tardiff, 2011). Albeit mutations in cTnT are the most common thin filament mutations, they account for only 3-5% of all cases of HCM; nonetheless, HCM patients with cTnT mutations have an increased likelihood of suffering a sudden cardiac death (Moolman et al, 1997) at least 26 known mutations have been found in the human cardiac TnT gene that are linked to HCM, including 23 missense

mutations, one deletion mutation, and one splicing donor site mutation (Varnava et al, 2001). Patients who present TnT mutations often show no or mild hypertrophy, myocardial disarray, and have a malignant phenotype associated with a high incidence of SD. The deletion of the 160 glutamic acid codon of the troponin T gene (Δ160E) was reported to be associated with a high incidence of sudden death in Caucasian patients (Watkins et al, 1995).

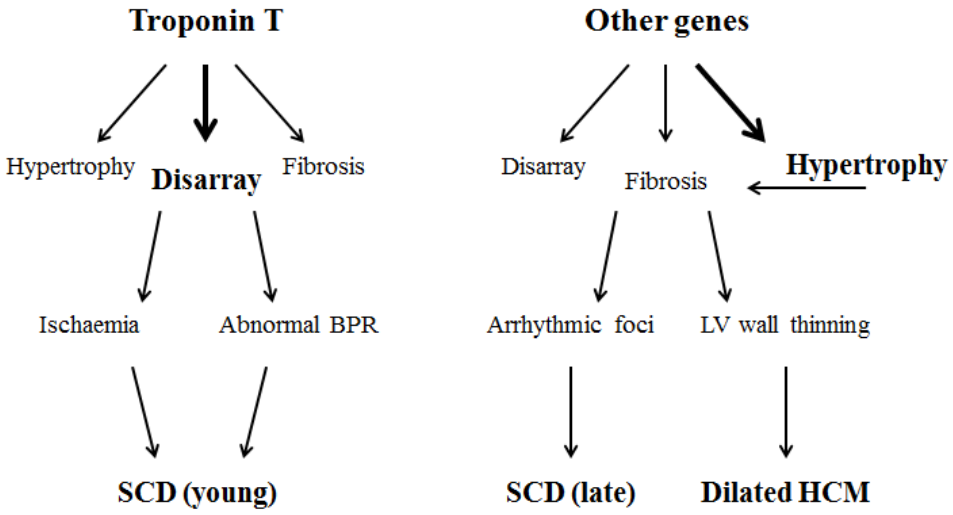

Figure 4: Relation between genotype, histology, phenotype, and sudden death. Diagram showing the genotype-phenotype correlation proposed for HCM associated cTnT mutation versus HCM With Unknown Genotype. BPR indicates blood pressure response to exercise; LV, left ventricle; and SCD, sudden cardiac death.

cTnI mutations account for 2-3% of all cases and are similarly associated with poor outcome in patients (Doolan et al, 2005). Tm mutations are less common (1-2%) (Van Driest et al, 2003) and are also associated with high risk of arrhythmias (Karibe et al, 2001). Thin-filament HCM is characterized by a low degree of hypertrophy, despite large myocytes disarray and interstitial fibrosis (Varnava et al, 2001). A seminal study (Watkins et al, 1995) showed that the clinical features associated with 3 different cTnT mutations were remarkably similar, comprising a reduced ventricular wall thickness and an increased prevalence of sudden death compared with patients with thick filament mutations.

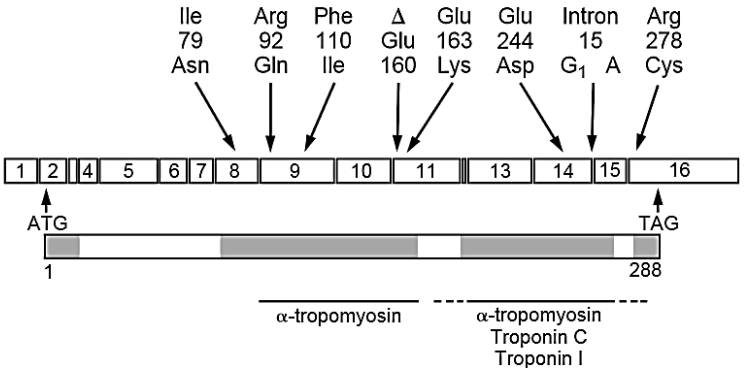

Figure 5: Eight Mutations in Cardiac Troponin T that Cause Familial Hypertrophic Cardiomyopathy. The schematic illustration of the cardiac troponin T gene is based on the rat genomic structure. Exons are indicated by boxes; the location of each mutation is shown. The initiation (ATG) and termination (TAG) codons are indicated. The peptide is represented below; shaded areas indicate high levels of conservation between cardiac and skeletal isoforms. The postulated binding sites are indicated for tropomyosin, troponin C, and troponin I. modified from (Watkins et al, 1995).

This apparent uniformity was subsequently challenged (Van Driest et al, 2002). The direct genotype-phenotype correlation established by early studies may have suffered from the pitfalls of mutations clustering due to founder effect (Moolman-Smook et al, 1999). In a Japanese study, where HCM patients with MHC or troponin T mutations were enrolled, sudden death has been found to be less frequent from what expected in both groups. Patients with charge change mutations, including Glul60del (Δ160E), showed general trends to develop systolic dysfunction. In a particular case family with a Glu163Arg mutation where a proband died of heart failure at age 47, while two children have developed septal hypertrophy. In other patients with a non-charge change mutation (Phe110Ile), the clinical course was benign, although the number of patients was small (Koga et al, 1996). Two subsequent reports identified a second independent mutation at residue 92 of cTnT (Arg92Trp) (Moolman et al, 1997; Varnava et al, 2001). In the study by Moolman, 64 the patient profile was similar to the previously described cTnT mutations, with minimal LVH, low disease penetrance via echocardiogram, and a high frequency of SCD, especially in males, late-onset (>35 years of age) hypertrophy of the interventricular septum with no evidence of progression to a dilated phenotype.

However, no studies so far have assessed on a large population whether the clinical course and outcome of patients with thin filament mutations differ from those bearing mutations in the thick filament.

Numerous preclinical studies pointed out that the causal biophysical abnormalities leading to disease manifestations in presence of thin filament mutations may be different from the "classical" thick filament mutations. Early studies on skinned cardiac preparations identified the increased Ca^{2+} sensitivity of myofilaments as a common alteration in thin filament mutations (Lin et al, 1996; Redwood et al, 2000). Studies on animal models have shown that selected mutations in cTnT in the mouse can result in a cardiomyopathy that includes hypertrophy and fibrosis (Tardiff et al, 1998) as well as an increased tendency for ventricular rhythm disturbances and Ca^{2+}-dependent changes in action potential morphology (Knollmann et al, 2003). Moreover, cardiac muscle from mutant mice shows specific alterations of contractile function with increased force production and slowed kinetics of contraction (Miller et al, 2001) that is directly associated with the increased Ca^{2+} sensitivity of myofilaments with mutant TnT. Furthermore, it was demonstrated that the increased susceptibility to arrhythmia in mutant

hearts is related with the increased Ca^{2+} sensitivity induced by thin filament mutations and can be observed early, even in the absence of any detectable cardiac hypertrophy or fibrosis (Baudenbacher et al, 2008).

Despite the widespread investigations related to HCM pathophysiology, the medical management of the disease has been largely unchanged over the past decades (Spoladore et al, 2012). So far, therapeutic approaches to HCM are based on the expertise of single clinicians and no evidence-based therapy, supported by studies on the pathogenic mechanisms of disease, is available. Moreover, none of the presently employed drug therapies has been shown capable of preventing arrhythmias and modifying disease progression in patients. The need of an effective preventive therapy is particularly required for thin filament mutation carrying patients.

REFERENCES

Adabag AS, Maron BJ, Appelbaum E, Harrigan CJ, Buros JL, Gibson CM, Lesser JR,Hanna CA, Udelson JE, Manning WJ, Maron MS (2008). Occurrence and frequency of arrhythmias in hypertrophic cardiomyopathy in relation to delayed enhancement on cardiovascular magnetic resonance. J Am Coll Cardiol; 51:1369-74.

Basso C, Thiene G, Corrado D, Buja G, Melacini P, Nava A (2000). Hypertrophic cardiomyopathy and sudden death in the young: pathologic evidence of myocardial ischemia. Hum Pathol;31:988–98.

Baudenbacher, F., Schober, T., Pinto, J.R., Sidorov, V.Y., Hilliard, F., Solaro, R.J., Potter, J.D., and Knollmann, B.C. (2008). Myofilament Ca2+ sensitization causes susceptibility to cardiac arrhythmia in mice.J Clin Invest 118, 3893-3903.

Belus, A., Piroddi, N., Scellini, B., Tesi, C., Amati, G.D., Girolami, F., Yacoub, M., Cecchi, F., Olivotto, I., and Poggesi, C. (2008). The familial hypertrophic cardiomyopathy-associated myosin mutation R403Q accelerates tension generation and relaxation of human cardiac myofibrils. The Journal of physiology 586, 3639-3644.

Camici PG, Crea F (2007). Coronary microvascular dysfunction. N Engl J Med; 356: 830–40.

Doolan A, Tebo M, Ingles J, Nguyen L, Tsoutsman T, Lam L, Chiu C, Chung J, Weintraub RG, Semsarian C (2005) Cardiac troponin I mutations in Australian families with hypertrophic cardiomyopathy: clinical, genetic and functional consequences. *Journal of molecular and cellular cardiology* 38: 387-393.

Geisterfer-Lowrance AA, Kass S, Tanigawa G, Vosberg HP, McKenna W, Seidman CE, Seidman JG (1990) A molecular basis for familial hypertrophic cardiomyopathy: a beta cardiac myosin heavy chain gene missense mutation. *Cell* 62: 999-1006.

Ho, C. Y., Sweitzer, N. K., McDonough, B., Maron, B. J., Casey, S. A., Seidman, J. G., et al. (2002). Assessment of diastolic function with Doppler tissue imaging to predict genotype in preclinical hypertrophic cardiomyopathy. Circulation, 105, 2992–2997.

Karibe A, Tobacman LS, Strand J, Butters C, Back N, Bachinski LL, Arai AE, Ortiz A, Roberts R, Homsher E, Fananapazir L (2001) Hypertrophic cardiomyopathy caused by a novel alpha-tropomyosin mutation (V95A) is associated with mild cardiac phenotype, abnormal calcium binding to troponin, abnormal myosin cycling, and poor prognosis. *Circulation* 103: 65-71.

Klues HG, Schiffers A, Maron BJ 1995. Phenotypic spectrum and patterns of left ventricular hypertrophy in hypertrophic cardiomyopathy: morphologic observations and significance as assessed by two-dimensional echocardiography in 600 patients. J Am Coll Cardiol.;26:1699-708.

Kokado, H., Shimizu, M., Yoshio, H., Ino, H., Okeie, K., Emoto, Y., Matsuyama, T., Yamaguchi, M., Yasuda, T., Fujino, N., et al. (2000). Clinical features of hypertrophic cardiomyopathy caused by a Lys183 deletion mutation in the cardiac troponin I gene. Circulation 102, 663-669.

Knollmann BC, Kirchhof P, Sirenko SG, Degen H, Greene AE, Schober T, Mackow JC, Fabritz L, Potter JD, Morad M (2003) Familial hypertrophic cardiomyopathy-linked mutant troponin T causes stress-induced ventricular tachycardia and Ca2+-dependent action potential remodeling. *Circulation research* 92: 428-436.

Koga Y, Toshima H, Kimura A, Harada H, Koyanagi T, Nishi H, Nakata M, Imaizumi T (1996) Clinical manifestations of hypertrophic cardiomyopathy with mutations in the cardiac beta-myosin heavy chain gene or cardiac troponin T gene. *Journal of cardiac failure* 2: S97-103.

Lin D, Bobkova A, Homsher E, Tobacman LS (1996) Altered cardiac troponin T in vitro function in the presence of a mutation implicated in familial hypertrophic cardiomyopathy. *The Journal of clinical investigation* 97: 2842-2848Maron, B.J. (2002). Hypertrophic cardiomyopathy: a systematic review. Jama 287, 1308-1320.

Marian AJ, Roberts R (2001) The molecular genetic basis for hypertrophic cardiomyopathy. *Journal of molecular and cellular cardiology* 33: 655-670.

Maron, B. J. (2003). Sudden death in young athletes. New England Journal of Medicine, 349, 1064–1075.

Maron, B. J., Spirito, P., Shen, W.-K., Haas, T. S., Formisano, F., Link, M. S., et al. (2007). Implantable cardioverter-defibrillators and prevention of sudden cardiac death in hypertrophic cardiomyopathy. JAMA, 298, 405–412.

Maron, B. J., Olivotto, I., Spirito, P., Casey, S. A., Bellone, P., Gohman, T. G., et al. (2000). Epidemiology of hypertrophic cardiomyopathy-related death. Revisited in a large non-referralbased patient population. Circulation, 102, 858–864.

Maron, B. J., & Spirito, P. (2008). Implantable defibrillators and prevention of sudden death in hypertrophic cardiomyopathy. Journal of Cardiovascular Electrophysiology, 19, 1118–1126.

Maron, B. J., McKenna, W. J., Danielson, G. K., et al. (2003). American college of cardiology/European society of cardiology clinical expert consensus document on hypertrophic cardiomyopathy. Journal of the American College of Cardiology, 42, 1687–1713.

Maron MS, Olivotto I, Betocchi S, Casey SA, Lesser JR, Losi MA, Cecchi F, Maron BJ (2003. Effect of left ventricular outflow tract obstruction on clinical outcome in hypertrophic cardiomyopathy. N Engl J Med.;348:295-303.

Maron MS, Maron BJ, Harrigan C, Buros J, Gibson CM, Olivotto I, Biller L,Lesser JR, Udelson JE, Manning WJ, Appelbaum E (2009). Hypertrophic cardiomyopathy phenotype revisited after 50 years with cardiovascular magnetic resonance. J Am Coll Cardiol.;54:220-8.

Maron MS, Olivotto I, Zenovich AG, Link MS, Pandian NG, Kuvin JT, Nistri S, Cecchi F, Udelson JE, Maron BJ (2006). Hypertrophic cardiomyopathy is predominantly a disease of left ventricular outflow tract obstruction. Circulation.;114:2232-9.

McLeod, C. J., Ackerman, M. J., Nishimura, R. A., Tajik, A. J., Gersh, B. J., & Ommen, S. R. (2009). Outcome of patients with hypertrophic cardiomyopathy and a normal electrocardiogram.Journal of the American College of Cardiology, 54, 229– 233.

Miller T, Szczesna D, Housmans PR, Zhao J, de Freitas F, Gomes AV, Culbreath L, McCue J, Wang Y, Xu Y, Kerrick WG, Potter JD (2001) Abnormal contractile function in transgenic mice expressing a familial hypertrophic cardiomyopathy-linked troponin T (I79N) mutation. *The Journal of biological chemistry* 276: 3743-3755.

Mogensen, J., Klausen, I.C., Pedersen, A.K., Egeblad, H., Bross, P., Kruse, T.A., Gregersen, N., Hansen, P.S., Baandrup, U., and Borglum, A.D. (1999). Alpha-cardiac actin is a novel disease gene in familial hypertrophic cardiomyopathy. J Clin Invest 103, R39-43.

Mogensen, J., Murphy, R.T., Kubo, T., Bahl, A., Moon, J.C., Klausen, I.C., Elliott, P.M., and McKenna, W.J. (2004). Frequency and clinical expression of cardiac troponin I mutations in 748 consecutive families with hypertrophic cardiomyopathy.Journal of the American College of Cardiology 44, 2315-2325.

Moolman-Smook JC, De Lange WJ, Bruwer EC, Brink PA, Corfield VA (1999) The origins of hypertrophic cardiomyopathy-causing mutations in two South African subpopulations: a unique profile of both independent and founder events. *American journal of human genetics* 65: 1308-1320.

Moolman JC, Corfield VA, Posen B, Ngumbela K, Seidman C, Brink PA, Watkins H (1997) Sudden death due to troponin T mutations. *Journal of the American College of Cardiology* 29: 549-555.

Nagueh, S. F., Kopelen, H. A., Lim, D. S., Zoghbi, W. A., Quinones, M. A., Roberts, R., et al. (2000). Tissue Doppler imaging consistently detects myocardial contraction and relaxation abnormalities, irrespective of cardiac hypertrophy, in a transgenic rabbit model of human hypertrophic cardiomyopathy. Circulation, 102, 1346–1350.

Nishimura, R. A., & Ommen, S. R. (2007). Hypertrophic cardiomyopathy, sudden death, and implantable cardiac defibrillators: How low the bar? JAMA, 298, 452–454. (Editorial).

Nistri S, Olivotto I, Betocchi S, Losi MA, Valsecchi G, Pinamonti B, Conte MR, Casazza F, Galderisi M, Maron BJ, Cecchi F (2006). Prognostic significance of left atrial size in patients with hypertrophic cardiomyopathy (from the Italian Registry for Hypertrophic Cardiomyopathy). Am J Cardiol.;98:960-5.

Olivotto I, Gistri R, Petrone P, Pedemonte E, Vargiu D, Cecchi F (2003b). Maximum left ventricular thickness and risk of sudden death in patients with hypertrophic cardiomyopathy. J Am Coll Cardiol.;41:315-21.

Olivotto I, Maron MS, Autore C, Lesser JR, Rega L, Casolo G, De Santis M,Quarta G, Nistri S, Cecchi F, Salton CJ, Udelson JE, Manning WJ, Maron BJ (2008a). Assessment and significance of left ventricular mass by cardiovascular magnetic resonance in hypertrophic cardiomyopathy. J Am Coll Cardiol.;52:559-66.

Olivotto I, Cecchi F, Gistri R, Lorenzoni R, Chiriatti G, Girolami F, Torricelli F, Camici PG (2006). Relevance of coronary microvascular flow impairment to long-term remodeling and systolic dysfunction in hypertrophic cardiomyopathy. J Am Coll Cardiol.;47:1043-8.

Redwood C, Lohmann K, Bing W, Esposito GM, Elliott K, Abdulrazzak H, Knott A, Purcell I, Marston S, Watkins H (2000) Investigation of a truncated cardiac troponin T that causes familial hypertrophic cardiomyopathy: Ca(2+) regulatory properties of reconstituted thin filaments depend on the ratio of mutant to wild-type protein. *Circulation research* 86: 1146-1152.

Seidman JG, Seidman C (2001) The genetic basis for cardiomyopathy: from mutation identification to mechanistic paradigms. *Cell* 104: 557-567.

Spoladore R, Maron MS, D'Amato R, Camici PG, Olivotto I (2012) Pharmacological treatment options for hypertrophic cardiomyopathy: high time for evidence. *European heart journal* 33: 1724-1733.

Tardiff, J.C., Hewett, T.E., Palmer, B.M., Olsson, C., Factor, S.M., Moore, R.L., Robbins, J., and Leinwand, L.A. (1999). Cardiac troponin T mutations result in allele-specific phenotypes in a mouse model for hypertrophic cardiomyopathy. J Clin Invest 104, 469-481.

Thierfelder, L., Watkins, H., MacRae, C., Lamas, R., McKenna, W., Vosberg, H.P., Seidman, J.G., and Seidman, C.E. (1994). Alpha-tropomyosin and cardiac troponin T mutations cause familial hypertrophic cardiomyopathy: a disease of the sarcomere. Cell 77, 701-712.

Tobacman, L.S., Lin, D., Butters, C., Landis, C., Back, N., Pavlov, D., and Homsher, E. (1999).Functional consequences of troponin T mutations found in hypertrophic cardiomyopathy. The Journal of Biological Chemistry 274, 28363-28370.

Van Driest SL, Ackerman MJ, Ommen SR, Shakur R, Will ML, Nishimura RA, Tajik AJ, Gersh BJ (2002) Prevalence and severity of "benign" mutations in the beta-myosin heavy chain, cardiac troponin T, and alpha-tropomyosin genes in hypertrophic cardiomyopathy. *Circulation* 106: 3085-3090.

Van Driest SL, Ellsworth EG, Ommen SR, Tajik AJ, Gersh BJ, Ackerman MJ (2003) Prevalence and spectrum of thin filament mutations in an outpatient referral population with hypertrophic cardiomyopathy. *Circulation* 108: 445-451.

Varnava AM, Elliott PM, Baboonian C, Davison F, Davies MJ, McKenna WJ (2001) Hypertrophic cardiomyopathy: histopathological features of sudden death in cardiac troponin T disease. *Circulation* 104: 1380-1384.

Watkins, H., Conner, D., Thierfelder, L., Jarcho, J.A., MacRae, C., McKenna, W.J., Maron, B.J., Seidman, J.G., and Seidman, C.E. (1995). Mutations in the cardiac myosin binding protein-C gene on chromosome 11 cause familial hypertrophic cardiomyopathy. Nat Genet 11, 434-437.

1.2 The functional contractile unit on striated muscle: the sarcomere

1.2.1 Structure of the sarcomere

The striation pattern in muscle cells, of which a sarcomere is one repeat, is the result of the alternating ordered arrays of thick and thin filaments into myofibrils (Squire, 1997). The sarcomere is the elementary contractile unit from which all striated muscles are made. These are about 2-2.5 µm long and link end-to-end to form long thin strands known as myofibrils. Myofibrils form the contractile apparatus inside each muscle fiber in which every myofibril has a parallel, longitudinal disposition and cylindrical shape of diameter around 1 µm.

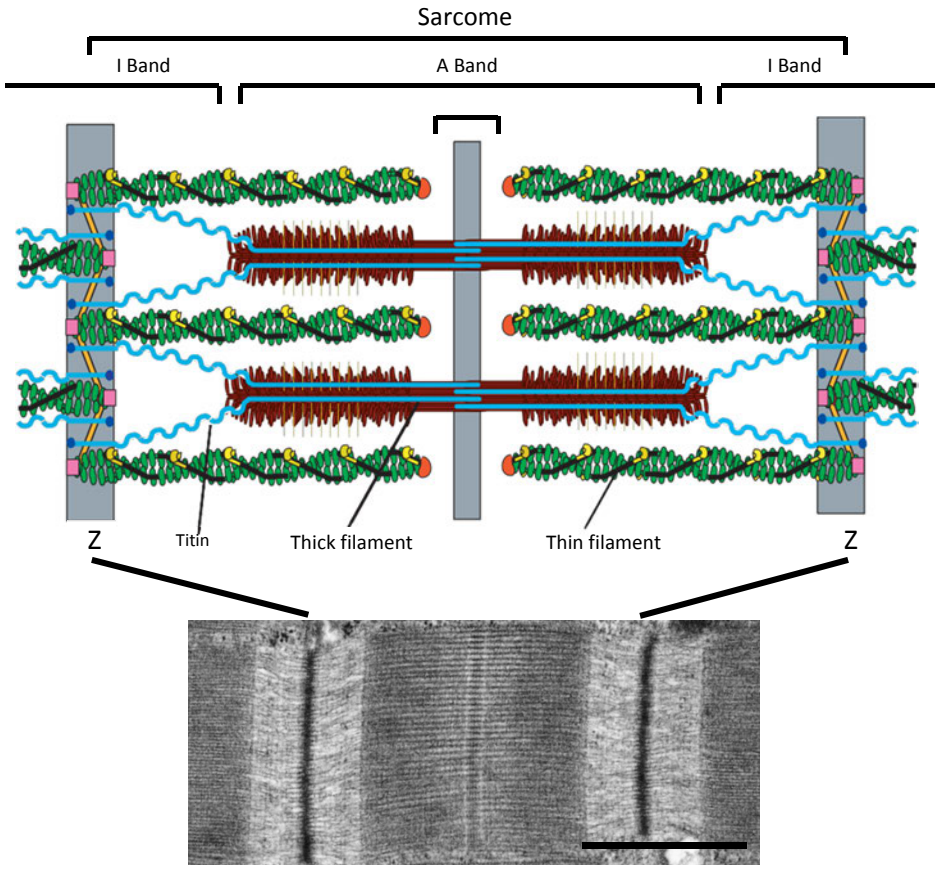

Figure 6: Major components of a cardiac muscle sarcomere. *Top:* Actin in green and myosin in red. Tropomyosin molecules (black lines) are associated with each other head to tail, forming two polymers per thin filament. Each tropomyosin molecule binds one troponin complex (troponins T, I and C; yellow). Thin filaments are polarized in muscle sarcomeres with the barbed ends anchored at the Z disk (edge of the sarcomere) by the crosslinking protein α-actinin (gold) and are capped by CapZ (pink squares). The C terminus of nebulette (a protein that shares sequence homology with the C-terminal domain of the skeletal muscle protein nebulin) extends partially into the Z disk. The third filament system is formed by titin, single molecules of titin reach from the Z line to the centre (M line) of the sarcomere. Titin interacts directly with several thick filament- associated proteins, such as myosin-binding-protein C (MyBP-C; yellow transverse lines). The N-terminal regions of titin molecules from opposite sarcomeres overlap in the Z lines, and the C-terminal regions of titin molecules from opposite half sarcomeres overlap in the M lines. Therefore, in myofibrils composed of many sarcomeric units, the titin filaments form a contiguous filament system. (Modified from Gregorio & Antin, 2000) *Bottom*: Electronmiscroscopic photograph of the ultrastructural organization of cardiac sarcomeres, unpublished data from our laboratory. Bar indicates 1000nm.

Sarcomeres consist of parallel arrays of ~ 1 µm -long thin filaments that interdigitate with 1.6 µm long thick filaments. The striations that characterize both cardiac and skeletal muscle and determine the repeating pattern of the sarcomere, are formed by alternating regions of higher and lower optical density, due to thick and thin filaments arrangement in each myofibril, named A and I bands, respectively. The sarcomere is bounded by optical dense Z-discs at the center of each I-band. The A-band is positioned around the lighter H-zone (Gregorio & Antin, 2000) (Fig. 6). The muscle shortening is associated to the reduction of width of I-band and H-zone, without any variation of A-band width (Squire, 1997). So, when sarcomere shortens, reduction of the distance between neighboring Z-line is related to the sliding of actin thin filaments towards the center of the sarcomere, causing the increase of overlapping of thin and thick filament, without any variation in the length of both filaments (Huxley, 1957; Huxley, 1969; Squire, 1997). Thick and thin filaments are formed by polymerization of the two principal contractile proteins, myosin and actin, respectively. Actin and myosin form the 'molecular motor' in muscles. Myosin works as an enzyme performing ATP hydrolysis under the allosteric control of actin such that actin binding initiates ATP product release and force generation in the myosin power stroke (Fig. 7**)**. There are different isoforms for many sarcomeric proteins in cardiac and skeletal muscles, specifically, cardiac isoforms are indicated with a "c" prefix (i.e. cardiac Myosin Binding Protein C, cMyBP-C).

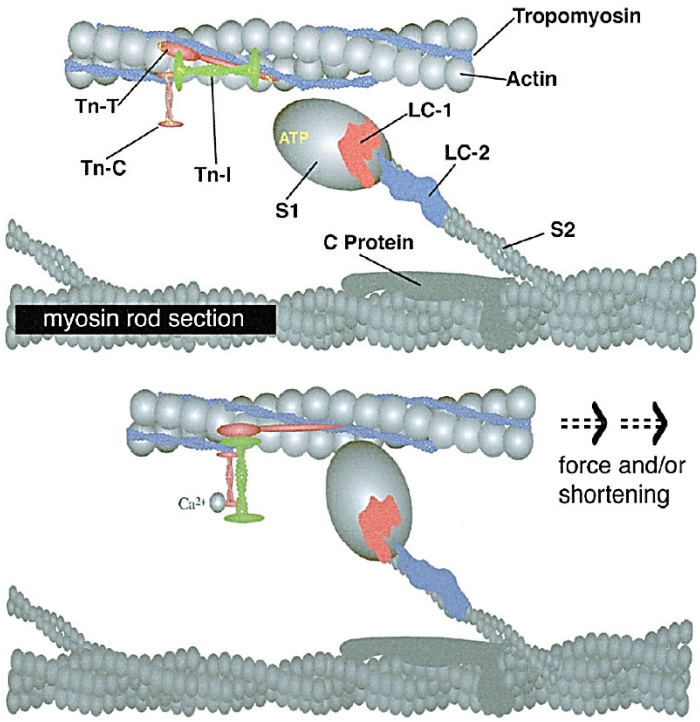

Figure 7: Thin and thick filaments interaction. The major proteins that are involved in contractile activation and regulation are shown in diastole (top panel) and systole (bottom panel) Myosin Heavy Chain (MyHC), the motor of contraction (it is a dimer but in the scheme is depicted as a single headed monomer) is made of different domains: the *myosin rod* composing the backbone of thick filaments, *S2*, connecting the rod to the myosin head, and the myosin head *S1* comprising the actin-binding, catalytic domain and the light chain binding domain (the lever arm of the motor protein). The other thick filament-associated proteins are the essential (ELC or LC-1, in red) and the regulatory (RLC or LC-2, in blue) myosin light chains, bound to the lever arm of *S1*, and C-protein (or cardiac Myosin Binding Protein-C, cMyBP-C in dark grey), a protein with poorly understood regulatory and structural functions. Thin filament proteins comprises, besides actin, the troponin complex (troponin C, TnC, troponin I, TnI, and troponin T, TnT) and tropomyosin. Modified from de Tombe; 2002.

The thick filaments are mainly composed by the motor protein myosin II. Myosin II is a polymer (6 chains) which is composed of two heavy chains (Myosin Heavy Chain, MHC of ≈ 200 kDa each), interconnected by a long twisted tail domain, and 4 light chains (LC). The extending domains of the myosin heavy chain are called the two myosin 'heads'. Two myosin light chains (MLC-1 and MLC-2) of ≈ 20 kDa are bound to the neck region of each head. The myosin 'head' is also called cross-bridge, since it bridges the gap between the thick myosin filaments and the thin actin filaments in muscle. The four light chains consist of two essential light chains (ELC, the MLC-1) and two regulatory light chains (RLC, the MLC-2) (Gordon et al, 2000) **(**Fig. 7). Each cross-bridge has an ATP binding site. Force and filament movement, in fact, depend on the energy released from ATP hydrolysis. In the presence of Ca^{2+}, the myosin cross-bridges bind to actin, promoting the release of Pi and then ADP. During this process a structural transition in the cross-bridge, suggested to be a change of tilt or change of shape, is thought to produce a relative sliding force between thin actin and thick myosin filaments. The cross-bridge can be released from actin when it binds another ATP molecule. In the heart, two different isoforms of MHC are present: α-myosin heavy chain (α-MHC) and β-myosin heavy chain (β-MHC). Human myosin is mainly composed of β-MHC and up to 5% of α-MHC.

Another important component of the thick filament is Myosin Binding Protein C (MyBP-C), a sarcomeric protein associated with the thick filaments, located in the cross-bridge containing A-band of the sarcomere (Fig. 7). To MyBP-C has been assigned a role in assembly and stability of the sarcomere as well as in the modulation of contraction (Oakley et al, 2004). In the myocardium, it has been demonstrated that cMyBP-C knockout mice are viable but show significant cardiac hypertrophy, myocyte disarray and fibrosis (Harris & Foord, 2000). Two models have been proposed for the arrangement of cMyBP-C in the sarcomere. In the first 'collar' model it is suggested that cMyBP-C molecules form a ring around the thick filament (Moolman-Smook et al, 2002). The second model proposes that the C-terminal of the molecule runs parallel to the myosin backbone, while the N-terminal domain interacts with neighboring actin filaments (Squire et al, 2003; Whitten et al, 2008). The C-terminal region of MyBP-C also contains binding sites for the giant protein titin.

The thin filament comprises F-actin helices, together with the so called "regulatory proteins": tropomyosin (Tm) and troponin (Tn) proteins in a 7:1:1 ratio. The thin filament consists mostly of the ≈ 45 kDa globular protein G-actin. G-actin monomers polymerize spontaneously to form the backbone of the thin filament, a double helix F-actin. Muscle thin filaments. The actin helix appears as two right-handed helices which twin slowly around each other (Holmes et al, 1990; Squire, 1997) . In striated muscle, tropomyosin (Tm) is wrapped around the F-actin backbone as a α-helical coiled-coil dimer. Tm modulates the actin-myosin interactions and functions to stabilize the actin structure. It comprises 284 aminoacid chains each spanning seven actin monomers and containing seven quasi-repeating regions. The Tm molecules are linked together through a head-to-tail association, which allows adjacent Tm molecules to function as a cooperative unit that spans 7 actin monomers. The Ca^{2+} binding protein complex, troponin (Tn), is bound to Tm (Kobayashi & Solaro, 2005; Wolska & Wieczorek, 2003). Troponin is a trimeric complex consisting of three subunits: troponin C (TnC), the Ca^{2+} binding subunit; Troponin I (TnI), the inhibitor of the acto-myosin reaction that shuttles between tight binding to actin and tight binding to the Ca^{2+}-TnC; and troponin T (TnT), the Tm binding subunit. Troponin subunits are present in different isoforms which distribution is tissue specific (fast skeletal muscle and slow skeletal muscle; miocardial) and also depend on development stage (Schiaffino & Reggiani, 1996). In cardiac muscle specific isoforms are present for all three subunits: cTnC, cTnI and cTnT.

1.2.2 Regulation of contraction: thin filament regulatory mechanism and E-C coupling

Regulation of actomyosin cross-bridge cycling by Tm and the Tn subunits is described by the three- state model of myofilament activation, whereby the position of the Tm coiled-coil dimer is in dynamic equilibrium between three position on actin (Lehrer & Geeves, 1998; Maytum et al, 1999; McKillop & Geeves, 1993). Ca^{2+} is the physiological activator of the contractile machinery. The interactions among the Tn subunits, Tm and actin are Ca^{2+} sensitive and allow Ca^{2+} induced conformational changes within the troponin complex, modification of the Tm position on the actin filament and the initiation of contraction (Gordon et al, 2000). During relax phase (or diastolic phase in the myocardium), the intracellular Ca^{2+} concentration is low and under these conditions TnI binds to actin-Tm and inhibits the binding of myosin and thereby force generation. During activation, (or systole, in the myocardium), intracellular Ca^{2+} concentration rises and triggers the contractile machinery by binding with the Ca^{2+} sensor: the TnC. As shown in fig. 8 skeletal muscle TnC contains two high affinity and two low affinity binding sites (Potter & Gergely, 1975), whereas, the cardiac TnC isoform (cTnC) has two high affinity sites, but only one low affinity binding site. The activation of the sarcomere occurs when Ca^{2+} binds to the low affinity site in cTnC, as the high affinity sites are always occupied by the ion.

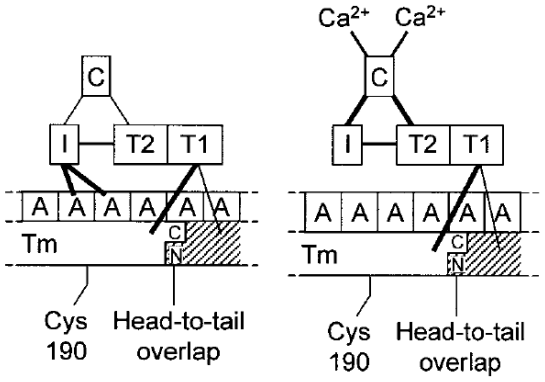

Figure 8: A model for molecular arrangement of Tn complex and Tm on the thin filament. The effect of Ca^{2+} binding to TnC on the interaction between the various thin filament proteins. A is actin, I is TnI, C is TnC, T1 is the NH2-terminal (1–158) portion of TnT, T2 is the COOH-terminal (159 –259) (*see below*) portion of TnT, Tm is tropomyosin with the NH_2 and COOH terminals indicated in the head-to-tail overlap region and the Cys-190 region indicated. Thicker lines imply stronger binding, and thinner lines imply weaker binding. No Ca^{2+} activating state where the ion is not bound to TnC triggering sites is shown on the left; whereas the state with Ca^{2+} bound to TnC sites is shown on the right. Note that Ca^{2+} binding to TnC enhances the TnC-TnI and TnC-TnT2 interactions and weakens the TnI-A interactions. This presumably allows the Tm to move on the surface of the actins opening up myosin binding residues. Modified from Gordon et al, 2000.

The relationship between free Ca^{2+} and isometric tension is very steep, much greater than would be expected on the basis of equilibrium binding of Ca^{2+} to the binding site on TnC (Shiner and Solaro, 1984). The transduction processes induced by Ca^{2+} binding that lead to activation of muscle contraction clearly involve cooperative interactions along the thin filament. Ca^{2+} binding induces a conformational change in TnC such that a hydrophobic region becomes exposed allowing interaction with TnI (Gagne et al, 1995; Slupsky & Sykes, 1995). In the absence of Ca^{2+}, this 'signaling pathway' is not triggered and Tn constrains Tm in a position that sterically

hinders myosin-S1 binding (Lehman et al, 1994; Xu et al, 1999). The movement of the troponin complex induces a conformational change in Tm, increasing its binding to actin, thereby revealing myosin-S1 binding sites on actin. Furthermore, upon forming strongly bound cross-bridges, the binding of additional cross-bridges is greatly enhanced in a cooperative manner, presumably by initiating the movement of tropomyosin to a third, more favorable position (Lehman et al, 2000; Lehrer & Geeves, 1998; Swartz & Moss, 1992; Tobacman & Butters, 2000).

A three-state model of the thin filaments has been proposed by Geeves et al. (1984) to explain the regulation of the interaction between actin, Tn, Tm and myosin (Figure 9). Tm can occupy three distinct positions on actin filament. Under relaxing condition, in absence of Ca^{2+}, Tm sterically blocks the interaction between actin and myosin heads in a 'blocked state'. Herein, not even weak myosin binding is possible. When Ca^{2+} starts to be present, Ca^{2+} starts to bind to TnC. This causes serial structural changes in all the components of Tn that allows movement of Tm to another position on actin filament and thereby the probability of formation of strong cross-bridges starts to increase. This is called 'closed or activated state'. Further increasing of Ca^{2+} concentration and the transition from weak to strong cross-bridges pushes Tm further to the 'open or activated state', further increasing the probability of strong mechanical transition and allowing full activation of thin filament and force generation by strong cross-bridges formation (Gordon et al, 2000; Lehman et al, 1997; Lehman et al, 1995).

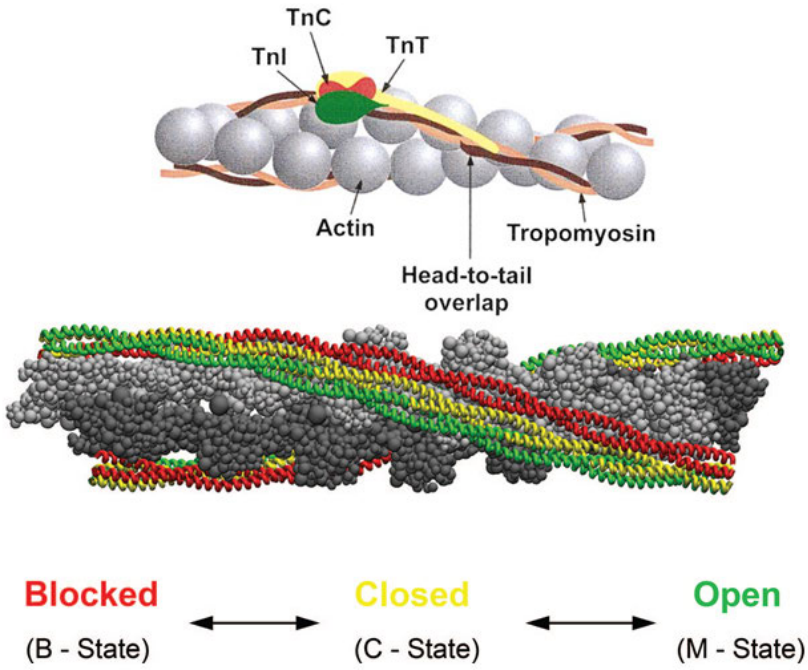

Figure 9: The 3-state model of myofilament activation. A model of molecular arrangement of Tn, Tm and actin in the thin filament. The various troponin subunits are indicated TnC (red), TnT (yellow), and TnI (green) as they lie along the two stranded tropomyosin shown as an a- (brown) and b-heterodimer (orange). The 3 average positions of Tm are depicted. Tm residues at the outer actin domain in the blocked state (red), Ca^{2+} binding to cTnC results in an azimuthal shift to the weakly bound closed state (yellow) in the actin inner domain, and myosin binding drives the final shift to the force-producing open state (green).

In the myocardium, activation of the contractile apparatus is initiated upon a transient increase in the cytosolic Ca^{2+} concentration. Under normal physiological conditions, calcium entry

during the plateau phase of the cardiac action potential is not sufficient to directly activate the myofilaments, but instead serves as a trigger to release calcium from the sarcoplasmic reticulum (Calcium Induces Calcium Release, CICR) (Bers, 2001). Collectively, this process is defined excitation–contraction coupling (E–C coupling). The key proteins involved in E-C coupling, such as DiHydro-Pyridine-Receptors (DHPR) and Sodium-Calcium-Exchangers (NCX) are located predominantly on the t-tubular membranes (Orchard et al. 2009,Yang D. et al. 2002, Pásek M. et al. 2008), adjacent to Ca^{2+} release-units in the Sarcoplasmic Reticulum (SR). Briefly, during the cardiac action potential, Ca^{2+}enters the cell through depolarization-activated Ca^{2+} channels as inward Ca^{2+} current (I_{Ca}), which contributes to the action potential plateau. Ca^{2+} entry triggers Ca^{2+} release from the sarcoplasmic reticulum (SR). The combination of Ca^{2+}influx and release raises the free intracellular Ca^{2+} concentration ($[Ca^{2+}]_i$), allowing Ca^{2+} to bind to the myofilament protein TnC, which then switches on the contractile machinery as previously described. For relaxation to occur $[Ca^{2+}]_i$ must decline, allowing Ca^{2+} to dissociate from Tn. This requires Ca^{2+} transport out of the cytosol by four pathways involving SR Ca^{2+}-ATPase, sarcolemmal Na^+/ Ca^{2+} exchange, sarcolemmal Ca^{2+}-ATPase or mitochondrial Ca^{2+} uniport (fig. 10).

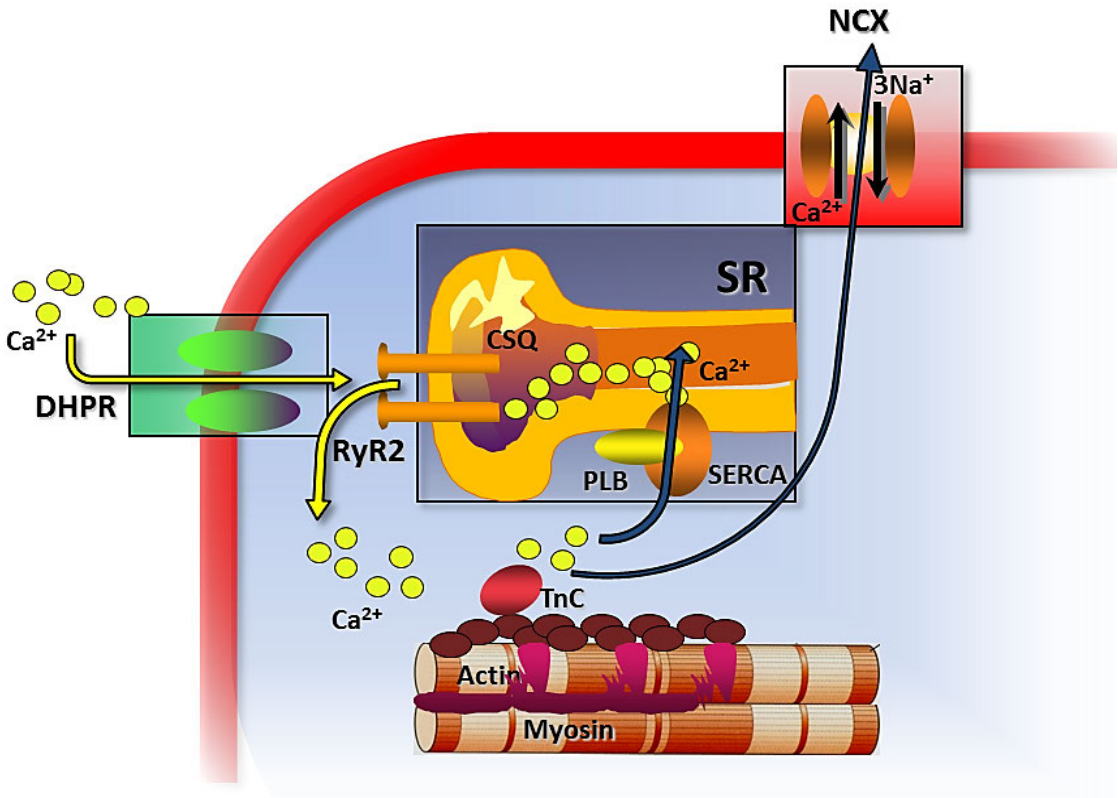

Figure 10: Cardiac Excitation-Contraction Coupling. During the cardiac action potential, Ca^{2+} enters the cell through depolarization-activated Ca^{2+} channels (DHPR) as inwardCa^{2+} current ($I_{Ca\text{-}L}$), which contributes to the action potential plateau. Ca^{2+} entry triggers Ca^{2+} release from the sarcoplasmic reticulum (SR), where a large amount of Ca^{2+} is stored bound to calsequestrin (CSQ). The Cardiac Ryanodine Receptor (RyR2) is the main SR Ca^{2+} release channel. The combination of Ca^{2+} influx and release raises the free intracellular Ca^{2+} concentration ($[Ca^{2+}]_i$), allowing Ca^{2+} to bind to the myofilament protein troponin C (TnC), which then switches on the contractile machinery. For relaxation to occur $[Ca^{2+}]_i$ must decline, allowing Ca^{2+} to dissociate from troponin. This requires Ca^{2+} transport out of the cytosol that occurs mainly by two pathways: SR Ca^{2+}-ATPase (SERCA) and sarcolemmal Na^+/Ca^{2+} exchange (NCX). Other pathways participate to cytosolic Ca^{2+} rise (e.g. reverse mode NCX, IP3receptor) and Ca^{2+} removal (e.g. sarcolemmal Ca^{2+}-ATPase or mitochondrial Ca^{2+}uniport), although with a minor contribution.

1.2.3 cTnT: the "glue" of the thin filament: structure and localization of the main cardiomyopathies-associated mutation

As explained above, the activation and inhibition of muscle contraction are primarily achieved by cTnC and cTnI respectively; however, these events cannot occur without cTnT. cTnT, in fact, anchors the Tn complex to the thin filament and also contributes to the Ca^{2+}dependent regulation of muscle contraction. Therefore, any functional and structural defects in cTnT may cause alteration of the Ca^{2+}regulation of muscle contraction. In his review of 1996, Tobacman described cTnT as "the glue" of the thin filament, because it links the cTnI:cTnC complex to TM-actin :"it touches them all" (Tardiff, 2011). Despite the cTnT linker's role in calcium signal propagation, little is known about its structure due to its hypervariability (Jin & Chong, 2010; Manning et al, 2012). cTnT consists of 298 aminoacids and is also named as TNNT2 from the name of gene that encode the cardiac isoform. cTnT is organized into 2 major functional domains TNT1 and TNT2. This classical organization is based on chymotryptic digest studies (Ohtsuki, 1979). The TNT2 domain is directly bound to cTnI: cTnC and comprises a significant portion of the rigid IT arm (residues 203 to 271) (see Fig. 11). The I-T arm is a coiled coil consisting of two helices, one from cTnI and the other from cTnT. It plays a key role in calcium signaling and represents the most stable region of the cTn complex in terms of subunit–subunit interactions.

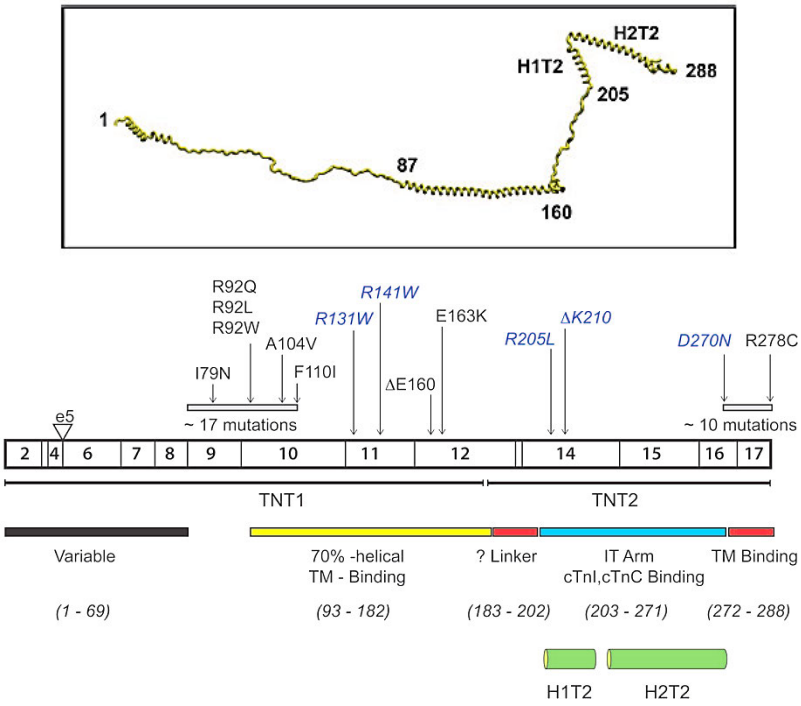

Figure 11: Distribution of HCM- and DCM-linked mutations in the cTnT N-terminal domain. This region of cTnT is highly conserved and the structure of the protein between residues 150 to 200 is poorly defined. Mutations that lead to hypertrophic or non-dilated ventricular remodeling are shown in *gray* and are contiguous to DCM-causing mutations (*black*). The disease-causing mutations in cTnT are highly clustered within 2 primary locations, all located in regions of the protein that are predicted to be highly mobile (modified from Tardiff, 2011).

TNT2 consists of 2α-helices (H1: 204 to 220; H2: 226 to 271) connected via a short 5-aa linker sequence (Fig. 12). Several of the known TNT2 mutations occur at the extreme N-terminal portion of the H1 helix and have been exclusively associated with Dilated Cardiomyopathy (DCM). The protein also includes the extended N-terminal, comprising the N-terminal "hypervariable" region and the largely α helical TNT1 and the extreme C-terminal (C-TnT) domains that were either not included in the cTn complexes that were crystallized or could not be resolved in the extant structures. These unresolved domains include more than 90% of the known disease-causing mutations in cTnT, and this lack of structural information limits our ability to understand the molecular pathogenesis of HCM. There is a flexible linker between TNT1 and TNT2 and little is known about its structure due to its hypervariability (Takeda et al 2003).

Approximally 65% of the cTnT mutation are found within or flanking TNT1, the N-terminal tropomyosin-binding domain of cTnT. TNT1 mutation trend to cluster at the N- and C- terminal ends of the domain, with two or several mutational hotspots occurring at residues 92 (i.e. R92Q, R92L, R92W) and 160-163 (i.e Δ160E, E163R, E163K). R92Q and Δ160E are consistently associated with a particularly poor clinical prognosis (Alcalai et al, 2008). Interestingly these mutations show significant differences in their molecular phenotype despite being located within the same functional domain (Haim et al, 2007; Palm et al, 2001). The mutational hotspot at residues 160-163 is located within a conserved, highly charged region (158-RREEEENRR-166). It has been recently shown that this region may unwind to form a flexible hinge that is necessary for normal thin filament regulation. Thus, mutations in TNT1 may alter the flexibility of TNT1, which is inversely proportional to the cooperativity of calcium activation of the thin filament. The flexibility of this region may be important for the transduction of Ca^{2+} activated signal for activation of the thin filament (Manning et al, 2012).

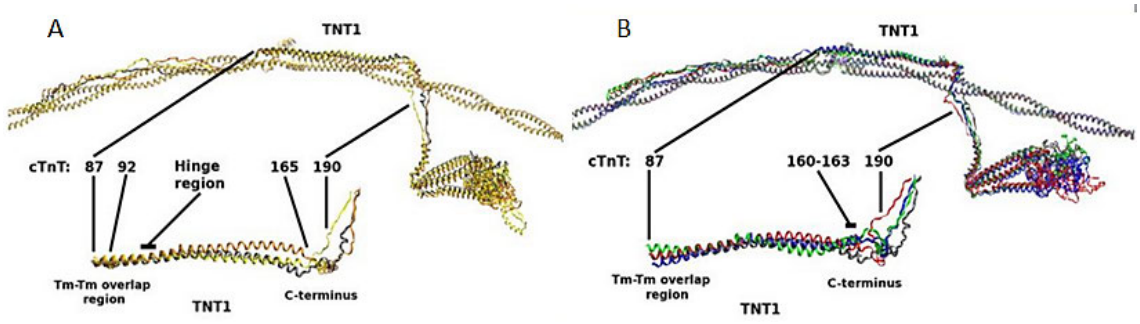

Figure 12: Two sets of cTnT mutations at opposite ends of TNT1. Mutations in residue 92 in the Tm-Tm overlap region of TNT1 and mutations in residues 160 and 163 in the C-terminal portion of TNT1 adjacent to the cTnT H1-H2 linker. (A) cTnT R92L and R92W mutations compared with WT. Top: Average structures of cTn with overlapping Tm–Tm for WT (gray), R92L (yellow), and R92W (orange) aligned with respect to Tm. Bottom: TNT1 is enlarged and rotated to highlight a noticeable shift in the average position of TNT1 for mutants R92L and R92W that results from decreased interactions between TNT1 and Tm. (B) cTnT ΔE160, E163K, E163R mutations compared with WT. Top: Average structures of cTn with overlapping Tm–Tm for WT (gray), ΔE160 (red), E163K (blue), and E163R (green) aligned with respect to Tm. Bottom: TNT1 is enlarged and rotated to highlight a noticeable shift in the average position of TNT1 for mutants ΔE160, E163K, and E163R that results from decreased interactions between TNT1 and Tm.

1.3.1 Primary and secondary changes related to cardiomyopathy-associated cTnT mutations

At present, there is no clear understanding as to why TnT mutations in particular pose a high risk for sudden death, as opposed to, for example, mutations in the myosin heavy chain, which usually cause a much greater degree of cardiac hypertrophy. Sudden cardiac death of HCM patients is often caused by ventricular tachyarrhythmias (Maron, 2000), but its cause remains unknown for patients with TnT mutations.
Disruption of cardiomyocyte Ca^{2+} homeostasis and excitation-contraction coupling has been shown to be an important early event in the pathogenesis of HCM (Semsarian et al, 2002). Increased [Ca^{2+}] in specific microdomains can also alter intracellular signaling pathways leading to adverse cardiac muscle remodeling.
How HCM-associated mutations in cTnT lead to different impaired cardiac function is not clear. In most cases, HCM is a disease that starts at the cardiac myofilament level triggering different remodeling of the heart. Each TnT mutation has somewhat different effects on myofilament properties though all mutations can be predicted to result in: (i) impaired relaxation, (ii) reduced diastolic compliance, (iii) reduced contractile reserve, (iiii) preserved systolic function under baseline conditions, and (iiiii) cardiac dysfunction under inotropic stimulation (Knollmann & Potter, 2001). A common feature shared by various HCM associated cTnT mutations is an increase in Ca^{2+} dependence of actomyosin interactions (Chandra et al, 2005). How such increase in Ca^{2+} sensitivity of force development leads to cardiac dysfunction is not understood. One possibility is that an enhanced Ca^{2+} sensitivity could provide a molecular basis for hypercontractility, which is a hallmark of these cTnT mutations. Consequently, this may lead to marked increases in sarcomeric ATP consumption, which could cause a mismatch between ATP synthesis and ATP usage by myocardial cells, exacerbated when stress is imposed on the heart.

1.3.2 Myofilament Ca^{2+} sensitivity

Increased myofilament Ca^{2+}-sensitivity has been reported as a common dysfunction in experimental models of HCM and has been proposed as a trigger of disease pathogenesis (e.g.(Marston, 2011). An augmented sensitivity to Ca^{2+} could affect cardiac myocyte relaxation and energetics and may contribute to electrical remodeling increasing the risk of arrhythmias (Baudenbacher et al, 2008). Recently, it has been reported that myofilament Ca^{2+} sensitization directly determines arrhythmogenic changes in cardiomyocyte Ca^{2+} homeostasis by increasing cytosolic Ca^{2+} buffering. This alteration in the intracellular Ca^{2+} handling could lead to proarrhythmic consequence such as pause-dependent potentiation of Ca^{2+} release, action potential prolongation, and triggered activity (Schober et al, 2012).
The high myofilament Ca^{2+} sensitivity found in human HCM samples could partly reflects a hypo-phosphorylation of PKA-targets. PKA-mediated phosphorylation of myofilament proteins such as cTnI, cMyBP-C, and titin, in fact, is thought to exert a positive lusitropic effect also by decreasing myofilament Ca^{2+} sensitivity and enhancing cross-bridge cycling kinetics. Phosphorylation of cTnI at the PKA sites Ser^{23} and Ser^{24} leads to a decrease in myofilament Ca^{2+} sensitivity through a conformational change of the troponin complex. This structural change reduces the affinity of Ca^{2+} binding to cTnC (Solaro et al, 1976; Takimoto et al, 2004; Zhang et al, 1995). It has been shown that frameshift *MYBPC3* mutations, causing

haploinsufficiency, enhanced Ca^{2+} sensitivity through hypophosphorylation of troponin I, secondary to mutation-induced dysfunction (van Dijk et al, 2009).
A recent study in human HCM with mutations in both thick- and thin-filament proteins showed higher myofilament Ca^{2+} sensitivity compared to donor samples. However, the higher Ca^{2+} sensitivity in sarcomere mutation positive HCM groups compared with non-failing donors coincided with lower phosphorylation levels of cMyBP-C and cTnI. Treatment of HCM samples with PKA increased phosphorylation of the PKA target proteins and normalized myofilament Ca^{2+} sensitivity in *MYBPC3* mut, *TPM1* mut, and sarcomere mutation negative HCM to values observed in non-failing donors. In contrast, after PKA, higher myofilament Ca^{2+} sensitivity was still present in *MYH7* mut and *TNNT2* mut, suggesting that the Ca^{2+}-sensitizing effect is primary caused by these mutations (Sequeira et al, 2013).

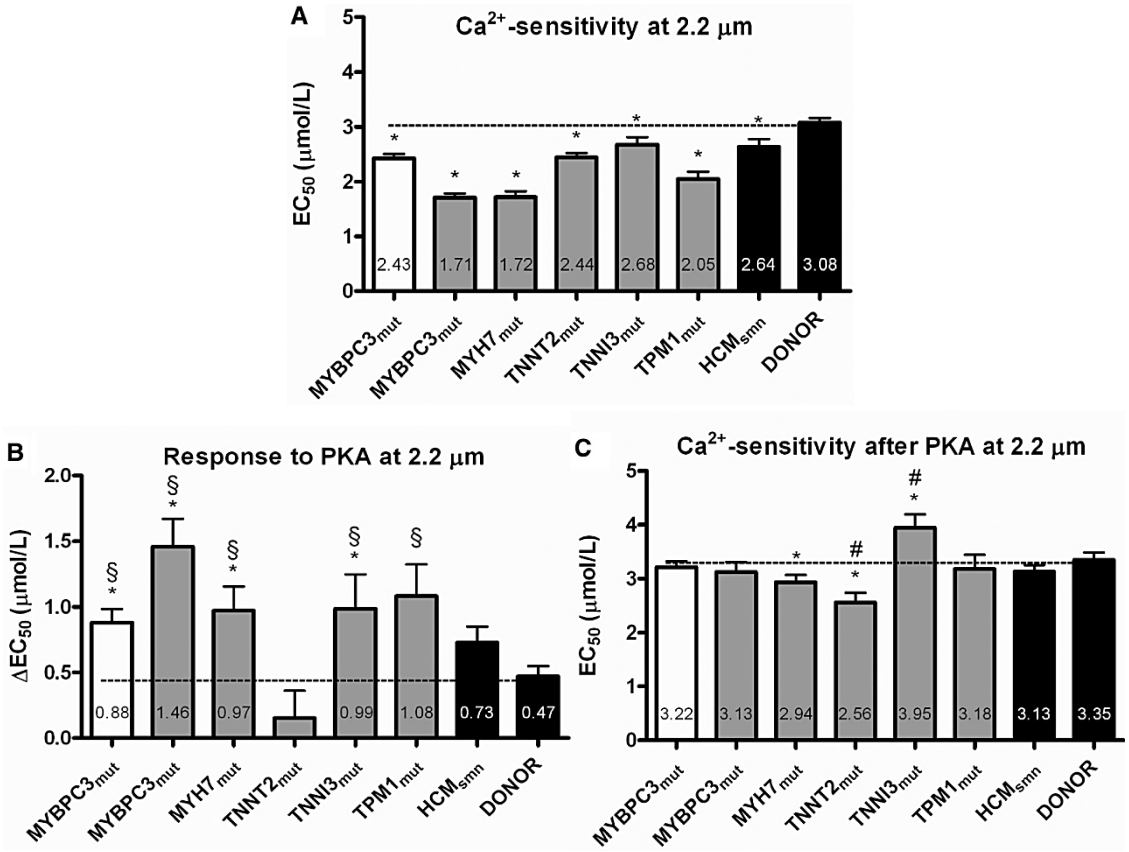

Figure 13: Myofilament Ca^{2+} sensitivity. A Myofilament Ca^{2+} sensitivity (EC50) was significantly higher in all HCM groups compared with donors. B The protein kinase A (PKA)–induced reduction (ΔEC50) in myofilament Ca^{2+} sensitivity was larger in HCM groups compared with donors, except in the *TNNT2*mut sample, in which PKA had no significant effect. C Myofilament Ca^{2+} sensitivity was similar in *MYBPC3*mut, *TPM1*mut, sarcomere mutation-negative HCM (HCMsmn), and donor after treatment with PKA, whereas it was higher than donor in *MYH7*mut and *TNNT2*mut. PKA-treated *TNNI3*mut cells showed a lower myofilament Ca2+ sensitivity compared with HCMsmn and donor. Open bar represents *MYBPC3* truncating mutation; solid gray bars represent missense mutations. **P*<0.05 vs donor; §*P*<0.05 vs *TNNT2*mut; #*P*<0.05 vs HCMsmn.

Many studies have shown that most HCM-TnT mutations alter the contractile properties of cardiac muscle, especially the Ca^{2+}sensitivity of force development and ATPase activity (see below) *in vitro* and *in vivo* (Gomes et al, 2004; Hernandez et al, 2001; Knollmann & Potter, 2001). HCM TnT mutants I79N, R92Q, F110I, E163K, and R278C increased Ca^{2+} sensitivity of force development when they were incorporated into porcine skinned cardiac fibers together with human cTnI and cTnC (Szczesna et al, 2000). Moreover, a transgenic mouse model, expressing the I79N mutation, has demonstrated similar properties (*i.e.* increase in the Ca^{2+} sensitivity of force development and ATPase activity) as well as other phenotypic properties of HCM, such as impaired diastolic function. Similar results have been seen at both molecular and physiological levels, implying that altered Ca^{2+}regulation of muscle contraction by TnT mutations might be the primary mechanism for TnT-linked HCM. There are strong evidences that ΔE160 TnT mutation increases Ca^{2+} sensitivity of both myofibrillar ATPase activity and force development of skinned fibers by increasing Ca^{2+} affinity of TnC (Harada et al, 2000; Tobacman et al, 1999). Although the mechanisms by which single point mutation in TnT may cause a Ca^{2+} sensitizing are still not clear, an increased Ca^{2+} sensitivity of force development might be explained by one of the following ways or a combination of them: i) increased Ca^{2+} affinity of TnC; ii) reduced inhibitory action of TnI, and iii) activation of the actomyosin interaction that indirectly leads to increased Ca^{2+} affinity of TnC (Harada & Potter, 2004).

1.3.3 E-C coupling alterations

The mechanisms underlying HCM cardiomyocyte adverse remodeling in E-C coupling components are still under investigation. One of the predicted consequences of the energy depletion hypothesis for HCM is that reuptake of Ca^{2+} into the sarcoplasmic reticulum will be compromised because of the extreme energy requirements of the cardiac SERCA pump. In support of this notion, spectroscopy studies in transgenic mouse models of HCM have shown that ATP availability is reduced to a level at which SERCA function will be compromised (He et al, 2007; Javadpour et al, 2003; Spindler et al, 1998). Increased Ca^{2+} concentrations in specific micro-domains would activate hypertrophy-signaling pathways and mutation-induced abnormalities in myocyte Ca^{2+} handling could activate pathological hypertrophy signaling cascades. This idea is strongly supported by studies in HCM mice showing that treatment with Ca^{2+} channel antagonists partially blocks the development of pathological hypertrophy. Elevated diastolic intracellular [Ca^{2+}] and altered function of other ion transporters may also render the myocardium vulnerable to the arrhythmias that underlie sudden cardiac death in HCM. The electromechanical profile of cardiomyocytes from HCM patients undergoing myectomy has been recently assessed and compared with that of cardiomyocytes from non-hypertrophic non-failing surgical patients by performing patch-clamp and intracellular Ca^{2+} studies (Coppini et al, 2013). Compared with controls, HCM cardiomyocytes showed prolonged action potential related to increased late Na^+ (I_{NaL}) and Ca^{2+} (I_{CaL}) currents and decreased repolarizing K^+ currents; increased occurrence of cellular arrhythmias; prolonged Ca^{2+}-transients and higher diastolic Ca^{2+}. Such changes were related to enhanced Ca^{2+}/calmodulin kinase II (CaMKII) activity and increased phosphorylation of its targets (Figure 14). Thus, an enhanced I_{NaL} seems to be a major contributor to the electrophysiological and Ca^{2+}dynamic abnormalities of ventricular myocytes and trabeculae from patients with HCM, suggesting potential therapeutic implications of I_{NaL} and CaMKII inhibition.

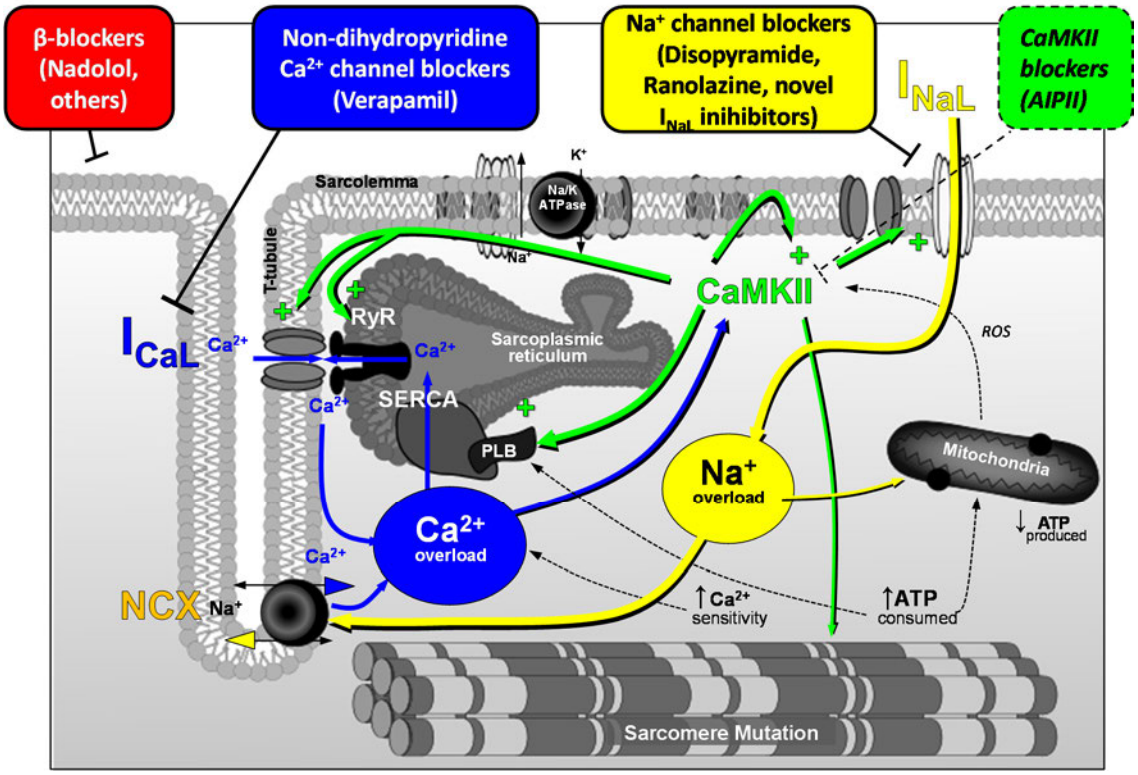

Figure 14: Targeting secondary alterations in HCM: electro-mechanical remodeling in human HCM cardiomyocytes. Sarcomeric mutations may cause a primary sustained increase of intracellular Ca^{2+} with multiple mechanisms: (i) increased sarcomeric ATP consumption that may lead to SERCA (and mithocondria) dysfunction and impaired Ca^{2+} removal; (ii) increased myofilament Ca^{2+} sensitivity that slows Ca^{2+} dissociation from the myofilaments and contributes to increased Ca^{2+} levels during diastole. Intracellular Ca^{2+} overload (in combination with increased production of reactive oxygen species) leads to sustained activation of CaMKII: increased phosphorylation of its downstream targets (Ca^{2+} channels, Ryanodine Receptors, phospholamban, Na+ channel) is responsible for the abnormalities observed in HCM cardiomyocytes, including increased I_{NaL}. Overall, these changes aggravate intracellular Ca^{2+} overload. The enhanced I_{NaL} is responsible for intracellular Na^{+} overload, which favors reverse over forward NCX mode. The latter contributes to cytosolic Ca^{2+} overload, further promoting CaMKII activation, thus setting up a vicious circle. (Coppini et al, 2013)

Furthermore, a loss of t-tubules in the sarcolemmal membrane has been shown: in hypertrophied HCM cardiomyocytes, capacitance/volume ratio is reduced compared to control cardiomyocytes, reflecting a disproportion between surfaces vs. volume growth. (Coppini et al, 2013; Lyon et al, 2009). The reduction of t-tubular density, usually paralleled by increased cell dimensions, can be an additional pathogenic element contributing to alteration in Ca^{2+} handling and mechanical impairment. A decreased t-tubule density with loss of t-tubular currents can hinder a synchronous SR Ca^{2+}-release throughout the myocyte leading to a prolongation of Ca^{2+}_i transient rise and decay (Ferrantini et al, 2014).

All these alteration have been also studied in animal models of HCM carrying sarcomeric mutations. These studies showed alterations of the kinetics of intracellular calcium transients (Szczesna-Cordary et al, 2007; Wang et al, 2006) and alterated properties of membrane electrical activity (Knollmann et al, 2003; Knollmann & Roden, 2008), such as changes in action potential duration (APD), APD adaptation to heart rate and alterations of repolarizing potassium currents, even in the absence of hypertrophy. The complexity of the potential role of

altered Ca^{2+} fluxes is exemplified by studies of patients and animal models harboring specific mutations in TnT. Mouse models demonstrate little or no hypertrophy. Measurement in Δ160E and R92L myocytes isolated from these models demonstrated (i) slower Ca^{2+} transient kinetics (ii) a significant reductions in SR Ca^{2+} load and uptake only Delta160E, and not R92L myocytes (iii) a significant Δ160E-specific reduction in the SERCA2a/PLB ratio, which may well underlie the observed alterations in Ca^{2+} homeostasis in Western blot analysis (Haim et al, 2007). Therefore, independent cTnT mutations result in significant mutation-specific effects in Ca^{2+} handling that may, in part, contribute to the observed clinical variability in cTnT-related FHC. Finally, all these functional changes observed in human HCM myocardium are likely a consequence of a complex remodelling process involving alterations of signaling pathways, rather than being a direct consequence of the causal sarcomeric mutations.

1.3.4 Molecular basis of HCM: Are alterations in Ca^{2+}-fluxes the initiating stimulus for pathological hypertrophy and arrhythmias?

Early functional *in vitro* studies have concluded that HCM mutations cause a loss of sarcomere mechanical function. Hypertrophy would then follow as a compensatory mechanism to raise the work and power output of the affected heart. However, subsequent *in vitro* and mouse model studies have suggested that HCM mutations enhance contractile function and myofilament Ca^{2+} sensitivity and impair cardiac myocyte energetics. It has been hypothesized that these changes may result in cardiac myocyte energy depletion, due to inefficient ATP utilization (Ashrafian H et al. 2003). More recent work with myofibrils isolated from affected human hearts supports the energy depletion hypothesis (Belus et al 2008, Ferrantini et al 2009). One of the predicted consequences of the energy depletion hypothesis for HCM is that reuptake of Ca^{2+} into the sarcoplasmic reticulum will be compromised because of the extreme energy requirements of the cardiac SERCA pump. In support of this notion, spectroscopy studies in transgenic mouse models of HCM have shown that ATP availability is reduced to a level at which SERCA function will be compromised (Spindler et al., 1998; Javadpour et al., 2003; He et al. 2007). Increased Ca^{2+} concentrations in specific micro-domains would activate hypertrophy-signalling pathways and mutation-induced abnormalities in myocyte Ca^{2+} handling could activate pathological hypertrophy signaling cascades. This idea is strongly supported by studies in HCM mice showing that treatment with Ca^{2+} channel antagonists partially blocks the development of pathological hypertrophy.

There is also evidence that the HCM phenotype can be rescued by manipulation of the Ca^{2+}handling properties of HCM myocytes (i.e. viral aided gene transfer of SERCA2a in neonatal hearts expressing mutant tropomyosin, Pena JR et al. 2006). This idea deserves additional study to see if results can be translated into animal models and finally into humans. In these studies, Ca^{2+} handling should be manipulated at multiple levels, from influx pathways to sarcoplasmic reticulum (SR) storage and release, to identify the most reliable strategy to inhibit the development of pathological phenotypes without negatively impacting cardiac function. Calcium influx reduction with diltiazem, proven effective in preventing development of hypertrophy in animal models, is being tested on young mutation-bearing patients: due to the negative inotropic effects, such drugs may severely affect exercise tolerance in patients leading to treatment withdrawal; moreover, long term effects of $I_{Ca\text{-}L}$ block in the heart are not clearly known. A more specific drug, that positively affects intracellular Ca^{2+}-handling with less side effects is therefore needed for effective HCM treatment.

New studies are also needed to define how altered Ca^{2+} fluxes on and off of troponin C (TnC) change the kinetics of the cytosolic free [Ca^{2+}] transient and what role this may play in arrhythmogenesis (Baudenbacher F et al. 2008). Details can be found in fig. 15, which clearly shows that TnT mutations, due to the increased myofilament Ca^{2+} sensitivity, directly lead to changes in action potentials and increased susceptibility to arrhythmias. In HCM, increased Ca^{2+} sensitivity of the myofilament can prolong the decay phase of the transient and thus delay relaxation.The complexity of the potential role of altered Ca^{2+} fluxes is exemplified by studies of patients and animal models harboring specific mutations in TnT. Patients and mouse models demonstrate little or no hypertrophy. Yet there are apparent alterations in Ca^{2+} fluxes in myocytes isolated from these models (Haim TE et al. 2007). Measures of myocyte mechanics and Ca^{2+} kinetics in HCM revealed a decreased rate of contraction, percent shortening, peak rate of relaxation, sarcoplasmic reticulum Ca^{2+} load, baseline Ca^{2+} levels, peak rate of Ca^{2+} rise and decline, Ca^{2+} peak amplitude, and SERCA/PLB ratios.

Additionally, altered intracellular calcium transients and variations of Ca^{2+}binding to the myofilaments can lead to changes in NCX current and/or other calcium dependent currents (transient outward potassium current,I_{to} and L-Type calcium current, $I_{Ca\text{-}L}$). In fact, animal models of HCM carrying sarcomeric mutations not only showed alterations of the kinetics of intracellular calcium transients (Wang Y et al., 2006; Szczesna-Cordary D et al, 2007) but also of the properties of membrane electrical activity (Knollmann BC et al. 2003; Baudenbacher F et al. 2008), such as changes in action potential duration (APD) and APD adaptation to heart rate and alterations of repolarizing potassium currents, even in the absence of hypertrophy.

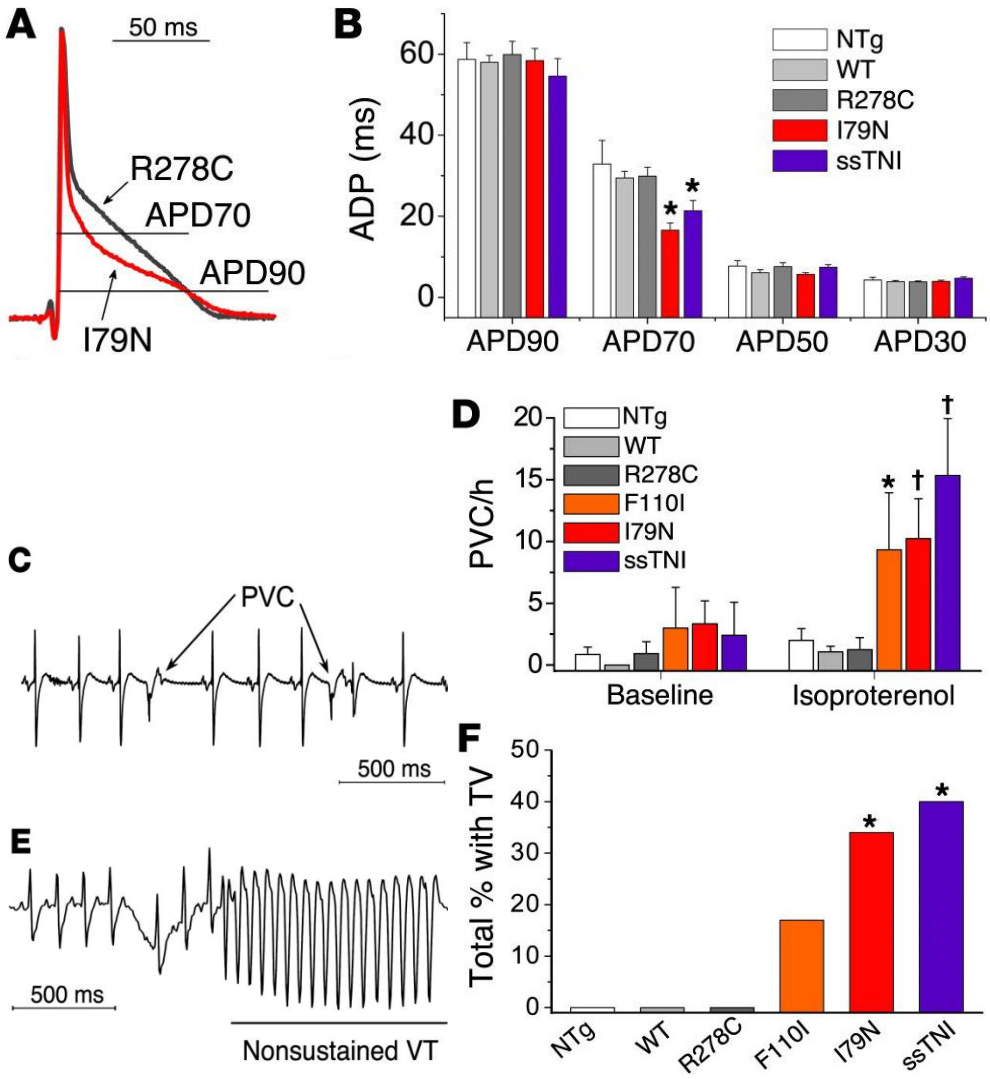

Figure 15: Ca^{2+} sensitization from troponin T mutation changes electrical properties and raises risk of arrhythmias. (A) Superimposed MAP records comparing the effect of the Ca^{2+}-sensitizing I79N and the nonsensitizing R278C TnT mutations on mouse ventricular AP. While the overall APD is unchanged, I79N hearts have a lower terminal repolarization phase. (C) Effect of isoproterenol on ventricular arhhythmias in anesthetized mice. ECG recording from an F110I mouse illustrating isoproterenol-induced PVCs (arrows). (D) Note the significantly higher PVC rate in mice with Ca^{2+}-sensitized (TnT mutant) myofilaments compared with normal myofilament Ca^{2+} sensitivity $*P < 0.05$, $^{\dagger}P < 0.005$ compared with WT, by Mann-Whitney *U* test. (E) Example of nonsustained VT recorded in an I79N mouse after isoproterenol injection. (F) VT incidence after isoproterenol injection. $*P < 0.05$ compared with WT, by Fisher's exact test; group sizes as in D. (Baudenbacher et al.2008).

Moreover, hypertrophic remodeling has been widely associated with secondary changes in transmembrane currents leading to modifications of AP (AP Prolongation) in models of secondary hypertrophy: these changes are known to contribute to Diastolic Dysfunction (DD) and are likely present in HCM, though never extensively investigated before.

Collectively these studies suggest that mutations in myofibrillar proteins often involve reactive changes in Ca^{2+} signaling that are likely to be required to ensure the pump function of the heart. If and how these changes in Ca^{2+}handling contribute to the associated hypertrophy and eventually cardiac dysfunction is an area that needs much more study.

REFERENCES:

Alcalai R, Seidman JG, Seidman CE (2008) Genetic basis of hypertrophic cardiomyopathy: from bench to the clinics. *Journal of cardiovascular electrophysiology* 19: 104-110.

Ashrafian H, Redwood C, Blair E, Watkins H. Hypertrophic cardiomyopathy:a paradigm for myocardial energy depletion. Trends Genet. 2003;19:263-268.

Baudenbacher F, Schober T, Pinto JR, Sidorov VY, Hilliard F, Solaro RJ, Potter JD, Knollmann BC. Myofilament Ca^{2+} sensitization causes susceptibility to cardiac arrhythmia in mice. J Clin Invest. 2008;118:3893-3903.

Gagne SM, Tsuda S, Li MX, Smillie LB, Sykes BD (1995) Structures of the troponin C regulatory domains in the apo and calcium-saturated states. *Nature structural biology* 2: 784-789.

Gordon AM, Homsher E, Regnier M (2000) Regulation of contraction in striated muscle. *Physiological reviews* 80: 853-924.

Gregorio CC, Antin PB (2000) To the heart of myofibril assembly. *Trends in cell biology* 10: 355-362.

Ferrantini C, Belus A, Piroddi N, Scellini B, Tesi C, Poggesi C. Mechanical and energetic consequences of HCM-causing mutations. J Cardiovasc Transl Res. 2009 Dec; 2 (4):441-51.

Ferrantini C, Coppini R, Sacconi L, Tosi B, Zhang ML, Wang GL, de Vries E, Hoppenbrouwers E, Pavone F, Cerbai E, Tesi C, Poggesi C, ter Keurs HE. Impact of detubulation on force and kinetics of cardiac muscle contraction. J Gen Physiol. 2014 Jun;143(6):783-97.

Haim TE, Dowell C, Diamanti T, Scheuer J, Tardiff JC. Independent FHC-related cardiac troponin T mutations exhibit specific alterations in myocellular contractility and calcium kinetics. J Mol Cell Cardiol. 2007;42:1098-1110.

Harris S, Foord SM (2000) Transgenic gene knock-outs: functional genomics and therapeutic target selection. *Pharmacogenomics* 1: 433-443.

Holmes KC, Popp D, Gebhard W, Kabsch W (1990) Atomic model of the actin filament. *Nature* 347: 44-49.

Huxley AF (1957) Muscle structure and theories of contraction. *Progress in biophysics and biophysical chemistry* 7: 255-318.

Huxley HE (1969) The mechanism of muscular contraction. *Science* 164: 1356-1365.

Jin JP, Chong SM (2010) Localization of the two tropomyosin-binding sites of troponin T. *Archives of biochemistry and biophysics* 500: 144-150.

Knollmann BC, Kirchhof P, Sirenko SG, Degen H, Greene AE, Schober T, Mackow JC, Fabritz L, Potter JD, Morad M. Familial hypertrophic cardiomyopathy-linked mutant troponin T causes stress-induced ventricular tachycardia and Ca^{2+}-dependent action potential remodeling.Circ Res. 2003 Mar 7;92(4):428-36. Epub 2003 Feb 6.

Kobayashi T, Solaro RJ (2005) Calcium, thin filaments, and the integrative biology of cardiac contractility. *Annual review of physiology* 67: 39-67.

Lehman W, Craig R, Vibert P (1994) Ca(2+)-induced tropomyosin movement in Limulus thin filaments revealed by three-dimensional reconstruction. *Nature* 368: 65-67.

Lehman W, Hatch V, Korman V, Rosol M, Thomas L, Maytum R, Geeves MA, Van Eyk JE, Tobacman LS, Craig R (2000) Tropomyosin and actin isoforms modulate the localization of tropomyosin strands on actin filaments. *Journal of molecular biology* 302: 593-606.

Lehman W, Vibert P, Craig R (1997) Visualization of caldesmon on smooth muscle thin filaments. *Journal of molecular biology* 274: 310-317.

Lehman W, Vibert P, Uman P, Craig R (1995) Steric-blocking by tropomyosin visualized in relaxed vertebrate muscle thin filaments. *Journal of molecular biology* 251: 191-196.

Lehrer SS, Geeves MA (1998) The muscle thin filament as a classical cooperative/allosteric regulatory system. *Journal of molecular biology* 277: 1081-1089.

Linke WA. Sense and stretchability: the role of titin and titin-associated proteins in myocardial stress-sensing and mechanical dysfunction. Cardiovasc Res.2008;77:637-648.

Manning EP, Guinto PJ, Tardiff JC (2012) Correlation of molecular and functional effects of mutations in cardiac troponin T linked to familial hypertrophic cardiomyopathy: an integrative in silico/in vitro approach. *The Journal of biological chemistry* 287: 14515-14523.

Maytum R, Lehrer SS, Geeves MA (1999) Cooperativity and switching within the three-state model of muscle regulation. *Biochemistry* 38: 1102-1110.

McKillop DF, Geeves MA (1993) Regulation of the interaction between actin and myosin subfragment 1: evidence for three states of the thin filament. *Biophysical journal* 65: 693-701.

Moolman-Smook J, Flashman E, de Lange W, Li Z, Corfield V, Redwood C, Watkins H (2002) Identification of novel interactions between domains of Myosin binding protein-C that are modulated by hypertrophic cardiomyopathy missense mutations. *Circulation research* 91: 704-711.

Oakley CE, Hambly BD, Curmi PM, Brown LJ (2004) Myosin binding protein C: structural abnormalities in familial hypertrophic cardiomyopathy. *Cell research* 14: 95-110.

Ohtsuki I (1979) Molecular arrangement of troponin-T in the thin filament. *Journal of biochemistry* 86: 491-497.

Palm T, Graboski S, Hitchcock-DeGregori SE, Greenfield NJ (2001) Disease-causing mutations in cardiac troponin T: identification of a critical tropomyosin-binding region. *Biophysical journal* 81: 2827-2837.

Pena JR, Szkudlarek AC, Goldspink PH. Neonatal gene transfer of SERCA2a alters hypertrophic gene expression and improves the response to beta-adrenergic stimulation in a FHC alpha-tropomyosin (Glu180Gly) mouse model (Abstract). Circulation. 2006;114:166.

Potter JD, Gergely J (1975) The regulatory system of the actin-myosin interaction. *Recent advances in studies on cardiac structure and metabolism* 5: 235-244.

Schiaffino S, Reggiani C (1996) Molecular diversity of myofibrillar proteins: gene regulation and functional significance. *Physiological reviews* 76: 371-423.

Semsarian C, Ahmad I, Giewat M, Georgakopoulos D, Schmitt JP, McConnell BK, Reiken S, Mende U, Marks AR, Kass DA, Seidman CE, Seidman JG. The L-type calcium channel inhibitor diltiazem prevents cardiomyopathy in a mousemodel. J Clin Invest. 2002;109:1013-1020.

Slupsky CM, Sykes BD (1995) NMR solution structure of calcium-saturated skeletal muscle troponin C. *Biochemistry* 34: 15953-15964.

Squire JM (1997) Architecture and function in the muscle sarcomere. *Current opinion in structural biology* 7: 247-257.

Squire JM, Luther PK, Knupp C (2003) Structural evidence for the interaction of C-protein (MyBP-C) with actin and sequence identification of a possible actin-binding domain. *Journal of molecular biology* 331: 713-724.

Swartz DR, Moss RL (1992) Influence of a strong-binding myosin analogue on calcium-sensitive mechanical properties of skinned skeletal muscle fibers. *The Journal of biological chemistry* 267: 20497-20506.

Szczesna-Cordary D, Jones M, Moore JR, Watt J, Kerrick WG, Xu Y, Wang Y, Wagg C, Lopaschuk GD. Myosin regulatory light chain E22K mutation results in decreased cardiac intracellular calcium and force transients.FASEB J. 2007 Dec;21(14):3974-85. Epub 2007 Jul 2.

Tardiff JC (2011) Thin filament mutations: developing an integrative approach to a complex disorder. *Circulation research* 108: 765-782.

Tobacman LS, Butters CA (2000) A new model of cooperative myosin-thin filament binding. *The Journal of biological chemistry* 275: 27587-27593.

Wang Y, Xu Y, Kerrick WG, Wang Y, Guzman G, Diaz-Perez Z, Szczesna-Cordary D. Prolonged Ca^{2+} and force transients in myosin RLC transgenic mouse fibers expressing malignant and benign FHC mutations.J Mol Biol. 2006 Aug 11;361(2):286-99. Epub 2006 Jun 27.

Whitten AE, Jeffries CM, Harris SP, Trewhella J (2008) Cardiac myosin-binding protein C decorates F-actin: implications for cardiac function. *Proceedings of the National Academy of Sciences of the United States of America* 105: 18360-18365.

Wolska BM, Wieczorek DM (2003) The role of tropomyosin in the regulation of myocardial contraction and relaxation. *Pflugers Archiv : European journal of physiology* 446: 1-8.

Xu C, Craig R, Tobacman L, Horowitz R, Lehman W (1999) Tropomyosin positions in regulated thin filaments revealed by cryoelectron microscopy. *Biophysical journal* 77: 985-992.

1.4.1 Role of Animal Models in HCM research

The development of relevant animal models has been instrumental in dissecting various pathogenic features of HCM. While human studies have been extremely useful in both clinical aspects of disease, as well as identification of disease genes, there are limitations in human studies, including genetic background variations, environmental influences, and tissue availability.

In order to gain insight into disease pathogenesis, mechanisms of the disease, and novel potential therapeutic targets in HCM, animal models of HCM have been developed as an invaluable "research tool". Such animal models provide an answer to these limitations, with inbred strains eliminating variability in genetic background and allowing for effective identification of gender differences in phenotype. Furthermore, the availability and extensive breeding capacity of animal models allow for the limitless investigation of vital organs, such as the heart, thereby providing tissues for a range of molecular investigations including histopathology, cellular, RNA, and protein studies. Such models have been able to confirm the causative gene defects in HCM, have allowed for exploration into the signaling pathways involved in pathogenesis and the role of genetic and environmental modifying factors on clinical outcome. Additionally, they have provided exciting insights into potential new therapeutic interventions for prevention or regression of disease. Although many animal models of HCM exist, the following is a brief description of some of the models based on the causative gene, that bear some of the most common mutations found in HCM patients.

1.4.2 HCM murine models carrying troponin T mutation

Many animal models of HCM have been developed, including Myosin heavy chain mutants (Geisterfer-Lowrance et al, 1990), Myosin-binding protein C mutants and recently developed tropomyosin and actin mutants. Our attention will be focused on the Troponin T mutants that will be employed in this study.

The cardiac troponin complex consists of three subunits: troponin I, troponin T, and troponin C. This complex is associated with the thin filament and acts as the calcium sensor, which, together with tropomyosin (TM), is responsible for the regulation of contraction and relaxation of striated muscle. cTnT binds the troponin complex to TM and is involved with the positioning of the troponin complex along the actin filament. Mutations in the cTnT gene are responsible for causing 5–15% of HCM cases (Thierfelder, L et al, 1994). Individuals with cTnT mutations generally exhibit mild or no ventricular hypertrophy, but have a high incidence of premature sudden death (Watkins H et al, 1995; Moolman JC et al.1997).

As previously described, TNT1 mutations tend to cluster at the N- and C-terminal ends of the domain, with mutational hotspots occurring at residues 92–96 and 160–163. Despite their location in the same domain, these mutational hotspots exhibit significant differences in their molecular and clinical phenotypes. A transgenic mouse model expressing a truncated mouse cTnT allele analogous to one found in HCM patients (Thierfelder et al, 1994), has been described (Tardiff et al, 1998).

Heterozygous mice expressing the truncated cTnT at low levels (<5%) developed cardiomyopathy and had significantly smaller ventricles (18-27% decrease in heart mass in both independent lines of cTnT-Myc truncation mice at 4–5 months of age when compared to either non-transgenic siblings) and impaired cardiac contractility and relaxation. Interestingly, the

same splice donor site mutation has also been generated in a transgenic rat model, which overexpresses the human truncated cTnT protein (Frey et al, 2000). These rats display features of FHC including diastolic dysfunction and increased susceptibility to ventricular arrhythmias, particularly during exertion or stress (Luedde et al, 2009).

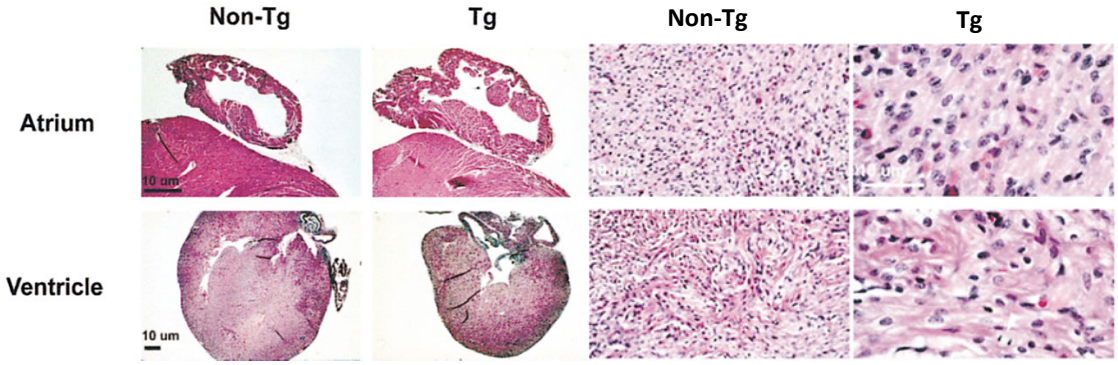

Figure 16: A, Atrial and ventricular hypertrophy in 5-months-old heterozygous cTnT-Myc-truncation mice. Representative cross-sections from paraffin-embedded hearts stained with hematoxylin and eosin. B, Cardiac TnT-Myc-truncation neonatal mice display myocellular disarray and degeneration similar to that found in patients with FHC (Tardiff et al, 1998).

Histopathological analysis of their hearts showed myocellular disarray and degeneration, but no fibrosis or myocyte hypertrophy (see Fig 16). The cTnT-truncation mice bred to homozygosis expressed twice the amount of truncated protein (5–10%) than their heterozygous littermates and died within 24 h of birth. This demonstrates an important relationship between the quantity of mutant protein expression and severity of disease presentation.

The Δ160E mutation in cTnT is caused by the in-frame deletion of three nucleotides encoding a glutamic acid at residue 160 (also reported as residue 163, as residues 160–163 are identical) and results in a severe form of HCM with several families exhibiting a high frequency of early sudden cardiac death (Pasquale et al, 2012; Watkins et al, 1995). Transgenic cTnT mouse line carrying 35% and 75% replacement of the endogenous cTnT with the Δ160E mutant form presented both mutation-driven changes in myofilament function: an increased ATPase activity and Ca^{2+} sensitivity (Chandra et al, 2005) and secondary Ca^{2+} handling alterations of cardiomyocytes. Both Δ160E-35% and Δ160E-70% exhibited dose-dependent shortened baseline sarcomere lengths and an impaired cardiomyocyte mechanics with significant decreases in resting intracellular calcium level, lower peak amplitude of the calcium transient and a decreased ability to remove calcium from the cytoplasm. Transgenic myocytes exhibit a decrease in calcium load and an impaired SERCA2a activity (Haim et al, 2007). Moreover, Δ160E hearts had significantly smaller ventricles, impaired cardiac contractility and relaxation, myocyte disarray and degeneration without fibrosis or myocyte hypertrophy. Δ160E mouse hearts exhibited extensive remodeling over time when compared to Non-Transgenic siblings. These results suggest that this mutation causes a progressive ventricular remodeling in mice that increases in severity with transgene dose and well replicate disease expression in patients.

A second cTnT transgenic mouse model was developed that expresses the missense mutation R92Q (Javadpour MM et al. 2003) within the TM-binding domain of cTnT, which is known to cause HCM in humans. Similar to the truncated cTnT model, R92Q mice had small left

ventricles, myocyte disarray, and lacked myocyte hypertrophy. In contrast, however, the R92Q hearts demonstrate significant interstitial fibrosis and up-regulation of hypertrophic markers. Studies with isolated cardiomyocytes from R92Q mice show increased basal sarcomere activation, impaired relaxation, and shorter sarcomere lengths. Measures of myocyte mechanics and Ca^{2+} kinetics in these mutants revealed a decreased rate of contraction, percent shortening, peak rate of relaxation, sarcoplasmic reticulum Ca^{2+} load, baseline Ca^{2+} levels, peak rate of Ca^{2+} rise and decline, Ca^{2+} peak amplitude, and SERCA/PLB ratios (Haim et al, 2007). Isolated working heart data are consistent, showing hypercontractility and diastolic dysfunction, both of which are common findings in patients with HCM. Moreover, both R92Q and Δ160E mice showed an increased frequency of arrhythmias (premature ventricular contractions) upon isoproterenol administration in the living animal as well as a slightly prolonged QRS and alterations in the atrio-ventricular conduction (Jimenez & Tardiff, 2011).

In contrast, patients who carry of the Arg-92-Leu (R92L) troponin T mutation often exhibit ventricular hypertrophy and eventually develop cardiac failure, while the frequency of sudden death is relatively low (Ertz-Berger et al, 2005).

A transgenic mouse expressing mutant R92L TnT was generated and tested: accordingly, mice carrying this mutation showed a significant degree of hypertrophy with a later onset (7-10 months) and increased myocyte size, as well as slowed cardiac relaxation and residual diastolic tension. Light microscopic analysis of ventricular sections from R92L adult mice revealed a broad range of histopathology consistent with that found in human mutant cTnT hearts, including myocyte disarray and degeneration, mild inflammatory cell infiltration, occasional hypertrophied cells, and minimal fibrosis. The R92L mice did not exhibit any significant induction of the hypertrophic gene program until late adulthood (10 months of age) (Guinto et al, 2009; Haim et al, 2007). Results from R92L myocytes showed mutation specific alterations in contraction and relaxation indexes at 2 months with improvements by 6 months. Alterations in Ca^{2+} kinetics remained consistent with mechanical data in which R92L exhibited severe diastolic impairments at the early time point that improved with increasing age.

In conclusion, although troponin T mutations are less common in patients, troponin T mutant mice are able to replicate all the different clinical phenotypes of human HCM: an early onset disease with scarce hypertrophy and fibrosis but high risk of arrhythmias (Δ160E), a restrictive-like disease presentation with fibrosis and severe diastolic dysfunction (R92Q), a later-onset presentation with hypertrophy, impaired relaxation but only slight increase of arrhythmogenic risk (R92L). Available troponin T mutant mice are therefore an optimal model to study the pathophysiology of human HCM and test the efficacy of specific therapies on subjects with different disease phenotypes.

REFERENCES:

Chandra M, Tschirgi ML, Tardiff JC (2005) Increase in tension-dependent ATP consumption induced by cardiac troponin T mutation. *American journal of physiology Heart and circulatory physiology* 289: H2112-2119.

Ertz-Berger BR, He H, Dowell C, Factor SM, Haim TE, Nunez S, Schwartz SD, Ingwall JS, Tardiff JC. Changes in the chemical and dynamic properties of cardiac troponin T cause discrete cardiomyopathies in transgenic mice. Proc Natl Acad Sci U S A. 2005 Dec 13;102(50):18219-24. Epub 2005 Dec 2.

Frey, N., Franz, W. M., Gloeckner, K., Degenhardt, M., Müller, M., Müller, O., et al. (2000). Transgenic rat hearts expressing a human cardiac troponin T deletion reveal diastolic dysfunction and ventricular arrhythmias. Cardiovascular Research, 47, 254– 264.

Geisterfer-Lowrance, A. A. T., Kass, S., Tanigawa, G., Vosberg, H.-P., McKenna, W., Seidman, C. E., et al. (1990). A molecular basis for familial hypertrophic cardiomyopathy: A β cardiac myosin heavy chain gene missense mutation. Cell, 62, 999–1006.

Guinto PJ, Haim TE, Dowell-Martino CC, Sibinga N, Tardiff JC (2009) Temporal and mutation-specific alterations in Ca2+ homeostasis differentially determine the progression of cTnT-related cardiomyopathies in murine models. *American journal of physiology Heart and circulatory physiology* 297: H614-626.

Haim TE, Dowell C, Diamanti T, Scheuer J, Tardiff JC. Independent FHC-related cardiac troponin T mutations exhibit specific alterations in myocellular contractility and calcium kinetics. J Mol Cell Cardiol. 2007 Jun;42(6):1098-110. Epub 2007 Mar 31.

Javadpour, M. M., Tardiff, J. C., Pinz, I., & Ingwall, J. S. (2003).Decreased energetics in murine hearts bearing the R92Q mutation in cardiac troponin T. Journal of Clinical Investigation, 112, 768– 775.

Jimenez J, Tardiff JC (2011) Abnormal heart rate regulation in murine hearts with familial hypertrophic cardiomyopathy-related cardiac troponin T mutations. *American journal of physiology Heart and circulatory physiology* 300: H627-635.

Luedde, M., Flögel, U., Knorr, M., Grundt, C., Hippe, H.-J., Brors, B., et al. (2009).Decreased contractility due to energy deprivation in a transgenic rat model of hypertrophic cardiomyopathy. Journal of Molecular Medicine, 87, 411–422.

Moolman, J. C., Corfield, V. A., Posen, B., Ngumbela, K., Seidman, C., Brink, P. A., et al. (1997). Sudden death due to troponin T mutations. Journal of the American College of Cardiology, 29, 549–555.

Pasquale F, Syrris P, Kaski JP, Mogensen J, McKenna WJ, Elliott P (2012) Long-term outcomes in hypertrophic cardiomyopathy caused by mutations in the cardiac troponin T gene. *Circulation Cardiovascular genetics* 5: 10-17.

Tardiff, J. C., Factor, S. M., Tompkins, B. D., Hewett, T. E., Palmer, B. M., Moore, R. L., et al. (1998). A truncated cardiac troponin T molecule in transgenic mice suggests multiple cellular mechanisms for familial hypertrophic cardiomyopathy. Journal of Clinical Investigation, 101, 2800–2811.

Tardiff JC, Hewett TE, Palmer BM, Olsson C, Factor SM, Moore RL, Robbins J, Leinwand LA (1999) Cardiac troponin T mutations result in allele-specific phenotypes in a mouse model for hypertrophic cardiomyopathy. *The Journal of clinical investigation* 104: 469-481.

Thierfelder, L., Watkins, H., MacRae, C., Lamas, R., McKenna,W., Vosberg, H.-P., et al. (1994). α-Tropomyosin and cardiac troponin T mutations cause familial hypertrophic cardiomyopathy: A disease of the sarcomere. Cell, 77, 701–712.

Watkins, H., Conner, D., Thierfelder, L., Jarcho, J. A., MacRae, C., McKenna, W. J., et al. (1995). Mutations in the cardiac myosin binding protein-C gene on chromosome 11 cause familial hypertrophic cardiomyopathy. Nature Genetics, 11, 434–437.

Watkins, H., McKenna, W. J., Thierfelder, L., Suk, H. J., Anan, R., O'Donoghue, A., et al. (1995). Mutations in the genes for cardiac troponin T and α-tropomyosin in hypertrophic cardiomyopathy. New England Journal of Medicine, 332, 1058–1064.

Watkins, H., Rosenzweig, A., Hwang, D. S., Levi, T., McKenna, W., Seidman, C. E., et al. (1992).Characteristics and prognostic implications of myosin missense mutations in familial hypertrophic cardiomyopathy. New England Journal of Medicine, 326, 1108–1114.

1.5.1 Current HCM therapies

In spite of considerable advances in understanding HCM genetics and pathophysiology, current pharmacological treatment of patients with HCM has remained largely empiric and unchanged over the past two decades. The primary emphasis in the management of patients with HCM has been on the risk of sudden cardiac death (SCD), as HCM is a common cause of SCD in the young (Maron, B. J. et al. 2009). Prudent use of automatic internal defibrillator/cardioverters (AICDs) has provided the physicians with an effective option for prevention of SCD in the high-risk patients (Maron, B. J. et al. 2000; Maron, B. J. et al. 2007). However, implantation of an AICD is associated with a high risk of unfavorable complications (e.g. infections, inappropriate discharges) and does not influence the underlying cardiac pathology (namely, myocyte hypertrophy, disarray, and interstitial fibrosis). Likewise, catheter based septal ablation and surgical myectomy, though effective in reducing the left ventricular outflow tract (LVOT) obstruction and alleviating symptoms (functional improvement), do not substantially alleviate the underlying arrhythmogenic substrate (Maron, B. J. et al. 2004; McLeod, C. J. et al. 2007; Ommen S et al. 2005;Seggewiss, H. et al., 2001; Woo A et al. 2005). In contrast, the tissue scar at the site of percutaneous septal ablation has the potential to increase the risk of ventricular arrhythmias (Sorajja, P et al. 2008 ; Talreja, D. R et al. 2004).

Current pharmacological treatment of human HCM, while is effective for symptomatic improvement, has not been established to prevent, attenuate, or reverse cardiac hypertrophy in humans with HCM or even impact the prognosis (Marian, A. J. 2008).The most commonly used pharmacological agents are the β-blockers, which are the mainstay of therapy and the first choice in the absence of a contraindication. The proposed mechanisms of effects include improved ventricular relaxation and increased diastolic filling time and, hence, improved left ventricular end diastolic pressure as well as perfusion. In addition, treatment with β-blockers is expected to reduce ventricular and supra-ventricular arrhythmias. An observational retrospective study in a mixed pediatrics HCM population suggests potential beneficial effects of high-doses β-blockers on total survival (Ostman-Smith, I. et al.1999). Otherwise, the benefits of β-blockers on mortality and the risk of SCD in patients with HCM and their impact on prevention or reversal of cardiac hypertrophy in HCM remain to be established.

Dihydropyridine calcium channel blockers, such as nifedipine are avoided in patients with HCM, because of the concern about the vasodilatory effects inducing hypotension, syncope, and possibly death. Overall, the clinical utility of Ca^{2+} channel blockers in treatment of patients with HCM is hindered by the risk of hypotension and syncope, at rest or particularly during exercise.

Disopyramide, a class I anti-arrhythmic drug, is used in conjunction with β-blockers to attenuate LVOT obstruction and improve symptoms (Sherrid M. V et al. 2005). The beneficial effects of disopyramide are largely due to its negative inotropic effects. Hence, it is most effective in patients with LVOT obstruction. Disopyramide does not reverse or attenuate cardiac hypertrophy in patients with HCM.

In conjunction with the implementation of a DNA-based diagnosis, pharmacological treatment/prevention of HCM is also likely to evolve and become largely individualized (mutation-specific). The diversity of the responsible mechanisms perhaps is best illustrated for the Ca^{2+} sensitivity of the myofilament, which varies according to the causal genes and is context dependent. For example, Ca^{2+} desensitizers would be expected to be beneficial in a large subset of HCM caused by mutations that increase the Ca^{2+}sensitivity of myofibrillar force generation. In contrast, such agents could potentially be harmful in a small subset that is caused by mutations that decrease the Ca^{2+} sensitivity of the myofibrils. Thus, one potential future

approach would be to individualize the therapy based on the specific mechanisms involved in the pathogenesis of the phenotype.
The opposite end of the spectrum of approach to treatment of HCM is to broaden the application of a specific therapy to various subtypes of HCM by targeting mechanisms that are involved in the "common" pathogenesis of cardiac hypertrophy in HCM as well as other pathological hypertrophy (Takimoto, E. 2007; Tirouvanziam, R. 2006). An example of such common mechanism is increased oxidative stress and pharmacological interventions targeted to reduce oxidative stress have been used successfully to reverse cardiac hypertrophy and fibrosis in animal models of HCM as well as in other hypertrophic states (Lombardi, R et al.2009). Specifically, potential beneficial effects of N-acetylcysteine (NAC) have been shown on reversal or prevention of hypertrophy and fibrosis in HCM. Very promising results have been obtained with NAC, which through multiple thiol-responsive mechanisms completely reversed established cardiac hypertrophy and fibrosis in three independent studies. Angiotensin II receptor blocker losartan, 3-hydroxy-3-methyglutarylcoenzyme A reductase inhibitors, mineralocorticoid receptor blocker spironolactone, statins (simvastatin and atorvastatin) are other molecules that have shown positive effects in animal models of HCM.

Table 2: Experimental pharmacological agents in treatment of human hypertrophic cardiomyopathy

Pharmacological agent	Mechanism of anti-hypertophic effects	Favorable effects	Unfavorable effects
Losartan	Blockade angiotensin II mediated pro-hypertrophic and pro-fibrotic signaling	Regression of fibrosis	No effects on cardiac hypertrophy in two small studies
	Reduces oxidative stress		Potential for hypotension and syncope
Statins	Inhibition of Rho-A and Rac1 small GTPases	Regression of hypertrophy and fibrosis	No effect on cardiac hypertrophy in two small pilot studies
	Reduces oxidative stress		Liver toxicity
			Skeletal myopathy
Spironolactone	Blockade of PKD	Regression of fibrosis	Hyperkalemia
	Blockade of TGF-β		Possible hypotension
	Reduces oxidative stress		
Calcineurin inhibitors	Inhibition of Calcineurin-NFATc hypertrophic pathway	Established anti-hypertrophic effect	Deterioration of cardiac structure and function in a mouse model of HCM
N-acetylcysteine	Reduces oxidative stress	No major side effects	Unpleasant taste for some unless mixed with juice/soda
	Thio-modifications of proteins and signaling molecules	Reverses established hypertrophy and fibrosis	

However, alterations of intracellular Ca^{2+}-handling are probably the earliest and most important changes leading to hypertrophy development and diastolic dysfunction and all other changes might be secondary to those. With the exception of $I_{Ca\text{-}L}$, no potential therapeutic targets directly affecting HCM-related E-C coupling alterations have been identified. Consequently, one major pathogenetic mechanism in HCM still remains devoid of an effective therapeutic measure. Moreover, none of the aforementioned drugs is specific for reverting changes occurring in HCM heart and bear significant undesired effects that may impact their effectiveness in patients. Therefore, the need for an effective and specific drug is still unmet.

1.5.2 Potential significance of Late Sodium Current ($I_{Na}L$) and Ranolazine in HCM

Recent studies pointed out the leading role of changes in Late Sodium Current ($I_{Na}L$) in different cardiac diseases. The classical role of voltage-dependent sodium channels in myocardium is to allow fast impulse propagation and to initiate action potential with a large and short-lasting inward current; however, it's been known for many years that a very small fraction of Na^+ current persists during the plateau phase of action potential, the "late" or "persistent" Na^+ current. This gave rise to a large number of studies in different models of cardiovascular pathology all pointing out that enhancement of Late-Na^+ current may be a consequence of different acquired cardiac diseases and may contribute to their pathogenesis: although a very small Na^+ current with slow inactivation is present in normal myocytes, abnormally large $I_{Na}L$ was found in cells from hearts of patients affected by end stage heart failure and in animal models of heart failure and post-myocardial infarction remodelling (Maltsev VA et al. 1998). Channels contributing to the transient peak and to the late persistent components of Na^+ current are exactly the same (NaV1.5). Therefore, rather than a varied expression of different I_{Na} channels isoforms, acquired diseases are thought to directly alter NaV1.5 channel structure (Valdivia CR et al. 2002). Hypoxia, oxygen free radicals (H_2O_2), ischemic metabolites (like oxidized lipids) and nitric oxide (NO) have been shown to rapidly and directly increase $I_{Na}L$ in experimental conditions (Xie LH et al. 2009), suggesting that peroxydation or nitrosylation of channels may directly alter their inactivation kinetics. In heart failure and myocardial infarction, due to reduced perfusion or inefficient metabolism, myocardial oxidative state is increased, possibly explaining the observed changes in $I_{Na}L$. Moreover, increased Ca^{2+}-Calmodulin and calmodulin kinase II (CaMKII) activity, both common features of myocardial remodelling, have been shown to increase $I_{Na}L$ (Wagner S et al. 2006). Whatever the reason of $I_{Na}L$ enhancement, this condition is always associated with a prolonged repolarisation causing a remarkable increase in AP duration and temporal variability: this leads to reduced repolarisation reserve and therefore increased incidence of EADs and potentially fatal arrhythmias (Antzelevitch C. 2006). Previously mentioned cardiac conditions are all characterized by increased susceptibility to perturbations of repolarisation (such as drugs acting on K^+ currents or electrolyte abnormalities) and overall increased risk of arrhythmias.

The increased Sodium influx not only bears the aforementioned electrophysiological consequences, but can directly alter intracellular calcium homeostasis. Although $I_{Na}L$ amplitude, even when pathologically increased, is less than 1/30 of peak I_{Na}, it lasts for a very long time (15-20 times the peak current): a substantial increase in $I_{Na}L$ may bring 50% more sodium into the cell for each beat, leading to a sustained increase in cytosolic Na^+ concentration $[Na]_i$, that has been found in failing myocytes (Noble D. 2006). Intracellular Na^+ directly regulates the function of sarcolemmal sodium calcium exchanger (NCX), the main responsible for the maintenance of intracellular calcium balance: increased $[Na]_i$ causes a reduced NCX function during diastole leading to insufficient Ca^{2+} extrusion; moreover, increased reverse mode activity of NCX during systole would bring more Ca^{2+} into the cell contributing to cellular calcium overload (Zaza A, 2008). Calcium overload has multiple effects on myocardial function: Ca^{2+} overloaded SR increases the probability of spontaneous calcium releases trough the ryanodine receptors (RyR) during diastole, possibly leading to arrhythmogenic delayed after depolarisations (DADs). Increased cytosolic calcium may also directly reduce the function of Ca^{2+}-dependent K^+ repolarizing currents, contributing to APD prolongation. Calcium overload is also associated with SR-release rate-dependent alterations (alternans) that contribute to APD alternans and inhomogeneity and thus to the development of reentry circuits. Chronically increased $[Ca^{2+}]_i$ leads to activation of numerous intracellular pathways: increased activity of

PKC, CaMKII and calcineurin not only acutely affects Ca^{2+} homeostasis and membrane currents but may also activate transcriptional factors ultimately leading to hypertrophic response. Concomitant increase of intracellular Na^+ and Ca^{2+} may alter mitochondrial function leading to altered ATP production: given the bigger ATP consumption caused by the increased function of Na^+K^+ATPase (to extrude excessive Na^+) and SERCA pump (to store excessive Ca^{2+}), chronic $I_{Na}L$ augmentation may lead to significant metabolic impairment. Moreover, increased intracellular Na^+ impairs the function of sarcolemmal Na^+/H^+ exchanger, thus lowering cytosolic pH: this last effect may also contribute to metabolic impairment and contractile dysfunction.
Altered intracellular Ca^{2+} handling leading to sustained high levels of intracellular calcium during diastole is crucial for the determining of impaired relaxation in HCM. Increased $I_{Na}L$ may significantly contribute to HCM-related diastolic dysfunction with different mechanisms: 1) Increased action potential duration renders calcium release longer and prolongs contraction: inhomogeneous prolongation of APD will increase variability of twitch duration in the ventricle, leading to uncoordinated relaxation. 2) Increased diastolic $[Ca^{2+}]_I$ leads to slower and incomplete myofilament inactivation and relaxation; this phenomenon is extremely more pronounced at high pacing rates, due to a more marked cytosolic Na^+ and Ca^{2+} overload. 3) Spontaneous Ca^{2+} releases induced by overload will generate diastolic after-contractions that will impair relaxation (Undrovinas NA et al. 2010)
However, the role of $I_{Na}L$ in familial HCM development and pathogenesis has never been investigated, neither in patients nor in animal models of HCM.
To summarize, $I_{Na}L$ augmentation not only alters membrane function but also has multiple consequences on Ca^{2+} handling, mechanics, metabolism and cell signalling and may significantly contribute to the pathogenesis of hypertrophic cardiomyopathy.
Given the important role of enhanced $I_{Na}L$ in cardiac diseases and the relatively insignificant role of late current in normal myocardial physiology, a selective blocker of $I_{Na}L$ would represent a specific and relatively safe therapeutic option for the treatment of diastolic dysfunction and Ca^{2+}-related arrhythmias in cardiac conditions including HCM.
({+/-})-N-(2,6-dimethil-phenil)-(4[2-hydroxy-3-(2-methoxyphenoxy)propyl]-1-piperazine, a compound more commonly known as Ranolazine, developed in the 90s as a cardiac specific partial fatty acid oxidation inhibitor, was first experimented as a possible antianginal compound due to its ability to shift cardiac metabolism from fatty acid to glucose consumption, that requires less O_2 to produce ATP (McCormack JG Circulation 1996): this metabolic modulatory effect of ranolazine was thought to be responsible for its clear protective effect on myocardial tissue subjected to ischemia/reperfusion damage. Ranolazine was found effective in reducing symptoms in two clinical trials on chronic stable angina patients (MARISA and CARISA). Its electrophysiological effects were discovered in 2004 (Antzelevitch and Belardinelli, 2004**):** ranolazine exerts a potent inhibition of $I_{Na}L$, with small or no effect on peak I_{Na}, within the therapeutic concentration range. In a large scale trial on non ST-elevation myocardial infarction patients (MERLIN-TIMI 36), ranolazine significantly reduced the incidence of ventricular tachycardia and atrial arrhythmias after the first event (Scirica et al, 2007). In models of experimentally increased $I_{Na}L$ (with the administration of ATX-II toxin) ranolazine reduced APD and completely abolished the increased propensity to develop arrhythmias. In patients affected by type 3 long-QT syndrome, ranolazine shortened QTc reducing susceptibility to arrhythmias; in all models of myocardial ischemia, ranolazine reduced ventricular arrhythmic vulnerability. Antiarrhythmic effect of the drug seems to be essentially due to $I_{Na}L$ block, which counteracts the multiple deleterious effects of $I_{Na}L$ augmentation we have discussed above (Shram G et al, 2004). More importantly, this almost selective effect makes ranolazine relatively

ineffective on normal, undiseased, myocardium, where $I_{Na}L$ is not increased, making this drug extremely safe.
$I_{Na}L$ block may not only help reducing cell Ca^{2+} overload secondary to elevation of intracellular Na^{+} (Wasserstrom JA. 2009). Ranolazine effectively prevented spontaneous calcium releases and after-contractions in myocytes from heart failure models (Undrovinas et al 2006, Song et al 2006) and significantly reduced the incidence of DADs in a Long QT 3 model (Lindegger N et al. JMCC 2009). As discussed above, by counteracting the indirect effect of $I_{Na}L$ augmentation on Ca^{2+} handling, ranolazine should be able to reduce contraction duration, speed up relaxation and reduce diastolic tension (Hwang H et al 2009). Accordingly, ranolazine was shown to increase wall motion and speed up diastolic filling rate in ischemic myocardium in patients without affecting systolic shortening (Hayashida, 1994); in a dog model of heart failure ranolazine shortened contraction without affecting peak exerted force. Similar results were obtained from specimens taken from end-stage heart failure patients: ranolazine reduced diastolic tension at higher stimulation frequencies without decreasing twitch force.
Ranolazine seems to reduce diastolic calcium without affecting systolic Ca2+-release: in models of heart failure, this drug may even improve systolic contraction because the reduced Ca^{2+} leakage from the SR would preserve the integrity of stores in spite of a global reduction of cell Ca^{2+} content (Sossalla, 2008). No evidence exists about a possible role of ranolazine in ameliorating diastolic function in familial HCM.

REFERENCES:

Antzelevitch C, Belardinelli L. The role of sodium channel current in modulating transmural dispersion of repolarization and arrhythmogenesis.J Cardiovasc Electrophysiol. 2006 May;17 Suppl 1:S79-S85. Review.

Hayashida W, van Eyll C, Rousseau MF, Pouleur H.Effects of ranolazine on left ventricular regional diastolic function in patients with ischemic heart disease.Cardiovasc Drugs Ther. 1994 Oct;8(5):741-7.

Hwang H, Arcidi JM Jr, Hale SL, Simkhovich BZ, Belardinelli L, Dhalla AK, Shryock JC, Kloner RA. Ranolazine as a cardioplegia additive improves recovery of diastolic function in isolated rat hearts.Circulation. 2009 Sep 15;120(11 Suppl):S16-21.

Lindegger N, Hagen BM, Marks AR, Lederer WJ, Kass RS.Diastolic transient inward current in long QT syndrome type 3 is caused by Ca2+ overload and inhibited by ranolazine.J Mol Cell Cardiol. 2009 Aug;47(2):326-34. Epub 2009 Apr 14.

Lombardi, R., Rodriguez, G., Chen, S. N., Ripplinger, C. M., Li, W., Chen, J., et al. (2009). Resolution of established cardiac hypertrophy and fibrosis and prevention of systolic dysfunction in a transgenic rabbit model of human cardiomyopathy through thiol-sensitive mechanisms. Circulation, 119, 1398–1407.

Maltsev VA, Sabbah HN, Higgins RS, Silverman N, Lesch M, Undrovinas AI.Novel, ultraslow inactivating sodium current in human ventricular cardiomyocytes.Circulation. 1998 Dec 8;98(23):2545-52.

Marian, A. J. (2008). Hypertrophic Cardiomyopathy.In R. E. Rackel & E. T. Bope (Eds.), Conn's current therapy (pp. 333–335). Philadelphia: Saunders-Elsevier.

Maron, B. J., Dearani, J. A., Ommen, S. R., Maron, M. S., Schaff, H. V., Gersh, B. J., et al. (2004). The case for surgery in obstructive hypertrophic cardiomyopathy. Journal of the American College ofCardiology, 44, 2044–2053.

Maron, B. J., Doerer, J. J., Haas, T. S., Tierney, D. M., &Mueller, F. O. (2009). Sudden deaths in young competitive athletes: analysis of 1866 deaths in the United States, 1980–2006. Circulation, 119, 1085–1092.

Maron, B. J., Shen, W. K., Link, M. S., Epstein, A. E., Almquist, A. K., Daubert, J. P., et al. (2000). Efficacy of implantable cardioverter-defibrillators for the prevention of sudden death in patients with hypertrophic cardiomyopathy. New England Journalof Medicine, 342, 365–373.

Maron, B. J., Spirito, P., Shen, W. K., Haas, T. S., Formisano, F., Link, M. S., et al. (2007).Implantable cardioverter-defibrillators and prevention of sudden cardiac death in hypertrophic cardiomyopathy.Journal of the American Medical Association, 298, 405–412.

McCormack JG, Barr RL, Wolff AA, Lopaschuk GD. Ranolazine stimulates glucose oxidation in normoxic, ischemic, and reperfused ischemic rat hearts.Circulation. 1996 Jan 1;93(1):135-42.

McLeod, C. J., Ommen, S. R., Ackerman, M. J., Weivoda, P. L., Shen, W. K., Dearani, J. A., et al. (2007). Surgical septal myectomy decreases the risk for appropriate implantable cardioverter defibrillator discharge in obstructive hypertrophic cardiomyopathy. European Heart Journal, 28, 2583–2588.

Noble D, Noble PJ. Late sodium current in the pathophysiology of cardiovascular disease: consequences of sodium-calcium overload.

Ommen, S. R., Maron, B. J., Olivotto, I., Maron, M. S., Cecchi, F., Betocchi, S., et al. (2005). Long-term effects of surgical septalmyectomy on survival in patients with obstructive hypertrophiccardiomyopathy. Journal of the American College of Cardiology,46, 470–476.

Ostman-Smith, I., Wettrell, G., &Riesenfeld, T. (1999). A cohort study of childhood hypertrophic cardiomyopathy: improved survival following high-dose beta-adrenoceptor antagonist treatment. Journal of the American College of Cardiology, 34, 1813–1822.
Seggewiss, H. (2001). Current status of alcohol septal ablation for patients with hypertrophic cardiomyopathy. Current CardiologyReports, 3, 160–166.

Scirica BM, Morrow DA, Hod H, Murphy SA, Belardinelli L, Hedgepeth CM, Molhoek P, Verheugt FW, Gersh BJ, McCabe CH, Braunwald E.

Sherrid, M. V., Barac, I., McKenna, W. J., Elliott, P. M., Dickie, S., Chojnowska, L., et al. (2005).Multicenter study of the efficacy and safety of disopyramide in obstructive hypertrophic cardiomyopathy. Journal of the American College of Cardiology,45, 1251–1258.

Song Y, Shryock JC, Wagner S, Maier LS, Belardinelli L. Blocking late sodium current reduces hydrogen peroxide-induced arrhythmogenic activity and contractile dysfunction.J Pharmacol Exp Ther. 2006 Jul;318(1):214-22. Epub 2006 Mar 24.

Sorajja, P., Valeti, U., Nishimura, R. A., Ommen, S. R., Rihal, C. S., Gersh, B. J., et al. (2008). Outcome of alcohol septal ablationfor obstructive hypertrophic cardiomyopathy. Circulation, 118, 131–139.

Sossalla S, Kallmeyer B, Wagner S, Mazur M, Maurer U, Toischer K, Schmitto JD, Seipelt R, Schöndube FA, Hasenfuss G, Belardinelli L, Maier LS. Altered Na(+) currents in atrial fibrillation effects of ranolazine on arrhythmias and contractility in human atrial myocardium.

Sossalla S, Wagner S, Rasenack EC, Ruff H, Weber SL, Schöndube FA, Tirilomis T, Tenderich G, Hasenfuss G, Belardinelli L, Maier LS.Ranolazine improves diastolic dysfunction in isolated myocardium from failing human hearts--role of late sodium current and intracellular ion accumulation.J Mol Cell Cardiol. 2008 Jul;45(1):32-43. Epub 2008 Mar 14.

Takimoto, E., & Kass, D. A. (2007).Role of oxidative stress in cardiac hypertrophy and remodeling.Hypertension, 49, 241–248.

Talreja, D. R., Nishimura, R. A., Edwards, W. D., Valeti, U. S., Ommen, S. R., Tajik, A. J., et al. (2004). Alcohol septal ablation versus surgical septal myectomy: comparison of effects on atrioventricular conduction tissue. Journal of the AmericanCollege of Cardiology, 44, 2329–2332.

Tirouvanziam, R., Conrad, C. K., Bottiglieri, T., Herzenberg, L. A., Moss, R. B., & Herzenberg, L. A. (2006). High-dose oralN-acetylcysteine, a glutathione prodrug, modulates inflammationin cystic fibrosis. Proceedings of the National Academy of Sciences of the United States of America, 103, 4628–4633.

Undrovinas AI, Belardinelli L, Undrovinas NA, Sabbah HN. Ranolazine improves abnormal repolarization and contraction in left ventricular myocytes of dogs with heart failure by inhibiting late sodium current.J Cardiovasc Electrophysiol. 2006 May;17 Suppl 1:S169-S177.

Undrovinas NA, Maltsev VA, Belardinelli L, Sabbah HN, Undrovinas A Late sodium current contributes to diastolic cell Ca2+ accumulation in chronic heart failure. J Physiol Sci. 2010 Jul;60(4):245-57. Epub 2010 May 19.

Valdivia CR, Nagatomo T, Makielski JC.Late Na currents affected by alpha subunit isoform and beta1 subunit co-expression in HEK293 cells.J Mol Cell Cardiol. 2002 Aug;34(8):1029-39.

Wagner S, Dybkova N, Rasenack EC, Jacobshagen C, Fabritz L, Kirchhof P, Maier SK, Zhang T, Hasenfuss G, Brown JH, Bers DM, Maier LS.Ca2+/calmodulin-dependent protein kinase II regulates cardiac Na+ channels. J Clin Invest. 2006 Dec;116(12):3127-38. Epub 2006 Nov 22.

Wasserstrom JA, Sharma R, O'Toole MJ, Zheng J, Kelly JE, Shryock J, Belardinelli L, Aistrup GL. Ranolazine antagonizes the effects of increased late sodium current on intracellular calcium cycling in rat isolated intact heart. J Pharmacol Exp Ther. 2009 Nov;331(2):382-91. Epub 2009 Aug 12.

Woo, A., Williams, W. G., Choi, R., Wigle, E. D., Rozenblyum, E., Fedwick, K., et al. (2005). Clinical and echocardiographic determinants of long-term survival after surgical myectomy in obstructive hypertrophic cardiomyopathy. Circulation, 111, 2033–2041.

Xie LH, Chen F, Karagueuzian HS, Weiss JN.Oxidative-stress-induced afterdepolarizations and calmodulin kinase II signaling. Circ Res. 2009 Jan 2;104(1):79-86. Epub 2008 Nov 26.

Zaza A, Belardinelli L, Shryock JC. Pathophysiology and pharmacology of the cardiac "late sodium current.". Pharmacol Ther. 2008 Sep;119(3):326-39. Epub 2008 Jul 1. Review.

Chapter 2: METHODS
"Old" and novel techniques to study cardiac function

The experiments described in this thesis investigate the structural, mechanical and electrophysiological properties of intact cardiomyocytes preparations from rodent hearts. A detailed description of the experimental protocols can be found in the results sections. In the present chapter we provide a detailed overview of all the experimental preparations employed in the study and the techniques used to achieve experimental results, particularly focusing on the novel techniques that were developed or modified and fine-tuned during the study. First we describe transgenic mouse model and the techniques employed to isolate viable intact myocytes from ventricles of mice (paragraph 2.1). Then we describe the methods employed to characterize the electrophysiological properties of cardiomyocytes (paragraph 2.2). Patch clamp, electrophysiological measurements and Ca^{2+} transients recordings were performed. Ca^{2+} indicators fluorescence was recorded with a PMT or a fast sensitive camera, the latter allowed us to identify localized intracellular calcium changes. Imaging techniques were employed (paragraph 2.3) to describe the morphological structure of t-tubular network in myocytes and intact tissue. RT-PCR was performed for the study and quantification of mRNA expression of membrane proteins (paragraph 2.5). Finally echocardiography and Cardiac MRI were performed on living mice. Set-up engineering and assembling as well as software programming was mostly made in our lab.

2.1 Transgenic mouse model

2.1.1 Animal model, genotyping and assessment of gross heart morphology

R92Q and E163R transgenic constructs were generated in Jil Tardiff lab (Albert Einstein Institute, New York, USA) via pronuclear injection as previously described (Tardiff et al, 1998). In brief, a *c-myc* tag engineered onto the N-terminal end of the construct is used to identify the transgene via PCR (forward primer: TCCTCTTCAGAGATGAGCTTT; reverse primer: ACCTAGAGGGAAAGTGTCTT). The mutations were introduced via the Quiczk Change Site Directed Mutagenesis kit (Stratagene). Transgenic lines expressing a mid-level of transgenic protein were backcrossed into C57Bl/6 background for at least 7 generations until a stable expression of the transgene was reached (about 50% of total cTnT). Two male R92Q and E163R progenitors were transferred in April 2011 from the Albert Einstein Institute to our Animal facility (CeSaL) in Florence. The progenitors were inbreeded with C57Bl/6 females and the colony was amplified for many generations. At four- to six-weeks of age mice were genotyped and at 6 to 8 months were used for the experiments. Sibling non transgenic (WT) mice were used to provide controls (paired for each set of experiments). Experimental protocols and animal maintenance were performed according to local ethical regulations for animal breeding and use.

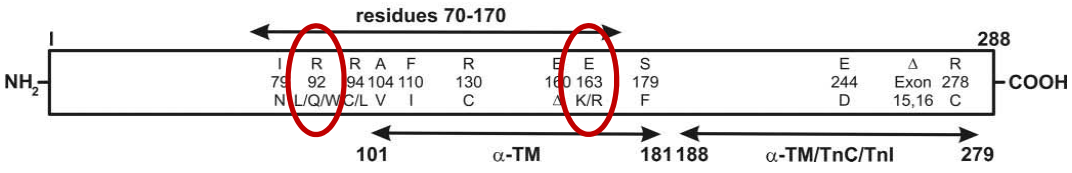

Figure 17 : Structure of cTnT and mutations associated with HCM.
Red circle identified R92Q and E163R mutation.

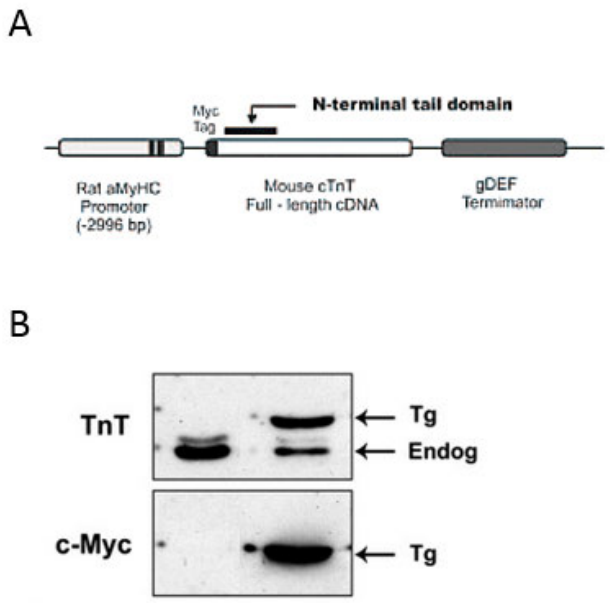

Figure 18: Characterization of mutant mice. (A) Scheme of the transgenic gene (modified from Briar R. Ertz-Berger et al, 2005). (B) Western blot analysis of heart homogenates and Non-Tg mice probed with antibodies, as indicated. TnT upper band represents c-myc tagged transgenic protein and lower band represents endogenous cTnT (modified from Moore et al, 2013).

Gross heart morphology and chambers dimensions, were quantified as heart /body weight, ventricle/body weight and atria/body weight ratios. Mouse body weight was assessed right before the sacrifice. Freshly isolated hearts from 6 month old mice were weighted right after perfusion in the Isenberg buffer (see the protocol below). Atria were dissected from the heart, maintaining the atria-ventricular ring attached to the ventricles. Then also right ventricles was separated from septum and left ventricles. Heart masses calculated with this method and normalized on the animal body weight provide numbers that are comparable to those obtained from hearts that were treated with fixatives (Moore et al, 2013).

2.1.2 Dissection of ventricular and atrial trabeculae

Left atrial and right ventricular trabeculae were selected because of their similarity with fascicles in the cardiac wall (Hanley et al. 1999, Baudino et al. 2006). Twelve month-old mice were heparinized (5000 UI/ml) and anesthetized by inhaled isoflurane. The heart was rapidly excised, perfused retrogradely via the proximal aorta with a modified Krebs-Henseleit solution (KH solution) and placed in a dissection dish beneath a binocular microscope (fig. 20). KH solution contained (mM): 120 NaCl, 5 KCl, 2 MgSO4, 1.2 NaH2PO4, 20 NaHCO3, 0.50 Ca^{2+} and 10 glucose, pH 7.4 equilibrated with 95%O_2 5%CO_2.
During retroperfusion and dissection the potassium concentration in the KH solution was raised to 15 mmol/L to stop spontaneous beating of the heart. BDM 20 mmol/L was also added to the solution to minimize contractures following cutting damages. Dissection was performed as

shown in figure 19. Free running atrial trabeculae were dissected from the left atrium as shown in figure 20.
Thin, unbranched, uniform trabeculae, running between the free wall of the right ventricle and the atrioventricular ring, were selected and carefully dissected by cutting through the atrioventricular ring on one end and removing a portion of the right ventricular wall on the other end (fig. 20).

Figure 19: Dissection dish. Diagonal (A), top (B) and lateral (C) view of the dissection dish. It consists of i) an internal chamber, with an elevated bottom made of Sylgard (Sylgard® 170 Silicone Elastomer) to pin the tissue during dissection; and ii) an external chamber (with lower bottom level) that works as a reservoir for solution overflow from the internal chamber. A metal cannula connected with the perfusion system comes out from the Sylgard bottom and has to be gently inserted into the aorta for coronary retro-perfusion. An external ring mounted around the internal chamber works as light support and allows tissue trans-illumination, that helps some phases of dissection (e.g. identification of small trabeculae under the atrio-ventricular ring).The dissection dish was designed by P.de Tombe and H.D.J. ter Keurs.

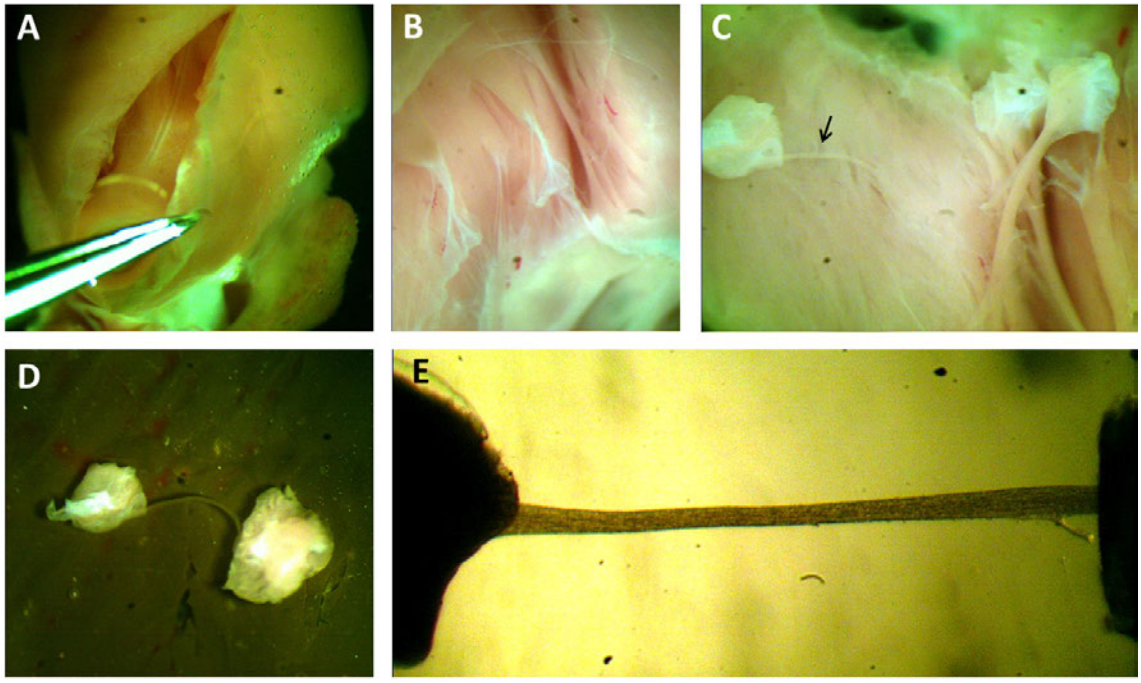

Figure 20: Dissection of right ventricular trabeculae. The free wall of the right ventricle is gently separated from the ventricular septum (A) and thin, unbranched, uniform trabeculae, running between the free wall of the right ventricle and the atrioventricular ring (B &C), are selected (e.g. trabecula indicated by the arrow) and carefully dissected by cutting through the atrioventricular ring on one end and removing a portion of the right ventricular wall on the other end. Dissected trabecula unloaded (D) and mounted (E).

The composition of modified Krebs-Henseleit solution was:

Table 3. *The composition of KH solution*

	Dissection solution	Experimental solution
	mM	**mM**
NaCl	**120**	**120**
KCl	**15**	**5**
$MgSO_4$	**2**	**2**
NaH_2PO_4	**1.2**	**1.2**
$NaHCO_3$	**20**	**20**
Glucose	**10**	**10**
$CaCl_2$	**1.5**	**2**
BDM	**20**	**-**
pH 7.4 with 95% O_2	5% CO_2	

2.1.3 Isolation of single cardiomyocytes from mouse hearts

Ventricular cardiomyocytes were isolated by enzymatic dissociation as previously described (Egorova et al, 2005). Briefly, the animal was heparinized (5,000 U/kg, i.p.) and deeply anesthetized with Isoflurane. The excised heart was immediately bathed in cell isolation solution and perfused retrogradely via the proximal aorta (Figure 21 A). Cell isolation solution contained 120 NaCl, 1.2 $MgCl_2$, 10 KCl, 1.2 KH_2PO_4, 10 glucose, 10 Hepes and 20 taurine, 5 pyruvate, oxygenated with O_2 (Table 3); pH 7.2 (adjusted with NaOH). The coronary arteries were then perfused with this solution at 37°C for 3-4 min at a constant flow of 3 mL/min. The solution was then switched to a recirculating enzyme solution made of the same buffer with the addition of 0.1 mg/mL Liberase (Liberase TM for mouse, Roche Applied Sciences). After 8-9 min, the ventricles were excised and cut into small pieces in buffer solution supplemented with 1 mg/ml BSA. (Figure 21 B). Gentle stirring facilitated further dissociation of the myocytes. The cell suspension (Figure 21 C) was let to settle and the cell pellet (~1 ml) was resuspended in Tyrode buffer (Table 5) supplemented with 0.05 mM $CaCl_2$ and 1 mg/ml BSA. Calcium concentration was gradually raised to 1.0 mM.

Table 4. *The composition of Isenberg buffer*

	mM
NaCl	**120**
KCl	**10**
KH_2PO_4	**1.2**
$MgCl_2$	**1.2**
Glucose	**10**
Taurina	**20**
Pyruvate	**5**
Hepes	**10**
pH 7.20 with NaOH - Filter	

Table 5. *The composition of Tyrode buffer*

	mM
NaCl	**140**
KCl	**5.4**
$MgCl_2$	**1.2**
Glucose	**10**
Hepes	**10**
pH 7.35 with NaOH	

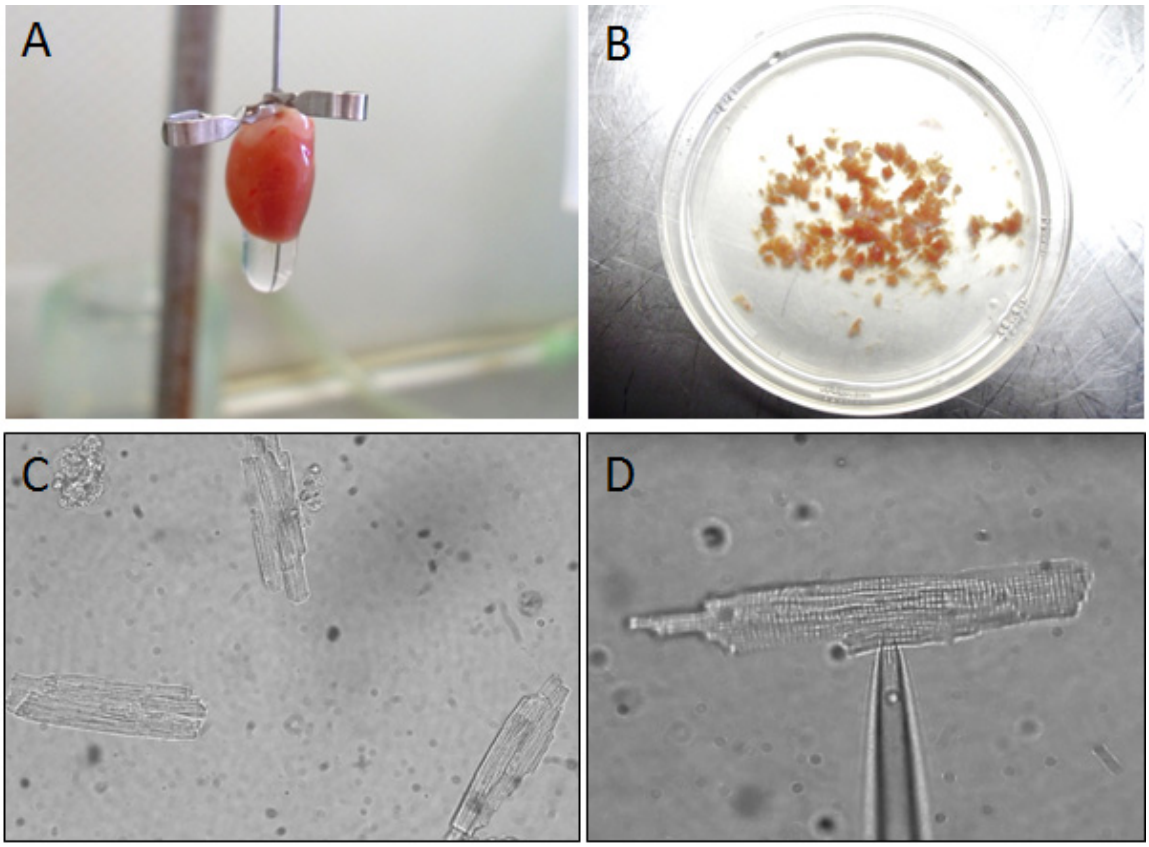

Figure 21: Enzymatic cell isolation. A) *Perfusion phase:* Cannulated heart retrogradely perfused at a constant flow of 3 mL/min at 37°C with the buffer for 3–4 min to wash out blood. B) *Cutting and stirring phase:* The ventricles were excised from the digested heart and cut into several pieces in buffer solution (with 1 mg/ml BSA). Gentle stirring facilitated myocyte dissociation. C) *Ca^{2+} adaptation phase:* The cell suspension was let to settle and the cell pellet (~1 ml) was resuspended in Tyrode buffer (0.05 mM $CaCl_2$, 1 mg/ml BSA). Calcium concentration was gradually raised up to 1.0 mM, by addition of 0.05 mM of $CaCl_2$ every 10-15 minutes.

2.2 Electrophysiological and intracellular Ca^{2+} measurements in intact cardiomyocytes

2.2.1 Set up for intracellular Ca^{2+} measurements from single cardiomyocytes and recording apparatus

Intact cardiomyocytes were enzymatically isolated (Paragraph 2.2) and used for action potentials, ionic currents and intracellular Ca^{2+} measurements. Action potentials were measured under current-clamp conditions using the perforated patch configuration of the patch clamp technique.

When electrophysiological measurements were not required, isolated myocytes were field-stimulated with short (<5ms) pulses by platinum electrodes mounted on the sides of cell bath for field stimulation. Fluoforte fluorescence emitted at 513 nm was measured during fixed excitation at 492 nm wavelength. The emitted fluorescence was acquired by a photomultiplier (Hamamatsu photonics) or by a high-speed camera (Photometrics Cascade 128+), to evaluate the global intracellular Ca^{2+} transient.

Myocytes were loaded with the calcium indicators Fluoforte (Enzo) for intracellular Ca^{2+} measurements. Fluoforte was loaded by incubating cells for 30 minutes in bath solution containing 10 μmol/L Fluoforte. After loading, cells were washed two times and were left 5-10 minutes in normal Tyrode solution. A small amount of the Cell-containing solution is transferred to a small (0.5-mL), temperature-controlled recording chamber and superfused by gravity with a six−line, heated microperfusor system (Warner Instruments), at a flow rate of 0.3 mL/min (temperature: 35°C). Main chamber solution is frequently cleaned by fast rate heated perfusion end placed at the chamber's side,that allows fast washout of chemicals in the bath. The end of the microperfusor system is a 3 barreled, 600 μm wide, square glass pipettes. Three different solutions can be conveyed into the pipette end, one for each of the 3 apertures. The cell under study was held within 300 μm from the tip of the multiline pipette. A computer controlled motor (Warner) allows fast (< 3 ms) change of the aperture facing the cell under study and fast exchange of the cell's extracellular environment. The recording chamber was mounted on the stage of an inverted microscope (Leica) modified for simultaneous patch clamping and Fluoforte epi-fluorescence. The temperature was kept at 35±0.5°C throughout the whole experiment and checked at the pipette tip with a fast-response digital thermometer (Warner).

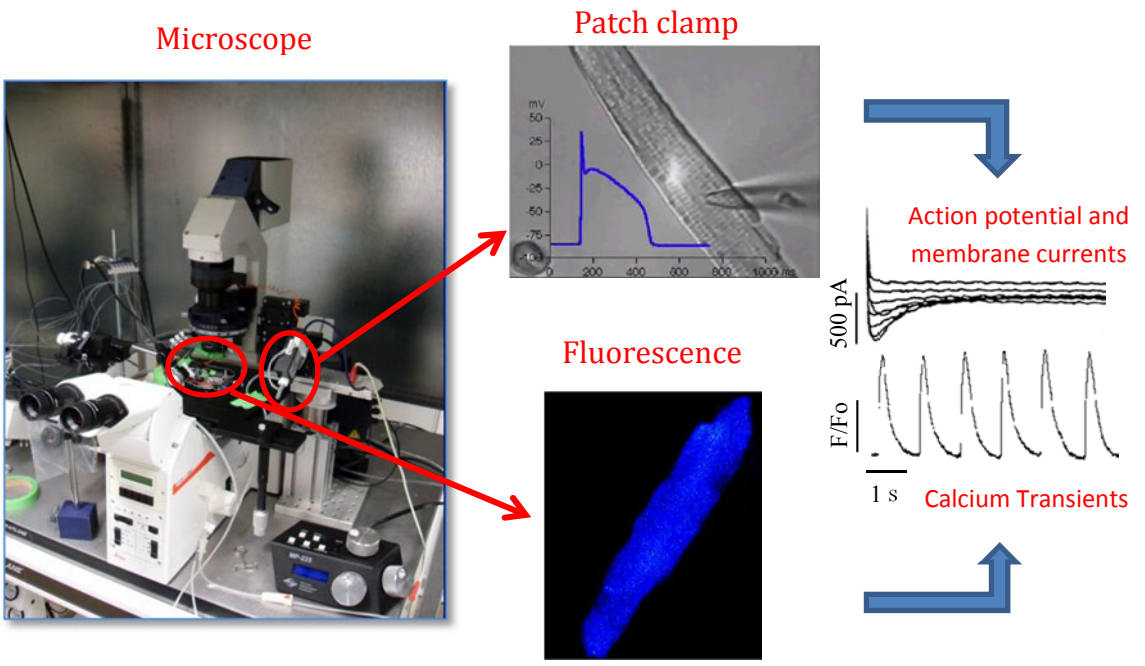

Figure 22: this equipment, in our laboratory, allows us to visualize and measure action potential and membrane currents and calcium transient.

2.2.2 Patch Clamp Methods and solutions

For perforated patch experiments, we used the amphotericin method (Rae J et al. 1991). For action potential recordings, the solution contained (in mM) 115 KMES (potassium *methanesulfonate), 25 KCl, 10 HEPES, 3MgCl2.* The giga-seal was obtained in normal Tyrode at 37°C, and the cell remained in that solution until attaining whole cell configuration (15–20 min; access resistance 11 MΩ). The standard Tyrode bath solution contained (in mmol/L) 136 NaCl, 5.4 KCl, 0.33 Na_2PO_4, 1.8 $CaCl_2$, 1 $MgCl_2$, 10 dextrose, and 10 HEPES-NaOH; pH was adjusted to 7.35 with NaOH. All junction potentials were corrected. Action potentials were elicited with short (3ms) current pulses, delivered regularly at three different frequencies of stimulation (1, 3 and 5 Hz). Membrane potential signals were measured with a Multiclamp 700B (Molecular Devices) patch-clamp amplifier and were filtered at 2 KHz and digitized through a 16-bit A/D converter (Digidata 1440A, sampling rate 5 KHz; Molecular Devices, Inc.). Trace acquisition and analysis was controlled by dedicated software (pClamp 10; Molecular Devices).

2.2.3 Drugs

Isoproterenol (ISO) (SIGMA) was stocked in distilled water solution with 1 mg/ml ascorbic acid as an anti-oxidant, and then used at 0.1 µM and 1 µM. Ranolazine (Gilead) was stocked in HCL 0.1M at the concentration of 0.2M.

2.2.4 Intracellular Ca^{2+}-transients measurements

Intracellular calcium measurements were simultaneously performed with membrane potential recordings on patched cells (see below). When electrophysiological measurements were not required, isolated myocytes were field stimulated with short (<5ms) pulses by platinum electrodes mounted on the sides of cell bath for field stimulation.

Fluoforte fluorescence emitted at 513 nm was measured during fixed excitation at 492 nm wavelength. At the end of the recording protocol each cell was mechanically permeabilized to record the maximal fluorescence. All measurements obtained with each cell were normalized using the maximal fluorescence as reference, after cell permeabilization.

2.2.5 Experimental Protocols on myocytes:

2.2.5.1 Current clamp protocols

Action potentials were elicited with small depolarizing stimuli lasting less than 3ms at different stimulation intervals. Stimulation frequencies used in this set of experiments were 1Hz, 3Hz and 5Hz. The cell was stimulated at each frequency for at least 1 minute before the measurements in order to reach steady state Action Potential Duration and Calcium Transient amplitude. In order to quantify the occurrence of arrhythmic events (Early after depolarization and delayed after depolarization), cells were stimulated at 5Hz for at least 30 seconds and then stimulation was abruptly stopped for 20 s, while recording intracellular Ca movements.

2.2.5.2 SR Calcium content

Steady state SR Calcium content at different stimulation frequencies
After 30-50ms conditioning depolarizing steps to 0mV at 1s interval (holding=80mV), bathing solution is rapidly switched from normal Tyrode to the same solution containing 10mM caffeine for 10s. Timing of solution change is adjusted in order to make the interval from the previous transient exactly equal to the interval between conditioning steps. During the 10s exposure to caffeine, depolarizing steps are interrupted to allow recording of caffeine-induced transmembrane current (I_{NCX}). Regular 1Hz depolarizing steps are resumed after caffeine exposure. Inward current during the 10s of caffeine exposure is integrated to calculate the total amount of charge crossing the membrane (C_{caff}). Total SR calcium content (expressed as mM per Liter of cytosol) is calculated as follows:

$$[Ca^{2+}]_{SR}\ (mM/L\ cyt.) = [(1+0.12)(C_{caff}/F*1000)]/(Cm*8.31)$$

Cm=membrane capacitance *F*=Faraday's number (96500 C/M)
Of note, cell volume is derived from cell capacitance using a fixed conversion factor[20]; non electrogenic Ca^{2+} extrusion modes are added by considering a 12% correction as in Bers DM et al.

2.3 Statistical Analysis

Means were compared by paired or unpaired *t* test and, wherever appropriate, by two-way analysis of variance (paired measurements). Data are expressed and plotted as the mean ± S.E. value obtained from a number of independent determinations. Statistical significance was defined as $p<0.05$ (N.S. = not significant). Absolute values of the variables and sample size for each experimental condition are provided in the figures and/or the respective legends.

2.4 Quantification of mRNA expression of membrane proteins

2.4.1 Cardiac samples

Samples were cleaned of blood and freeze in liquid nitrogen within 5 minutes from excision and were stored at -80°C for further use.

2.4.2 RNA isolation

Total RNA from each frozen cardiac sample was isolated and DNase-treated with the RNAeasy Fibrous Tissue Mini Kit (Qiagen) following manufacturer's instructions. Isolated RNA was quantified (spectrophotometric absorbance at 260 nm) and purity was confirmed by the A260/A280 ratio. Integrity of total RNA was evaluated by ethidium bromide staining on a denaturing agarose gels. RNA samples were stored at –80°C.

2.4.3 Total RNA Reverse transcription

Single-stranded cDNA was synthesized from 2 μg total RNA using the High Capacity cDNA Reverse Transcription Kit (Applied Biosystems) following manufacturer's instructions. Reverse transcription was performed at 25 °C for 10 min, 37°C for 120 min and stopped by incubating at 85 °C for 5 sec.

2.4.5 Real-Time PCR

The genes selected for quantification were investigated using predesigned TaqMan® Gene Expression assays (TaqMan® MGB probe and primers; Applied BioSystems, USA). The real-time RT-PCR reactions were performed using TaqMan® Gene Expression Master Mix (Applied BioSystems) in a 20 μl reaction volume containing 50 ng of cDNA for the different tested genes genes. All reactions were performed in triplicate and included a negative control. PCR reactions were carried out using an ABI Prism 7500 Sequence Detection System (Applied Biosystems). Cycling conditions were: 2 min at 50˚C, 10 min at 95˚C, and 40 cycles of 15 s at 95˚C and 1 min at 60˚C. Relative quantification of the mRNA level for the different genes was determined by the 7500 system software which uses the comparative method (ΔΔCT). In brief, the threshold cycle (Ct) difference of the index gene and the reference gene, calculated from each specimen, is subtracted from the average Ct of the control group; this value is used as the exponent of 2 to calculate ΔΔCt for each specimen. For all mRNA quantification assay, GAPDH was used as

reference gene. In order to validate GAPDH as a reference gene, GAPDH mRNA was compared with ribosomal RNA 18S and expression level calculated as ΔΔCt (not shown).

2.5 Confocal Microscopy

Laser scanning confocal imaging is an imaging technique that can address many of the limitations of traditional fluorescence microscopy. Because confocal imaging allows for visualizing a very narrow plane of focus, much of the interference that results from autofluorescence and out-of-focus blur, can be removed. Other advantages of confocal microscopy and its sophisticated optics include the use of specific excitation wavelengths, as well as the ability to employ detectors that exclude autofluorescence from other emission spectra. In addition, z-stack series of images can be easily combined to assemble three-dimensional reconstruction of many of the unique structure within cardiomyocytes and cardiac tissue.

After cell isolation (see paragraph 2.2), the cells were resuspended in Tyrode buffer supplemented with 0.05 mM $CaCl_2$ and 1 mg/ml BSA. Calcium concentration was gradually raised to 1.0 mM. Then one ml of this solution was incubated for 20 minutes with 5 µl of [Di-4-AN(F)EPPTEA], a selective membrane dye. The cell suspension was let to settle and the cell pellet was resuspended in one or less ml of clean Tyrode buffer. The solution with cells was placed atop confocal-imaging optimized borosilicate glass chamber slide (MaTek).

We used a similar method for imaging of intact cardiac tissue. A small piece of tissue was put in an eppendorf with 1 ml of tyrode solution and 10 µl of dye and incubated for 30 minutes. Then the sample was washed with clean tyrode solution and put in glass chamber. A drop of tyrode solution was placed atop the piece of tissue to prevent drying and facilitate the acquisition. The excitation wavelength was 488 nm and the emission filter was 504-649 nm. Finally, assembly of three-dimensional reconstructions was accomplished by acquiring multiple narrow-spaced z-stack images along the vertical axis.

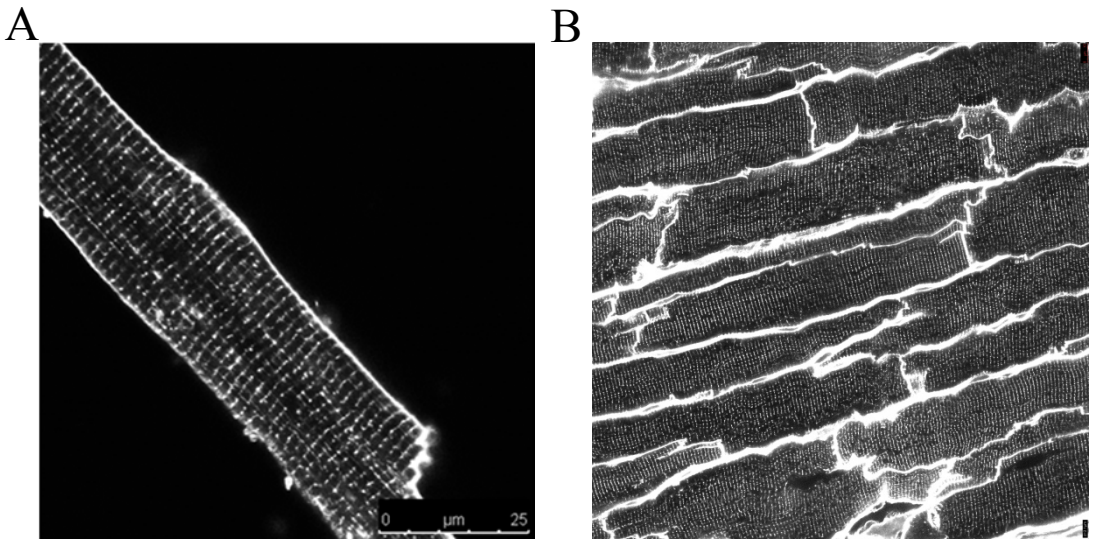

Figure 23: Examples pictures of confocal acquisition, single cell (A) and piece of tissue (B).

2.6 Long-term treatment of murine models with Ranolazine

Mice was treated with ranolazine added to their chow (0.5% ranolazine/0.03% ketoconazole), in order to get the desired plasma levels of the drug (8-15 μM). The half-life of ranolazine in mice is very short, thus ketoconazole was added to inhibit the metabolism of the drug (chow made from Research Diets Company). The combination of 0.5% Ranolazine + 0.03% Ketaconazole mixed in chow has been demonstrated to be effective to get to desired plasma levels of ranolazine for most time of the day.
R92Q mice, fed with ranolazine-containing chow since birth, was sacrificed at one, three, six and twelve months of age and compared to age-matched untreated mice (see graph below). Each of the litters is obtained by crossing a WT female with a heterozygous mutant male, thus mutation carriers were 50% of the littermates on average. Mice were genotyped at 1 month of age, allowing a direct comparison between WT mice and mutation-carriers of the same age. Therefore we had a total of 4 treatment branches: treated and untreated WT mice, treated and untreated TnT mutant mice. By treating also WT mice, we ensured that ranolazine does not exert any damage when used at an early age.

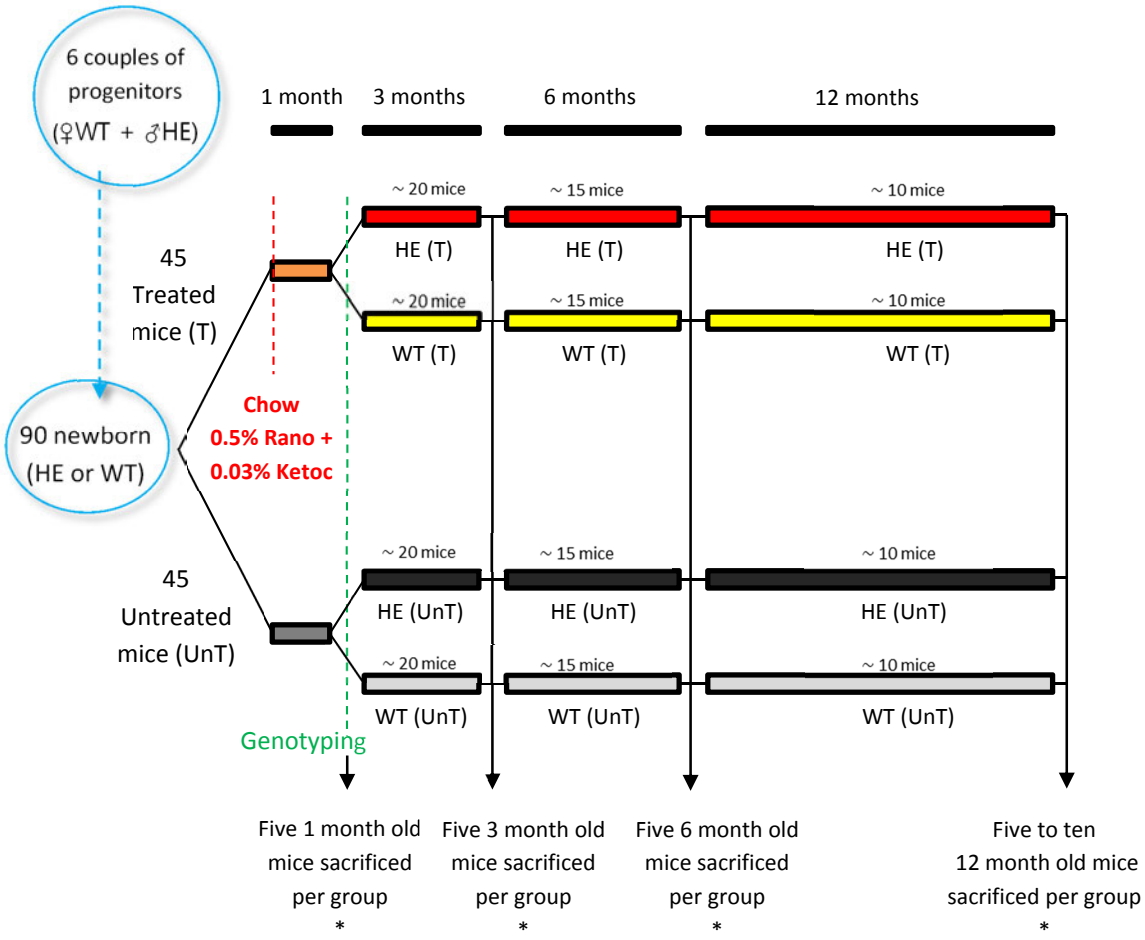

Figure 24: Work plan of long-term treatment of R92Q mice with ranolazine.

2.8 Echocardiography

In collaboration with Toscana Life Sciences (TLS) we performed echocardiographic measurements in living mice. We divided the mice into three groups: WT, R92Q (Keto) and R92Q (Rano). To visualize morphological changes and alteration of cardiac functions, and evaluate the chronic effects of the drug. For these measurements we use the dedicated instrumentation Visualsonics Vevo 2100. Mice were first anesthetized with isoflurane (induction, 4%–5%; maintenance, 1%–2.5% in oxygen from a precision vaporizer) in an induction chamber and then positioned prone on a heated bed. In each mouse, the following acquisitions were performed:

- Parasternal Long Axis (PSLAX) view was used to measure the thickness of the interventricular septum (IVS), and the left ventricle posterior wall (LVPW), as well as the left ventricular interior diameter (LVID).
- Short Axis (SAX) views were acquired to calculate volume changes with Simpson LV cavity reconstruction (see below)
- Simpson's LV volume reconstruction: we acquired one long axis view and 3 short axis views evenly spaced around a mid-level view at the level of the papillary muscles, one towards the apex or distal portion of the heart, and one towards the base or proximal portion of the heart. From this measurements we can calculate LV volume at end-diastole and end-systole, thereby obtaining precise evaluation of cardiac output, ejection fraction and stroke volume.
- PV Flow: these measurements are performed in the pulmonary artery acquired just below the pulmonary valve. These measurements involve measuring the velocity and gradient of flow through this vessel using Doppler acquisitions. From these measurements we can calculate the cardiac output my measuring the total blood flow in the pulmonary artery.
- LV Diastolic Function: these measurements are designed to be used on the mitral valve flow. The mitral valve E and A peaks are measured. The E peak is the "early" peak, while the A peak is the "atrial" peak. E/A ratio is also calculated as an indicator of the overall diastolic function. Along with these measurements the isovolumic relaxation time (IVRT) and the isovolumic contraction time (IVCT) are measured; both of these are times when the muscles are contracting however there is no change in the volume of the ventricle to cause blood flow, therefore they appear as flat lines on the PW Doppler spectrum. The deceleration of blood flow through the mitral valve can also be measured. They Myocardial Performance Index is another calculation preformed on the Mitral Valve PW. The no flow time (NFT) is measured from the time when the A peak reaches baseline to the time where the next E peak begins; while the aortic ejection time (AET) is measured as the time where the spectrum falls below the baseline, indicating flow out through the aorta.

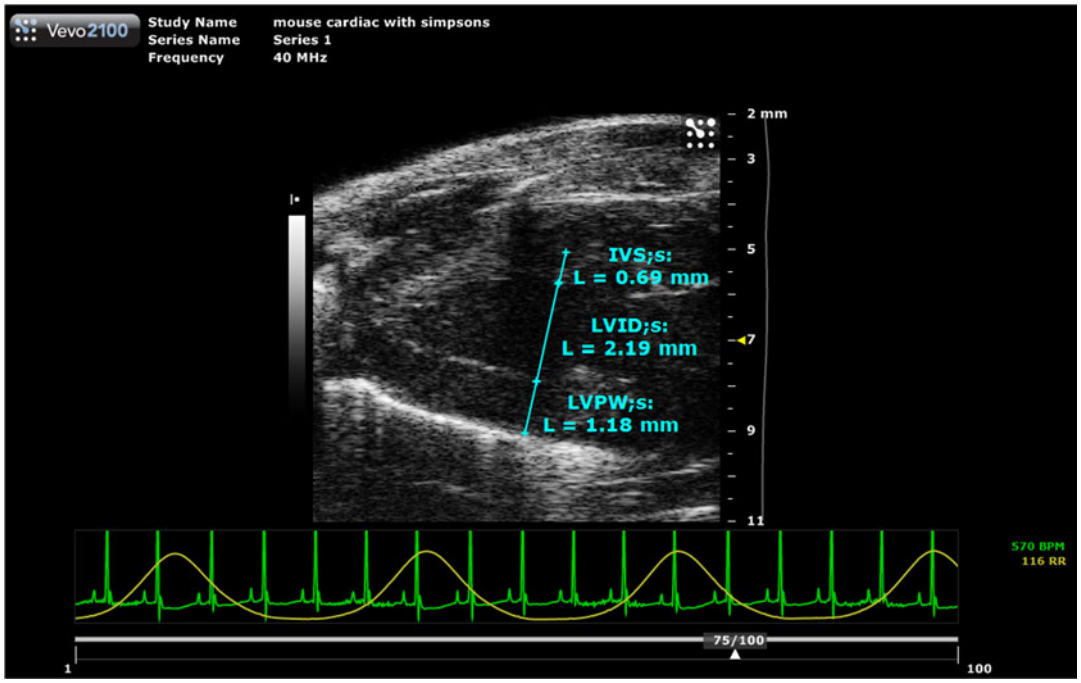

Figure 25: Parasternal Long Axis (PSLAX) and IVS, these measures provide the thickness of the interventricular septum.

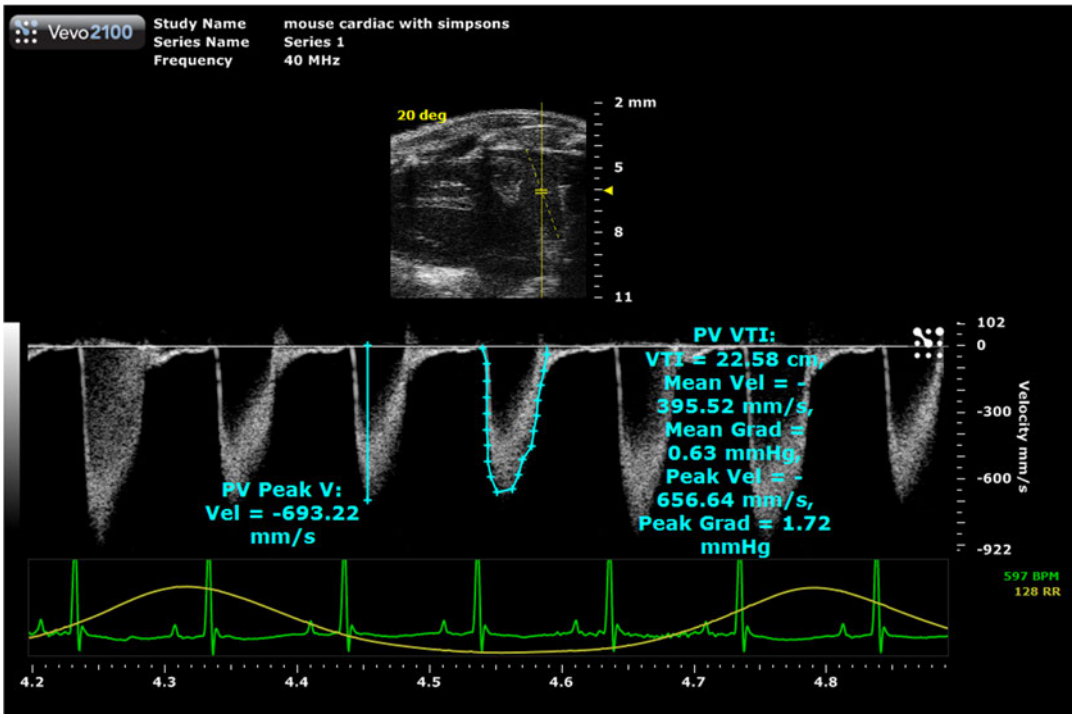

Figure 26: PW Flow: the PV Peak measures the peak velocity of the blood flow; the PV VTI measures the velocity time interval of the blood flow.

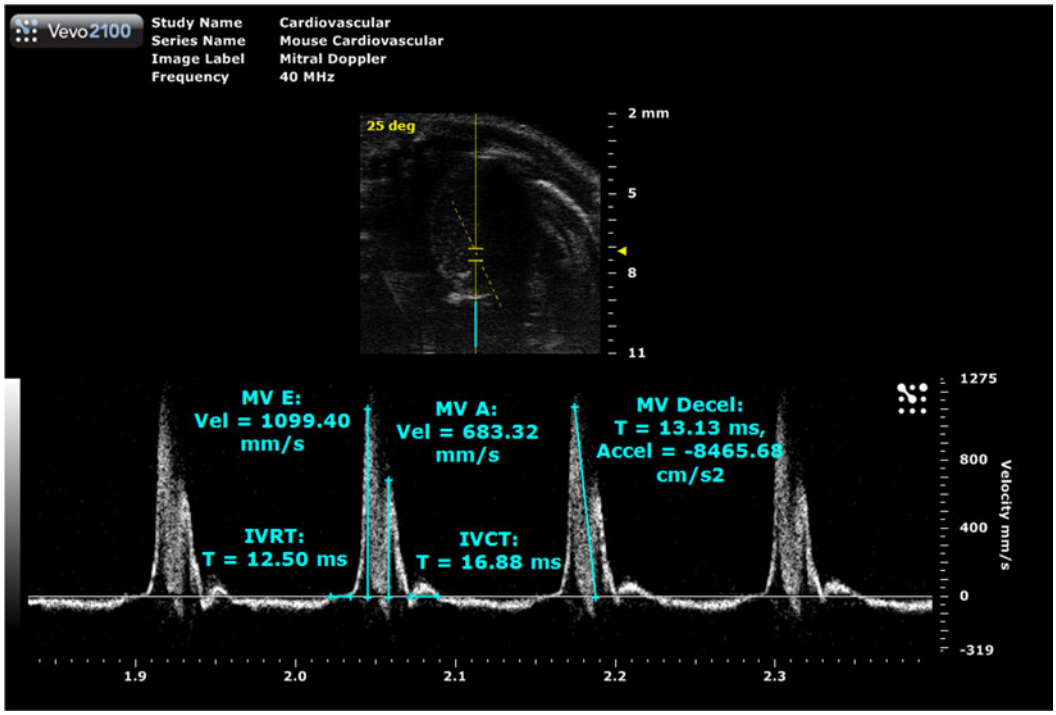

Figure 27: LV Diastolic Function and Mitral Valve Flow.

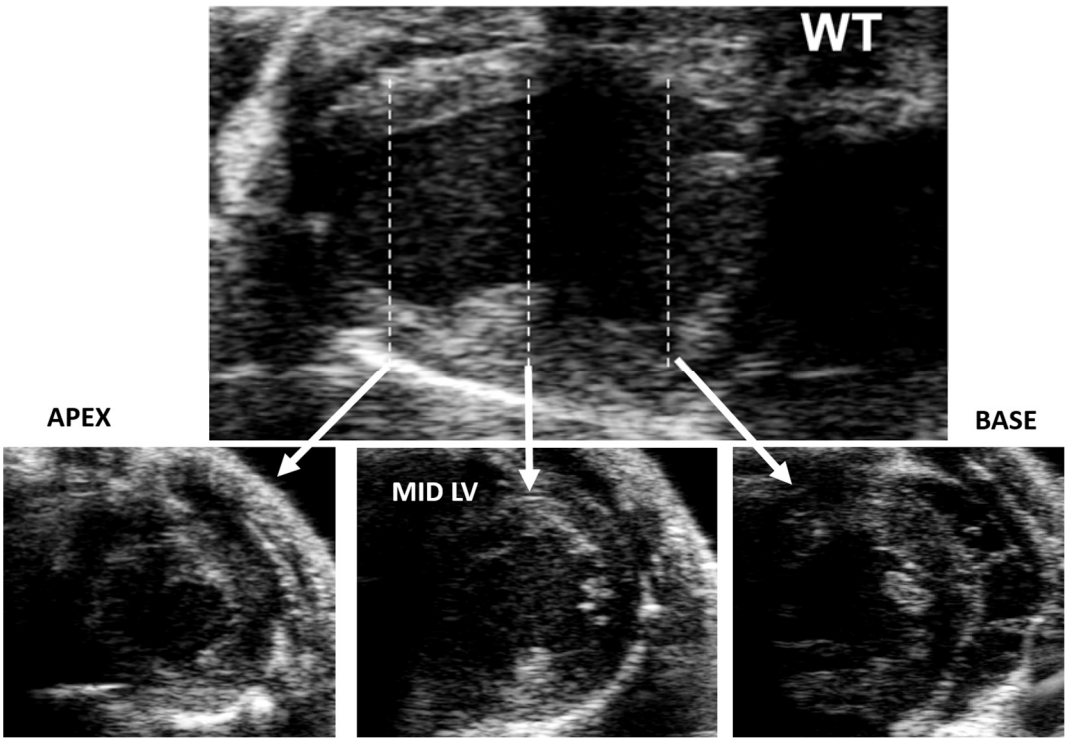

Figure 28: examples of Simpson's measures, for each of the 3 short axis views (apex, mid and base level) the endocardium should be traced in systole and diastole. We also made 3D reconstruction.

2.9 Cardiac Magnetic Resonance Imaging (MRI)

In collaboration with Siena Biotech S.p.A. we performed cardiac magnetic resonance imaging in WT, R92Q Keto and R92Q Rano mice. A Brucker Pharmascan 7T small animal MRI scanner was used to acquire MRI images, equipped with a 740 mT/m gradient coil. A 72-mm-diameter quadrature transmit coil was used in combination with a 4 element phased-array receive coil (Bruker). Mice were first anesthetized with isoflurane (induction, 4%–5%; maintenance, 1%–2.5% in oxygen from a precision vaporizer) in an induction chamber and then positioned supine on a water-heated bed in the MRI scanner. CMR images were acquired with ECG and respiratory gating (model 1025 L; SAII, Stony Brook, NY). For LV/RV size and function, short-axis cine gradient-echo images were obtained with full LV coverage (repetition time, 5.9 milliseconds; echo time, 2.2 milliseconds; temporal resolution, 20–30 milliseconds; in-plane spatial resolution, 100–120×180–210 μm; slice thickness, 1 mm; no gap). Manually traced epicardial and endocardial contours at end systole and end diastole were used to determine the LV and RV end-diastolic volume, LV/RV end-systolic volume, and LV myocardial mass using the Simpson rule, as well as LV and RV ejection fraction.
Gadolinium diethylenetriaminepentacetic acid (Magnevist, Berlex, Wayne, NJ) was injected intravenously (tail vein) in a single bolus dose of 0.5 mmol/kg. Myocardial T1 was measured in a mid-LV slice once before contrast and 35-40 minutes after contrast using a Look-Locker technique (repetition time, 2.5 milliseconds; echo time, 1.8 milliseconds; flip angle, 10°; in-plane resolution, 190 μm; slice thickness, 1 mm). For 6 myocardial segments and the blood pool, signal intensity was plotted versus time after inversion. T1 values were obtained by nonlinear least-squares fitting of the curves of signal intensity versus time after inversion to an analytic expression for the magnitude of the signal measured during the inversion recovery and correction for the radiofrequency pulse effects on the inversion recovery. The reciprocal of T1 (R1=1/T1) was used to calculate extracellular volume (ECV). ECV was calculated using the following expression: $ECV = (1 - \text{hematocrit}) * (R1_{MusclePost} - R1_{MusclePre}) / (R1_{BloodPost} - R1_{BloodPre})$. For the purposes of this analysis, hematocrit was considered to be 0.45.
Of note, the LV/RV size/function protocol (see above) was performed in each animal between the Pre and the Post contrast acquisitions.
A total of 12 mice for each of the three groups underwent MRI.

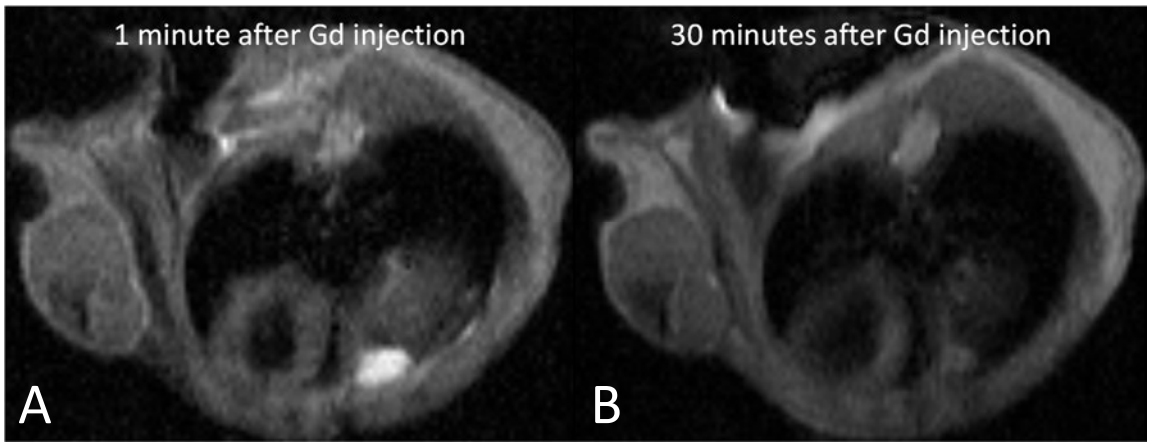

Figure 29: examples of MRI acquisition and administration of gadolinium: A) one minute after Gd injection; B) 30 minutes after Gd injection.

REFERENCES

Baudino TA, Carver W, Giles W, Borg TK (2006) Cardiac fibroblasts: friend or foe? *American journal of physiology Heart and circulatory physiology* 291: H1015-1026.

Bers DM. Excitation contraction coupling and cardiac contractile force. Second edition. Kluwer Academic Publishers 2001; Chapters 1 and 7.

Briar R. Ertz-Berger*†, Huamei He‡, Candice Dowell*, Stephen M. Factor†§, Todd E. Haim*, Sara Nunez*, Steven D. Schwartz*, Joanne S. Ingwall‡, and Jil C. Tardiff*† Changes in the chemical and dynamic properties of cardiac troponin T cause discrete cardiomyopathies in transgenic mice PNAS _ December 13, 2005.

de Tombe PP, ter Keurs HE (1990) Force and velocity of sarcomere shortening in trabeculae from rat heart. Effects of temperature. *Circulation research* 66: 1239-1254.

Coelho-Filho OR, Shah RV, Mitchell R, Neilan TG, Moreno H Jr, Simonson B, Kwong R, Rosenzweig A, Das S, Jerosch-Herold M. Quantification of cardiomyocyte hypertrophy by cardiac magnetic resonance: implications for early cardiac remodeling. *Circulation* 2013 Sep 10;128(11):1225-33.

Egorova MV, Afanas'ev SA, Popov SV (2005) A simple method for isolation of cardiomyocytes from adult rat heart. *Bulletin of experimental biology and medicine* 140**:** 370-373.

Hanley PJ, Young AA, LeGrice IJ, Edgar SG, Loiselle DS (1999) 3-Dimensional configuration of perimysial collagen fibres in rat cardiac muscle at resting and extended sarcomere lengths. *The Journal of physiology* 517 (Pt 3): 831-837.

Moore RK, Grinspan LT, Jimenez J, Guinto PJ, Ertz-Berger B, Tardiff JC (2013) HCM-linked 160E cardiac troponin T mutation causes unique progressive structural and molecular ventricular remodeling in transgenic mice. *Journal of molecular and cellular cardiology* 58**:** 188-198.

Rae J, Cooper K, Gates P, Watsky M Low access resistance perforated patch recordings using amphotericin B. Journal of Neuroscience Methods 1991;37-1:15-26.

Tardiff JC, Factor SM, Tompkins BD, Hewett TE, Palmer BM, Moore RL, Schwartz S, Robbins J, Leinwand LA (1998) A truncated cardiac troponin T molecule in transgenic mice suggests multiple cellular mechanisms for familial hypertrophic cardiomyopathy. *The Journal of clinical investigation* 101: 2800-2811.

Tardiff JC, Hewett TE, Palmer BM, Olsson C, Factor SM, Moore RL, Robbins J, Leinwand LA (1999) Cardiac troponin T mutations result in allele-specific phenotypes in a mouse model for hypertrophic cardiomyopathy. *The Journal of clinical investigation* 104: 469-481.

Chapter 3: AIMS

The main goal of the project is to demonstrate the effectiveness of ranolazine, a selective blocker of late sodium current, on transgenic mouse models of hypertrophic cardiomyopathy. We divided the work into three subsequent phases:

Aim 1 – Phenotypic and biophysical characterization of TnT-mutant mouse models of HCM

Hypertrophic cardiomyopathy (HCM) in patients is characterized by left ventricular hypertrophy in the absence of other systemic and cardiac disease. HCM is one of the main overall causes of fatal cardiac arrhythmias. Moreover, most HCM patients develop a severe diastolic dysfunction that impacts life quality and may slowly lead to deterioration of cardiac function and heart failure. However, very limited information is available on the cellular basis of arrhythmias and diastolic dysfunction in HCM myocardium. Studies on myocardial samples from patients with HCM are made extremely difficult by the scarce availability of material and the intrinsic variability among patients. The use of animal models of HCM can overcome these limitations and allow us to perform a more complete characterization of the pathways determining the cellular pathophysiology of HCM without the confounding effects of unpredictable contributors. Two different mouse transgenic knock-in lines bearing HCM-mutations of the cardiac troponin T gene are employed for the study (R92Q and E163R), providing a wide spectrum of different HCM-related phenotypes. Troponin T mutant mice are able to replicate the different clinical phenotypes of human HCM: a restrictive-like disease presentation with fibrosis and severe diastolic dysfunction (R92Q), an early onset disease with scarce hypertrophy and fibrosis but high risk of arrhythmias (E163R).
The main objectives for this first part are: (i) to breed and amplify the mouse colonies and identify mutation carriers via detection of the mutated allele, (ii) to set up a method to isolate viable ventricular cardiomyocytes from diseased mouse hearts; (iii) to define the electrophysiological properties of remodeling of ventricular myocytes, measuring action potential characteristics; (iv) to analyze alterations in the kinetics and amplitude of Ca^{2+} transients of myocytes from diseased hearts; (v) to assess contractile alterations of intact trabeculae; (vi) to assess the presence of structural and functional alterations of the t-tubules; (vii) to identify the molecular substrate of functional alterations, focusing on transcriptional modification of ion channels using qRT-PCR.

Aim 2 – *In vitro* effects of ranolazine on intact cells and trabeculae from HCM mouse models

No specific therapy exists to date that is able to reduce the burden of arrhythmias and improve diastolic function in HCM. A valuable pharmacological therapy for HCM still remains an unmet medical need. Ranolazine, a selective late sodium current blocker, was previously tested by our group on human samples from HCM patients. Ranolazine selectively shortened action potential duration, hastened calcium transients' kinetics and ameliorated muscle relaxation in HCM samples. To assess Ranolazine therapeutic potential in HCM, we aim to test the drug on HCM mouse models expressing mutations of TnT and bearing different disease phenotypes.

The main objectives for this second part are: (i) to study the effects of ranolazine on action potential duration and properties in ventricular myocytes; (ii) to investigate potential beneficial effects of ranolazine on intracellular Ca^{2+} handling and contraction of ventricular myocardium.

Aim 3 – *In vivo* treatment of murine models with ranolazine

As a consequence of extensive family screening programs, subjects carrying HCM-associated mutations are more and more commonly identified before the onset of disease (i.e. in the pre-hypertrophic stage) (Olivotto et al. 2012). Despite the increasing need, no drugs in current use are capable to prevent phenotype development and adverse cardiac remodeling in HCM mutation carriers. Reduction of intracellular Ca^{2+} obtained by long-term treatment with the Ca-channel blocker diltiazem prevented disease expression in transgenic mice with a MYH7 mutation (Semsarian et al. 2002). We have previously shown that ranolazine is beneficial in human HCM (Coppini et al. 2013), as it leads to a sustained reduction of intracellular Ca^{2+}.
The third aim of this thesis is to assess whether long-term oral treatment with ranolazine since birth is capable to prevent the HCM phenotype and the associated myocardial remodeling.
Mice were treated with ranolazine added to their chow (0.5% Ranolazine/0.03% ketoconazole), in order to get the desired plasma levels of the drug (8-15 μM). Mice are genotyped at 1 month of age, allowing a direct comparison between WT mice and mutation-carriers of the same age. Therefore we had a total of four treatment branches: treated and untreated WT mice, treated and untreated TnT mutant mice. We compared the behavior of WT, R92Q-untreated and R92Q-treated 1 year old mice, by performing echocardiography and cardiac MRI assessments. Then mice were sacrificed for ex vivo assessments on cells and trabeculae.
The main objectives for this third part are: (i) to study the long-term effects of ranolazine; (ii) evaluate its possible effects on early myocardial remodeling; (iii) verify the preventive effects on the progression of the disease.

To summarize, the main purposes of this thesis are:
- Phenotypic and biophysical characterization of TnT mutant mouse models of HCM;
- Acute effect of ranolazine on intact cells;
- Long-term treatment of mouse models with ranolazine.

REFERENCES:

Olivotto I, Cecchi F, Poggesi C, Yacoub MH. Patterns of disease progression in hypertrophic cardiomyopathy: an individualized approach to clinical staging. Circulation Heart failure 2012;5:535-46.

Semsarian C, Ahmad I, Giewat M et al. The L-type calcium channel inhibitor diltiazem prevents cardiomyopathy in a mouse model. The Journal of clinical investigation 2002;109:1013-20.

Coppini R, Ferrantini C, Yao L et al. Late sodium current inhibition reverses electromechanical dysfunction in human hypertrophic cardiomyopathy. Circulation 2013;127:575-84.

Chapter 4: RESULTS

Two different mouse transgenic knock-in lines bearing HCM-mutations of the cardiac troponin T gene were employed for the study: R92Q and E163R. The models were provided by Prof. Jil Tardiff and have been created and characterized at the A. Einstein College of Medicine, Bronx, New York (NY). Overall characteristics of the two models have been extensively described. In brief, R92Q mice show a restrictive-like disease presentation with fibrosis and severe diastolic dysfunction; E163R mice show an early onset disease with scarce hypertrophy and fibrosis but high risk of arrhythmias. The two models summarize different possible disease phenotypes in patients and, taken together, they represent an optimal test bench for drugs aimed at reducing the burden of HCM. The mouse lines were bred and genotyped in the Center for Animal handling (CeSAL) of the University of Florence. All procedures involving animal use was performed in agreement with local ethical regulations.

4.1 - Phenotypic and biophysical characterization of TnT mutant mouse models of HCM

4.1.1 - Amplification of murine colonies and identification of mutation carriers through the recognition of the mutant allele

The two mouse colonies have been bred and amplified from the original received progenitors. Heterozygous male mice were crossed with WT females. Each mouse has been tested for the presence of mutations and more than 120 mice carrying mutated troponin T have been generated and identified. Some of the generated mice were used for a complete characterization of the cardiac disease phenotype associated with the mutation.

4.1.2 – Morphological characterization of TnT mutant mouse models

We first investigated the changes of cardiac function of the two transgenic mouse models by performing echocardiographic studies.
A total of 12 WT, 11R92Q and 11 E163R mice were used for this study. Each animal was anesthetized with 4% isoflurane in an indction chamber and prepared for echocardiography. For these measurements we used the dedicated instrumentation Visualsonics Vevo 2100. The mouse was anesthetized during the whole procedure (isoflurane 2%). According to the experimental protocol (see methods), we performed a number of structural and functional measurements such as LV volumes and wall thickness, cardiac output and ejection fraction, stroke volume and atrial areas. Starting from the Parasternal Long Axis view of the heart (PSLAX) (fig. 30A), the assessment of LV volumes and wall thickness show marked alterations in both mutant mouse lines as compared with controls (WT). In particular, R92Q and E163R mice show an increased ejection fraction and diastolic septal thickness, as well as a significantly increased systolic wall thickening, when compared to WT (fig. 30C-F). Moreover, R92Q mice show a significant decrease of diastolic and systolic LV volumes with regards to WT, while E163R mice didn’t show any significant difference (fig. 30B). Stroke volume and cardiac output resulted slightly but significantly increased in E163R mice vs. WT, while they did not differ from controls in R92Q mice (fig. 30D).

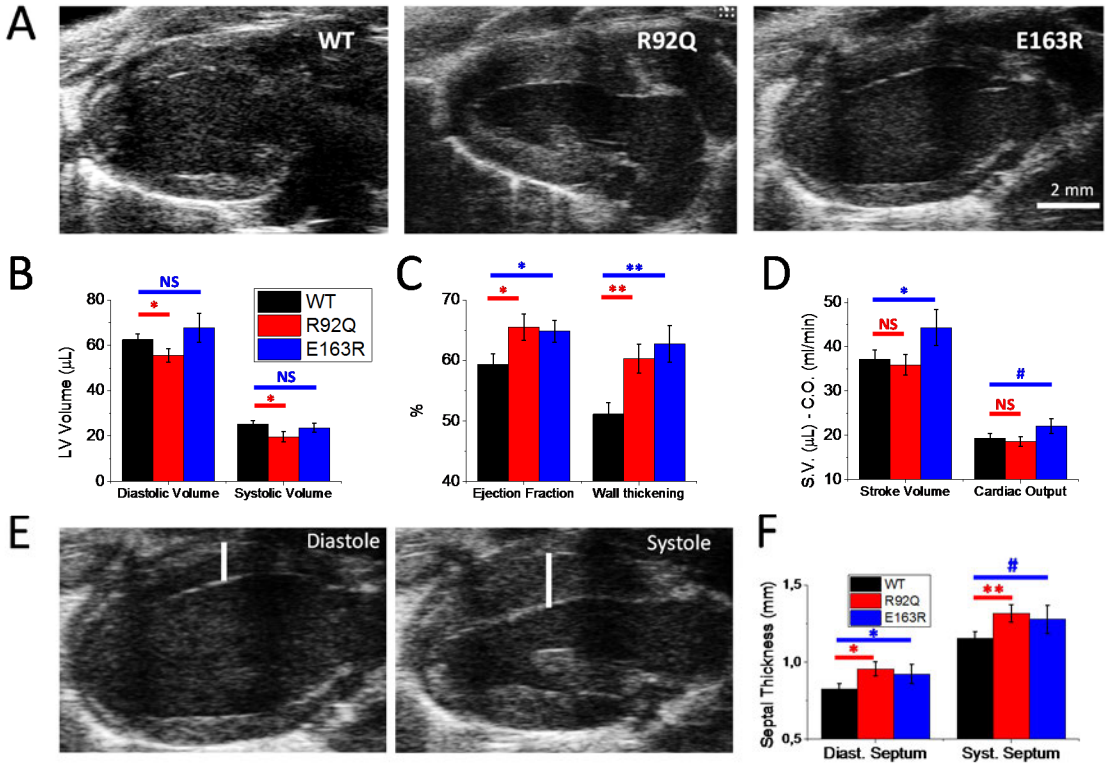

Figure 30: Echocardiographic assessment of LV volumes and wall thickness: increased ejection fraction and septal dimension in R92Q and E163R vs WT mice. A) Representative echocardiographic images of parasternal long axis of the three kind of mice. B) Diastolic and systolic volume. C) Ejection fraction and wall thickening. D) Stroke volume and cardiac output. E) Representative echocardiographic images of diastole and systole wall thickness. F) Diastole and systole septum.

Next we focused on diastolic dysfunction; the assessment are based on the analysis of mitral valve flow and left atrium area. For evaluation of mitral valve flow we used the Doppler technique and measured the mitral valve E and A peaks: the "early" peak E (passive ventricular relaxation) and the "atrial" peak A (late LV filling due to atrial contraction). In normal conditions peak A is lower than peak E and we can discriminate two separate peaks: this always occurred in WT mice. The left ventricle was not altered and therefore the filling of the heart chamber was mainly dependent on the passive relaxation of the cardiac left ventricle itself.
Instead, the data obtained show the presence of important diastolic alterations in HCM mice; in fact in R92Q mice peak A resulted higher than peak E and the two peaks were partially fused together. The peak A overrides the peak E because the left ventricles was stiffer due to the progression of the disease, thus implying a reduction and slowing of LV relaxation. As a consequence, the left atrium had to bear a greater effort to overcome this deficiency.
This also occurred in E163R mice, the two peaks were separated but the peak A resulted higher, as compared with the control (fig. 31A).This was further confirmed by E/A ratio analysis: data showed a significant reduction of E/A ratio in both mutant mice compared to WT (fig. 31B), with greater impairment in R92Q as compared with E163R.
Then, continuing with the analysis, the left atrial size results larger in both mutant mouse lines with regards to WT. Additionally, R92Q mice showed larger left atria than E163R (fig. 31C-D). This correlates with what mentioned previously: the left atrium was enlarged because it had to

carry a greater load due to the increased stiffness of the left ventricle. Mutant mouse hearts appear to implement these compensatory mechanisms to counteract the progression of the disease.

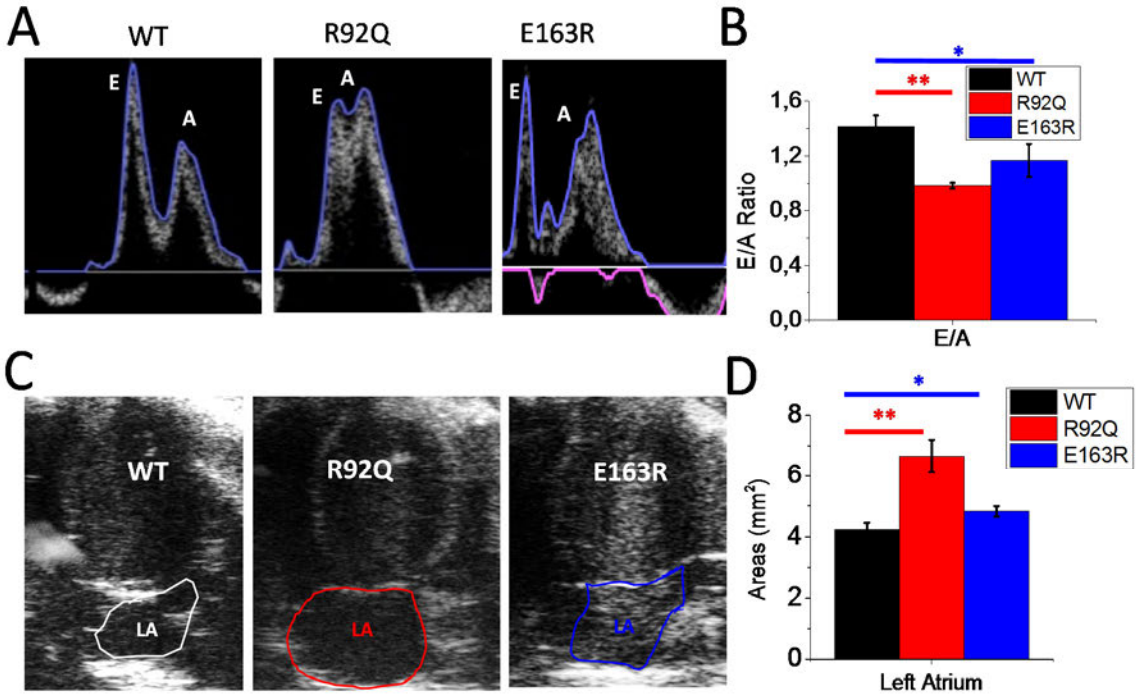

Figure 31: Transmitral blood flow and atrial dimension: impaired diastolic function in mutant mice vs WT. A) Representative images of mitral valve flow of WT, R92Q and E163R mice. B) E/A ratio of peaks E and A. C) Representative 4-chamber (apical) views highlighting atrial dimension in WT, R92Q and E163R mice. D) Left atrium areas.

4.1.3 - Set up a method to isolate viable ventricular cardiomyocytes from diseased mouse hearts.

Isolation of cardiomyocytes from WT hearts has been carried out using a standard Langendorff method. Briefly, a mouse was heparinized (8,000 U/kg, i.p.) and deeply anesthetized with Isoflurane. The excised heart was immediately bathed in cell isolation buffer and cannulated through the aorta. The cannulated heart was then retrogradely perfused at a constant flow of 3 ml/min. at 37°C with the buffer for 3-4 min. The perfusate was then switched to the enzyme solution (20 ml), the same buffer supplemented with 0.1 mg/ml Liberase TM Research Grade (Roche Applied Sciences). The solution was recirculated for 8-9 min. From the digested heart, the ventricles were excised and shredded into several pieces in buffer solution. Gentle stirring facilitated dissociation of the tissue. The cell suspension was let to settle and the cell pellet (~0.1 ml) was resuspended in buffer supplemented with 0.05 mM $CaCl_2$ and 1 mg/ml BSA. Calcium concentration was gradually raised up to 1.8mM. Viable cells from diseased hearts could not be easily obtained by applying this method. In order to obtain viable cells from diseased hearts, enzyme concentration and exposure time had to be adjusted and fine-tuned and that required

quite a lot of work. Finally, the adjustments led to obtain a total of ~500000 viable and calcium-tolerant cells from each mutant mouse heart.

4.1.4 – Analyze the alterations in the kinetics and amplitude of Ca^{2+} transients recoded from diseased myocytes.

After cell isolation, cardiomyocytes were loaded with the calcium indicators Fluoforte (Enzo) for intracellular Ca^{2+} measuraments. Fluoforte fluorescence emitted at 513 nm was measured during fixed excitation at 492 nm wavelength. The emitted fluorescence was acquired by a photomultiplier, to evaluate the global intracellular Ca^{2+} transient. After loading, cells were washed two times and were left 5-10 minutes in normal Tyrode solution. A small amount of the cell-containing solution was transferred to temperature-controlled recording chamber and superfused by gravity with a six−line, heated microperfusor system, at a flow rate of 0.3 mL/min (35°C). Main chamber solution is frequently cleaned by fast rate heated perfusion end placed at the chamber's side, allowing fast washout of chemicals in the bath.
Marked cell were submitted to rate of 1, 3, 5 Hz to simulate heart rate changes. Data obtained show that, compared to WT, R92Q mice had smaller calcium transients (reduced amplitude at the 3 frequencies investigated), with a slower rate of decay: indeed, the duration of calcium transient at 50% and 90% of the decay phase was markedly prolonged at all frequencies. Additionally, diastolic calcium concentration was increased and tended to increase more upon rise in frequency (fig. 32 left column). On the contrary, in E163R cardiomyocytes the amplitude of calcium transient was unchanged and their kinetics was not slower, as compared to WT. However, like in R92Q cells, diastolic calcium concentration was markedly increased with regards to WT (fig. 32 right column).

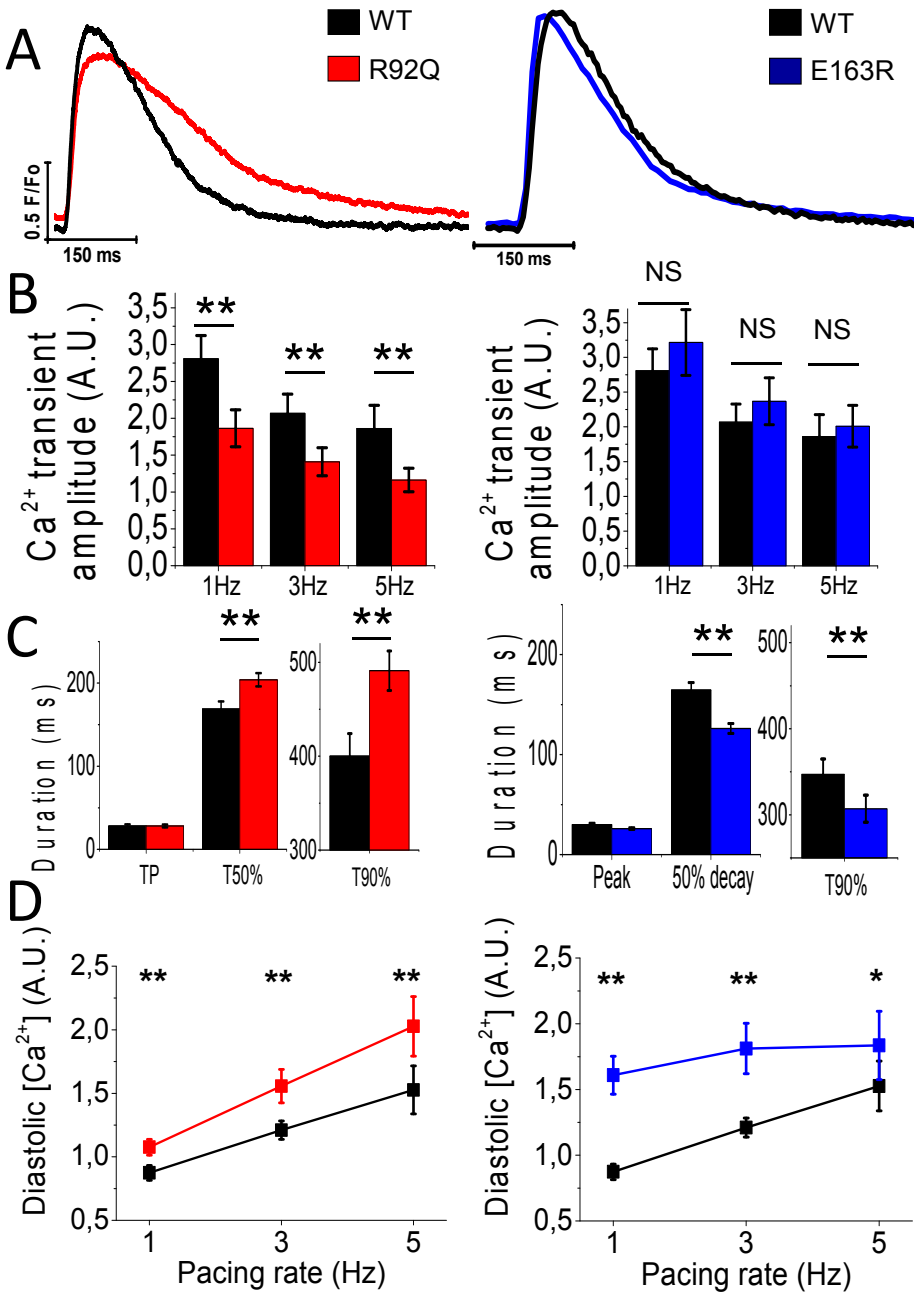

Figure 32: A) Representative graphs of calcium transient (1 Hz) of mutant mice (R92Q and E163R) compare to WT. B) Calcium transient amplitude (1, 3, 5 Hz). C) Duration of calcium transient (Time to peak, 50% and 90% of decay). D) Diastolic calcium concentration (pacing rate 1, 3, 5 Hz).

4.1.6 - Conclusion part I

Data obtained confirm that transgenic mutant mice are a good experimental model and reflect the main features of human disease. In fact, mutant mice show left ventricular hypertrophy, LV hypercontractility, disorganization of Ca^{2+} handling in cardiomyocytes, diastolic dysfunction and contractile abnormalities. The pathological phenotype, both at whole heart and at cellular level, was more marked in R92Q mice as compared to E163R. Therefore we concluded that R92Q mouse line is a good candidate for testing novel drugs for the treatment of HCM.

4.2 – *In vitro* effect of ranolazine on intact cells and trabeculae from HCM mouse models

4.2.1 - Effects of ranolazine on electrophysiological properties of remodeling of ventricular myocytes, measuring action potential characteristics

After the complete pathophysiological characterization of cells and trabeculae from mutant mouse hearts, acute effects of ranolazine was tested on a number of cellular parameters.
A preliminary dose-response experiment was performed for some tests; 10μM concentration was employed throughout the experiments, as it is generally considered a medium-high dose compatible with plasma and tissue level of the drug measured in regularly treated patients.
We first investigated the effect of ranolazine on action potentials. After cells isolation the action potentials was measured under current-clamp conditions, using either the whole-cell perforated patch configuration of the patch clamp technique, and elicited with small current pulses at 1Hz and 5Hz.
Compared to WT, R92Q cardiomyocytes showed slightly shorter action potentials. Ranolazine did not affect the normal action potential of WT cardiomyocytes, both at 1 Hz and at 5 Hz (fig. 33A). On the contrary, in R92Q preparations, the application of ranolazine induced a significant reduction of the action potential duration (fig. 33B) at all frequencies investigated.

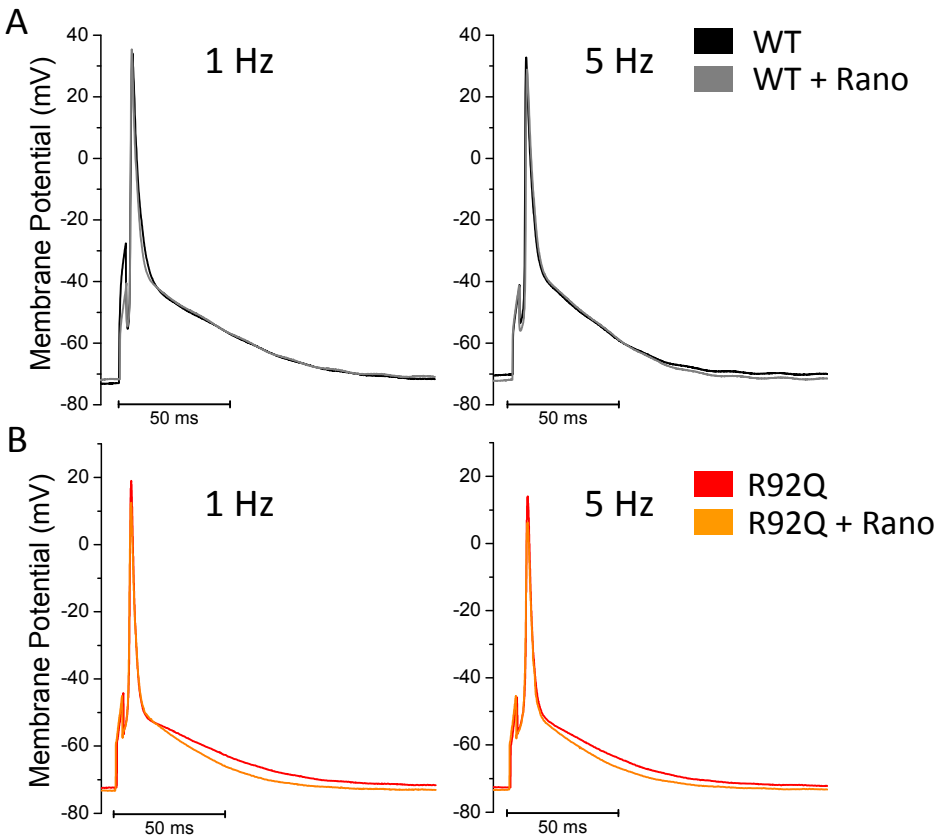

Figure 33: action potential and ranolazine effects: representative traces of action potential recording at 1 and 5 Hz of WT (A) and R92Q (B) mice compare to the same cells after the application of ranolazine. Data from: n WT: 15 cells (3 mice); n R92Q: 19 cells (4 mice).

In particular, by analyzing the individual steps of the action potential we can better distinguish the effects of ranolazine. Data obtained show that in WT cardiomyocytes ranolazine did not affect either of the three measured parameters (APD20, APD50 and APD90), neither at 1 Hz nor at 5Hz (fig. 34A). Instead, in R92Q mice cardiomyocytes, ranolazine reduced action potential duration at APD50 and APD90 steps, while there wasn't any difference of APD20. Besides, these differences were more pronounced at 5 Hz stimulation rate than at 1Hz (fig. 34B): this is probably related with the use-dependent Na-channel inhibition that has been observed with the drug.

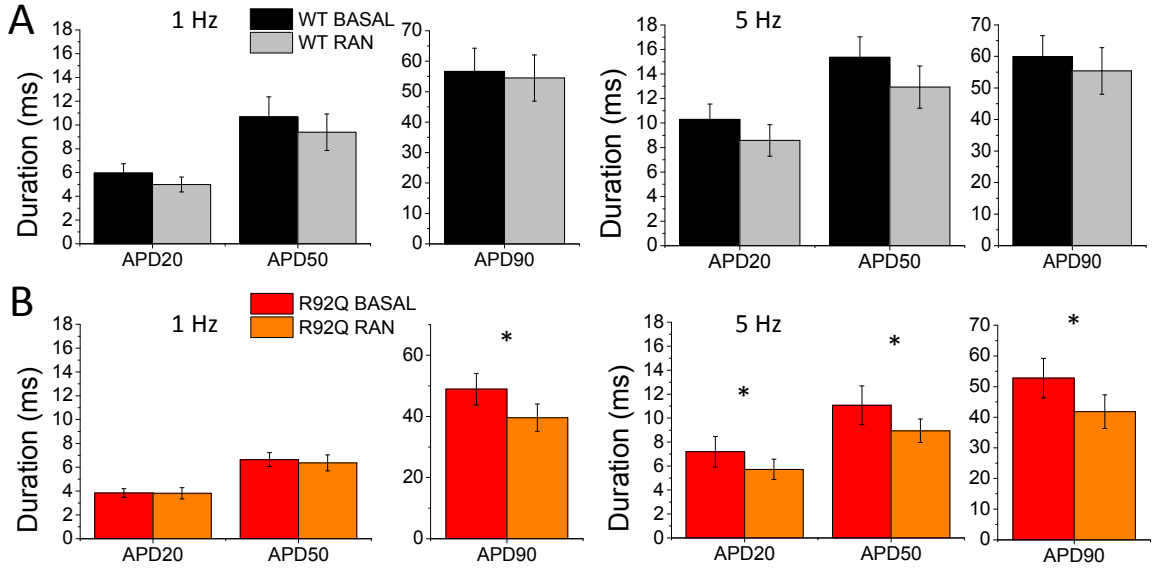

Figure 34: representative graphs of action potential divided in APD20, APD50 and ADP90. A) WT samples compared to the same cells after the application of ranolazine. B) R92Q samples compared to the same cells after the application of ranolazine. *=p<0.05 at paired t-test.

4.2.2 - Analyze the effects of ranolazine in the kinetics and amplitude of Ca^{2+} transients on myocytes from mutant mice

We repeated the previously –shown intracellular Ca experiments (paragraph 4.1.5) and applied ranolazine on single isolated cells from WT and mutant mice. Ranolazine did not alter the normal activity of the cells from WT mouse hearts, as calcium transient amplitude and kinetics were maintained.
Data obtained show that in WT cardiomyocytes, ranolazine did not affect calcium transient properties, at any frequency of stimulation. Also, diastolic calcium concentration was unchanged by the drug (fig. 35).
Instead the application of ranolazine on cells from mutant mice improved the kinetics of calcium fluxes and reduced calcium abnormalities during the diastolic phase.
In particular, the data obtained shown on R92Q preparation showed that ranolazine hastened calcium transient kinetics and reduced diastolic calcium concentration (fig. 36A).
In contrast, in E163R preparation ranolazine did not affect the kinetics of calcium transients, even if it significantly reduced the level of diastolic calcium (fig. 36B).
These results may be related to the efficacy of ranolazine to restore the proper flow of calcium via normalization of intracellular sodium.

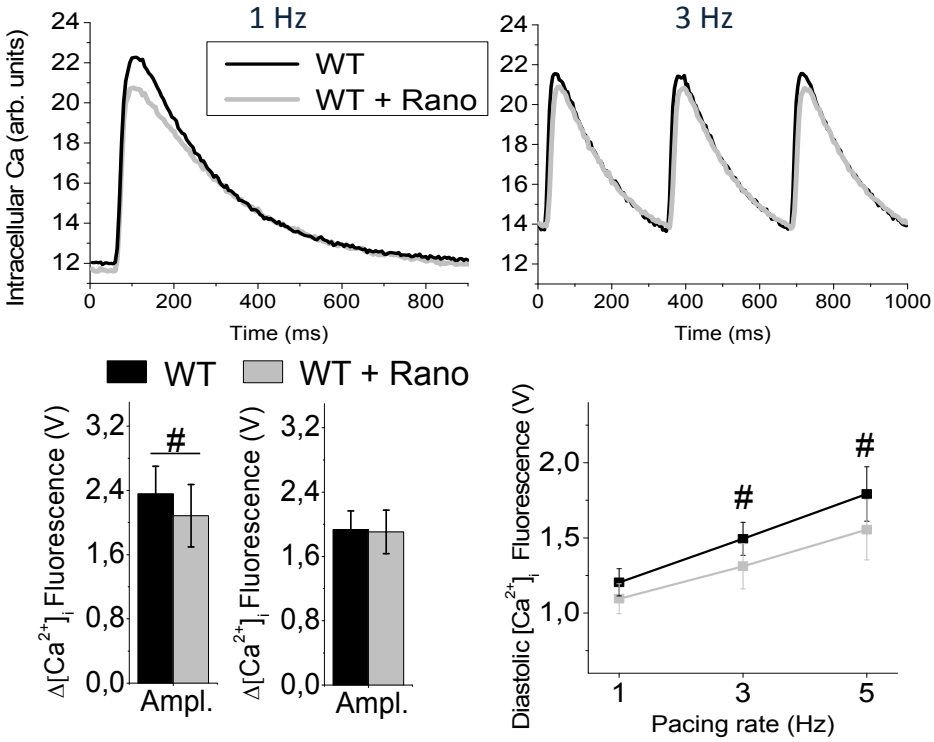

Figure 35: Representative traces and graphs of calcium transient (1, 3 Hz), calcium transient amplitude and diastolic calcium concentration of WT mice compare to the same cells after the application of ranolazine.

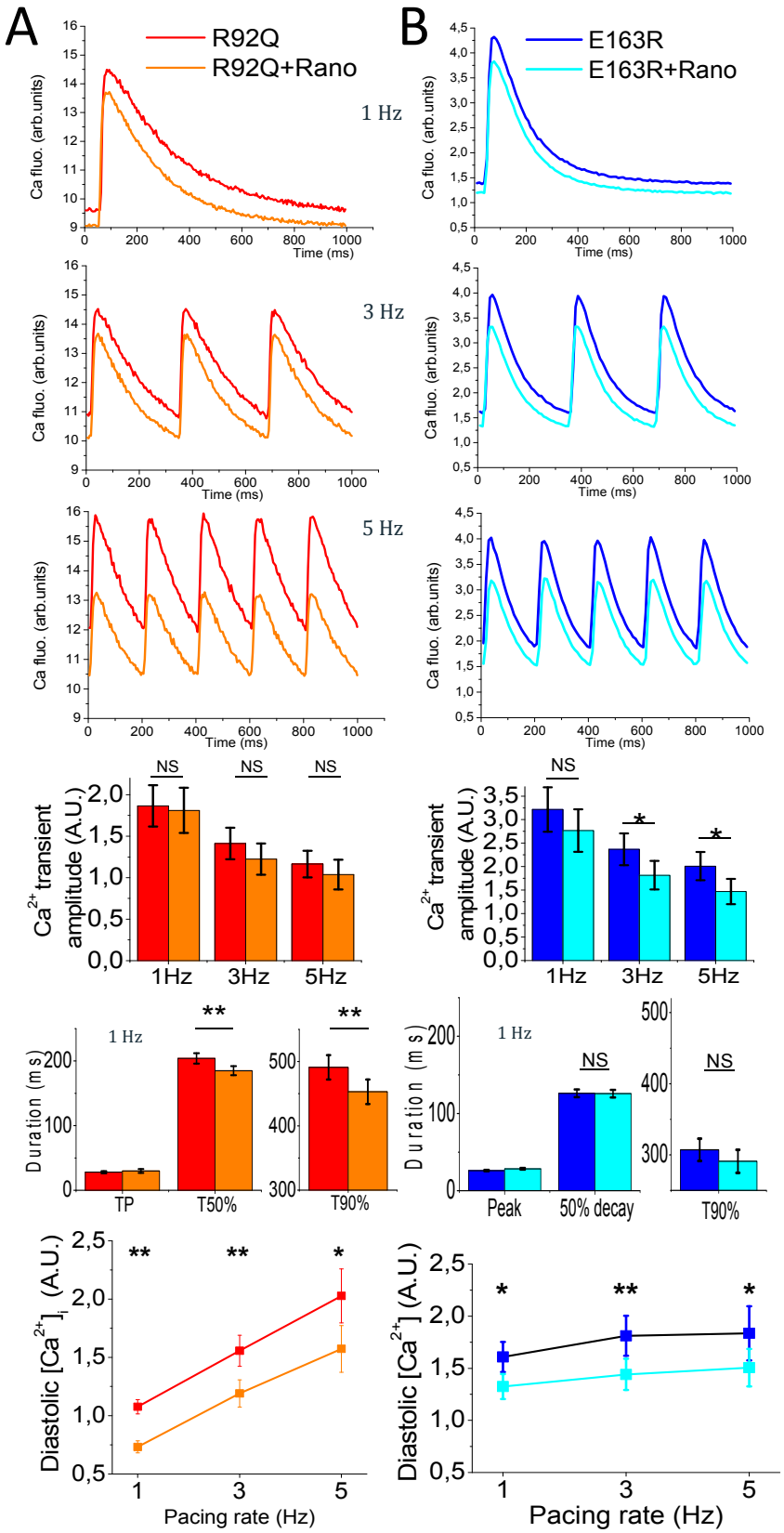

Figure 36: Representative traces and graphs of calcium transient (1, 3, 5 hz), calcium transient amplitude, duration of the transient and diastolic calcium concentration of mutant mice compare the same cells after the application of ranolazine. Column A) R92Q samples; column B) E163R samples.

4.2.3 – Spontaneous calcium release: assessment of arrhythmic events and effects of ranolazine

For the assessment of spontaneous calcium release we used a new protocol, after a strong stimulation at high frequency (5Hz) for single cells and 3-6 Hz for trabeculae, the stimulus is abruptly interrupted and so we can see the spontaneous beats. In single cells, these spontaneous events can be discriminated into calcium waves (i.e. spontaneous calcium release events which did not evoke a contraction of entire cell), and premature peaks (i.e. spontaneous global Ca transients involving the whole cell).
Mutant mice have a higher rate of spontaneous activity, in comparison to WT, evidenced both in single cells and in trabeculae (fig. 37). At the level of single cells, R92Q mice show an increased frequency of spontaneous peaks, while E163R show a higher rate of calcium waves. Trabeculae show a remarkable increase of spontaneous beats during pauses, which is more marked in R92Q preparations.
Moreover, in the presence of β-adrenergic stimulus (isoproterenol 10^{-6} M), the rate of spontaneous events severely increased: both R92Q and E163R showed a comparably higher occurrence of spontaneous events, as compared to WT, unveiling that the effect of Iso was more pronouced in mutant mice than in WT.
The treatment with ranolazine was able to reduce the frequency of the peaks and the spontaneous calcium waves evoked by isoproterenol in both mutant mouse lines. Remarkably, the rates of calcium waves or spontaneous calcium transients in cells, as well as the rate of spontaneous beats in trabeculae, were brought back or even below the baseline levels upon application of ranolazine.
Such results highlight the potential antiarrhythmic role of ranolazine in HCM.

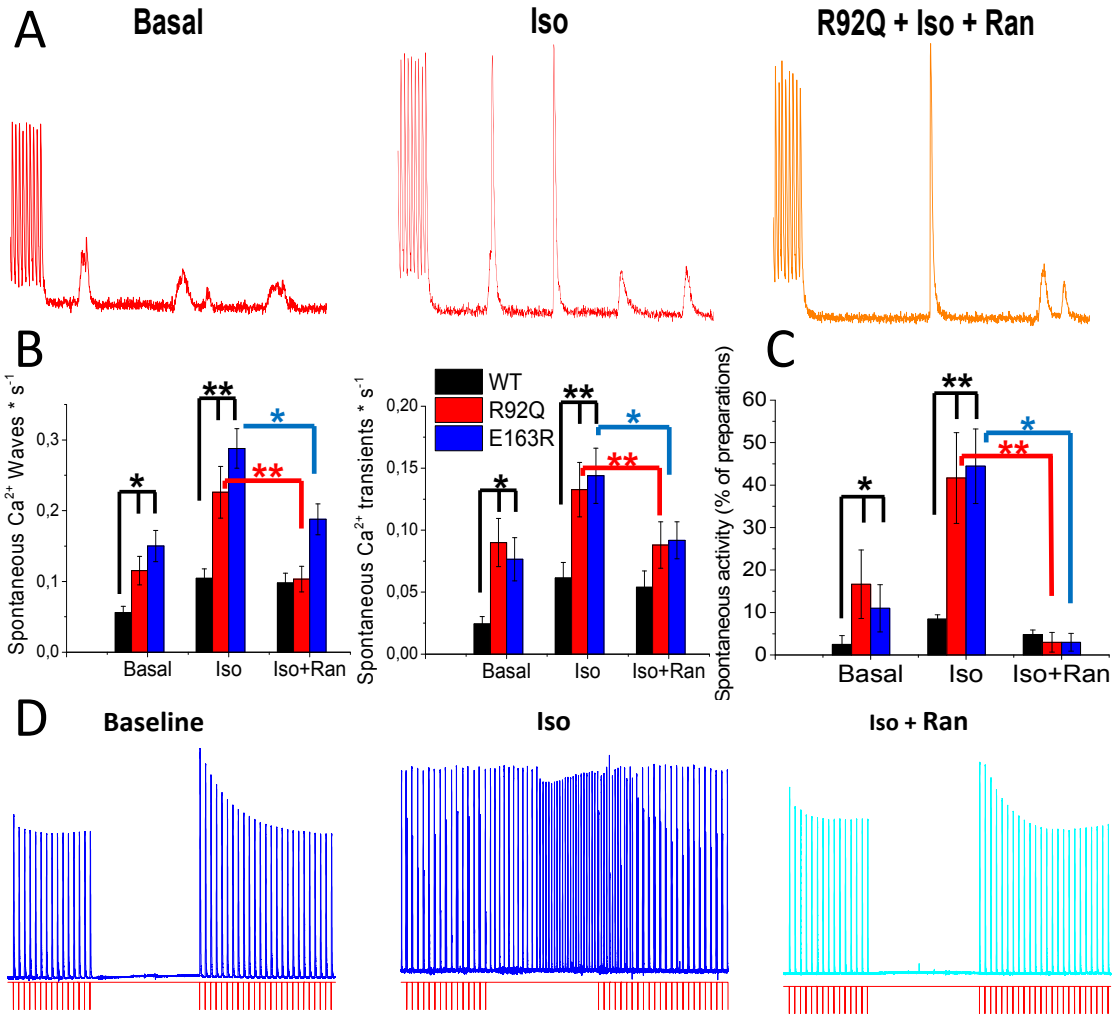

Figure 37: Spontaneous calcium release - arrhythmic events: A) representative traces and graphs of calcium release in cell isolated from R92Q mice (basal condition, Isoproterenol, Isoproterenol and ranolazine); B) spontaneous calcium waves and transients in WT, R92Q and E163R cells (basal condition, Isoproterenol, Isoproterenol and ranolazine); C) spontaneous activity in trabeculae dissected from WT, R92Q and E163R samples and tested in basal conditions, Isoproterenol, Isoproterenol + ranolazine; D) representative graphs of spontaneous activity in E163R trabeculae (basal condition, Isoproterenol, Isoproterenol and ranolazine).

4.2.4 – Conclusions part II

Acute administration of ranolazine in preparations from adult R92Q mice leads to hastened calcium transients, reduced diastolic calcium and abolishes arrhythmic spontaneous activity. As in human HCM, the beneficial effects of ranolazine on R92Q myocardium are likely mediated by the consequences of late sodium current inhibition.
In E163R preparations, myocardial arrhythmogeneicity is not accompanied by remodeling of ion currents and thus appear to be a direct consequence of increased myofilaments calcium sensitivity or anomalies of RyR2 function. Therefore the beneficial effects of ranolazine on calcium mediated spontaneous activity in E163R myocardium supports the hypothesis that the anti-arrhythmic effect of ranolazine can also be mediated by mechanisms other that INaL inhibition (i.e. reduction of myofilaments calcium sensitivity or RyR2 inhibition).
This data confirm that R92Q are the best candidate for a long term treatment with ranolazine.

4.3 - *In vivo* treatment of murine models with ranolazine

4.3.1 – Work plan of treatment

Following the characterizations of TnT mutant mouse models and the assessment of ranolazine *in vitro* effects, we started the phase three of the project: to test the effects of long term *in vivo* administration of ranolazine in mutant mice. We focused only on R92Q mutant mice for obvious economic reasons. In addition, R92Q mice show, in contrast to E163R, a marked hypertrophy, calcium fluxes alterations and other typical features seen in human HCM. Furthermore, the effects of ranolazine, when administrated acutely on cells and trabeculae, were more pronounced in R92Q praparations than in E163R. In fact, ranolazine was able to hasten calcium transients, reduce diastolic calcium and nearly abolished arrhythmic spontaneous activity in R92Q cells and trabeculae. However we may, in the future, repeat the *in vivo* treatment also on E163R mice.
Mice were treated with ranolazine added to their chow; the drug dosage in the chow was selected in order to get the desired plasma levels of the drug (8-15 μM). The half-life of ranolazine in mice is very short, thus ketoconazole was added to inhibit the metabolism of the drug. The combination of 0.5% Ranolazine + 0.03% Ketoconazole mixed in chow has been demonstrated to be effective to get to desired plasma levels of ranolazine for most time of the day (data courtesy of Luiz Belardinelli). R92Q mice, fed with ranolazine-containing chow since birth, were sacrificed at twelve months of age and compared to age-matched untreated mice. Therefore we had a total of 4 treatment branches: treated and untreated WT mice, treated and untreated TnT mutant mice. Since we found no difference between treated and untreated WT mice (data not shown), we will consider just one control group, that is ranolazine-treated WT, for the following experiments.

4.3.2 – Morphological assessment of R92Q mice during treatment with ranolazine

During drug administration we monitored cardiac function through echocardiography in mice of 10/12 months of age. The presented results are from 12 WT, 11 R92Q untreated and 11 R92Q treated mice.
As in the first part of the study (paragraph 4.1.2), the assessment of LV volumes and wall thickness confirmed a severe alteration of cardiac morphology in the untreated mutant mice when compared with controls. R92Q untreated mice, in fact, showed an increased ejection fraction and septal thickness and a significantly higher fractional wall thickening compared to WT. In contrast, 1-year old treated R92Q mice did not show the typical morphological alterations seen in untreated mutant mice. There were no increased ejection fraction and septal dimensions, and fractional wall thickening was at the same levels of WT mice (fig. 38).
Short axis analysis showed a significant effect of the administration of ranolazine in mutant mice. R92Q untreated mice, in fact, in comparison to WT, showed a reduction in the size of the chamber of the left ventricle (i.e. decreased LV end diastolic and end systolic volumes). Instead, R92Q treated mice showed only a slight reduction in the size of the chamber of the left ventricle in comparison to WT (fig. 39).
The analysis of mitral valve flow confirms the presence of diastolic dysfunction in R92Q untreated mice. In fact, the peak A was higher than peak E, the two peaks were fused together and E/A ratio was reduced, when compared to WT.

Instead, in R92Q treated mice the peak A was lower than peak E, the two peaks were usually separated and E/A ratio was only minimally reduced, when compared to WT and was significantly higher than untreated R92Q mice (fig. 40C-D).
Continuing with the analysis, the left atrial size was larger in mutant untreated mice than in WT. While in R92Q treated mice the left atrial size was found similar to WT (fig. 40A-B).
These results suggested that the long-term administration of ranolazine is able to prevent the stiffening of the left ventricle, allowing a normal diastolic function, and therefore also the enlargement of the left atrium that in this way no longer needs to compensate for the left ventricular dysfunction. This was confirmed by the presence of a near normal transmitral flow and by the normal size of the left atrium in R92Q treated mice.
These morphological data showed how the administration of ranolazine since birth reduced the expression of the pathological phenotype in mutant mice. Administration of ranolazine seems to prevent, or at least markedly mitigate, the structural and morphological changes typical of the disease.

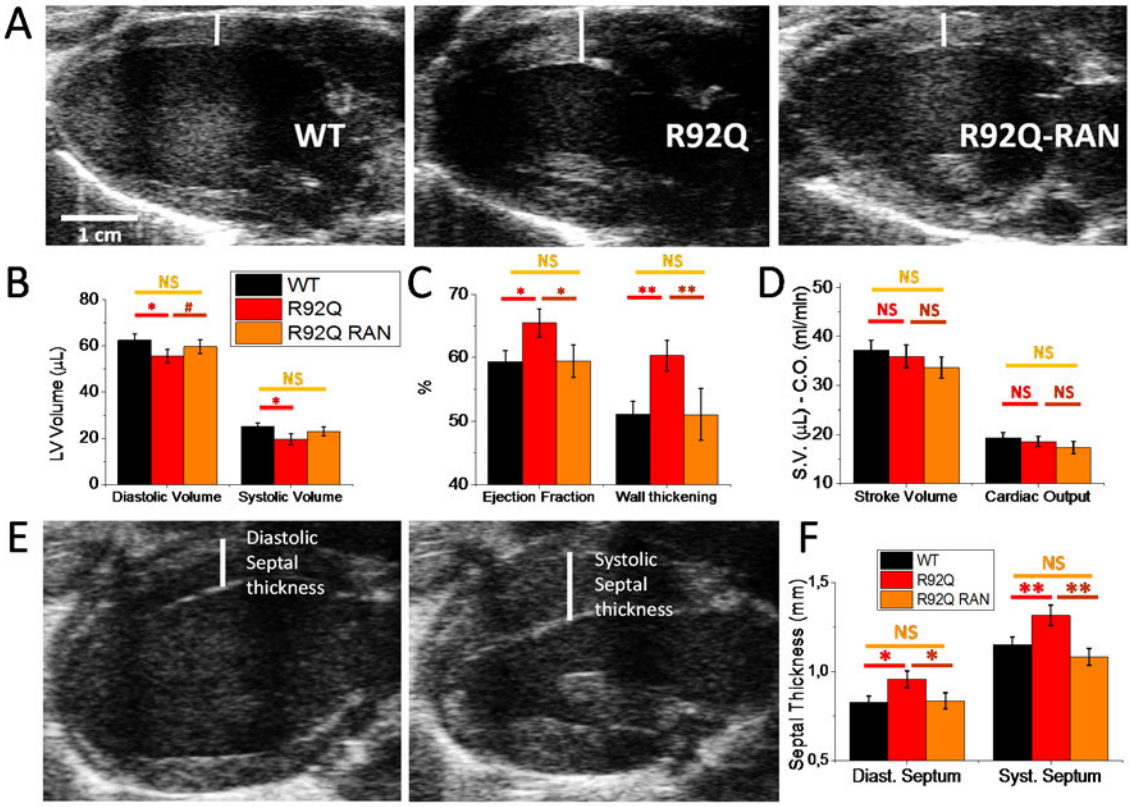

Figure 38: Echocardiographic of LV volumes and wall thickness in R92Q mice during *in vivo* treatment: decreased ejection fraction and septal dimension in R92Q treated mice vs untreated. A) Representative echocardiographic images of parasternal long axis of WT, R92Q untreated and R92Q treated mice. B) Diastolic and systolic LV volume. C) Ejection fraction and wall thickening. D) Stroke volume and cardiac output. E) Representative echocardiographic images of diastole and systole wall thickness. F) Diastole and systole thickness septum. *=p<0.05; **=p<0.01; NS=p>0.05, unpaired t-test.

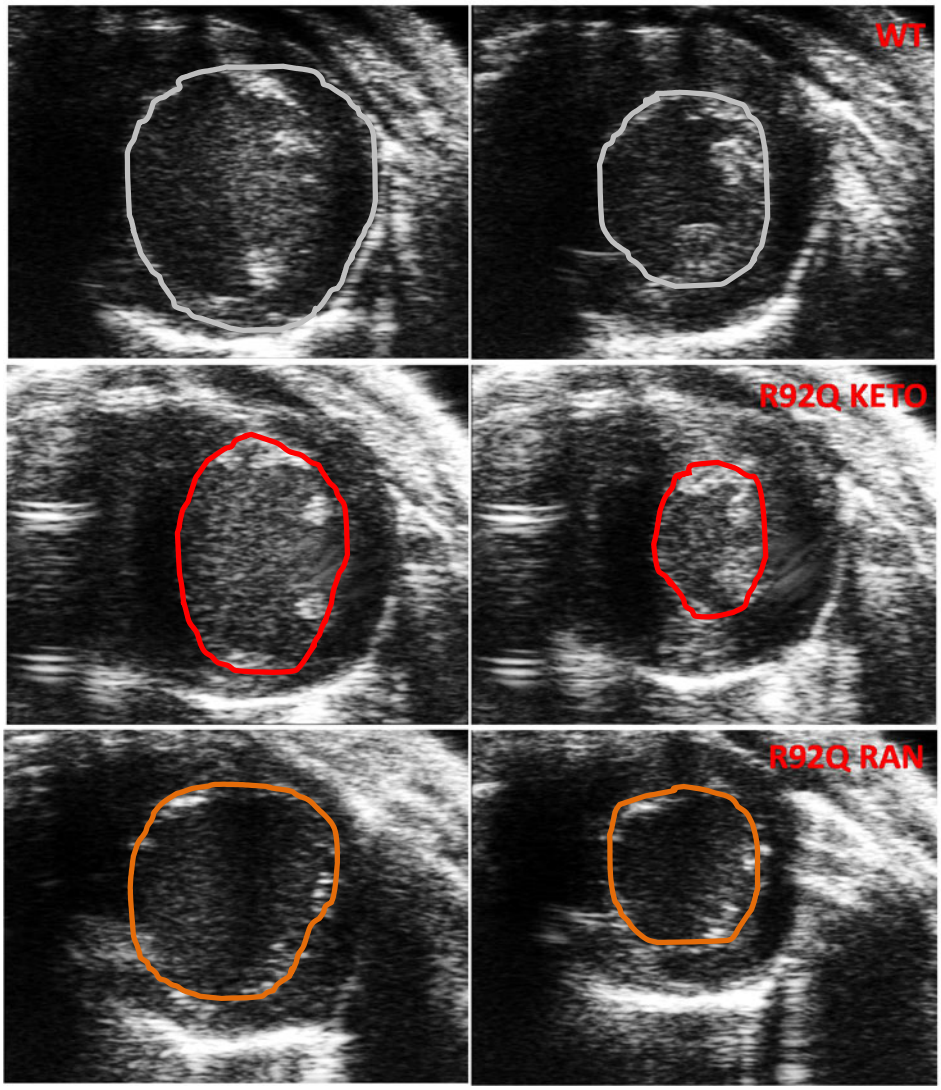

Figure 39: eco short axis during *in vivo* treatment: representative echocardiographic images of short axis (mid-level) in diastole and systole from WT, R92Q Keto (untreated) and R92Q Rano (treated) mice.

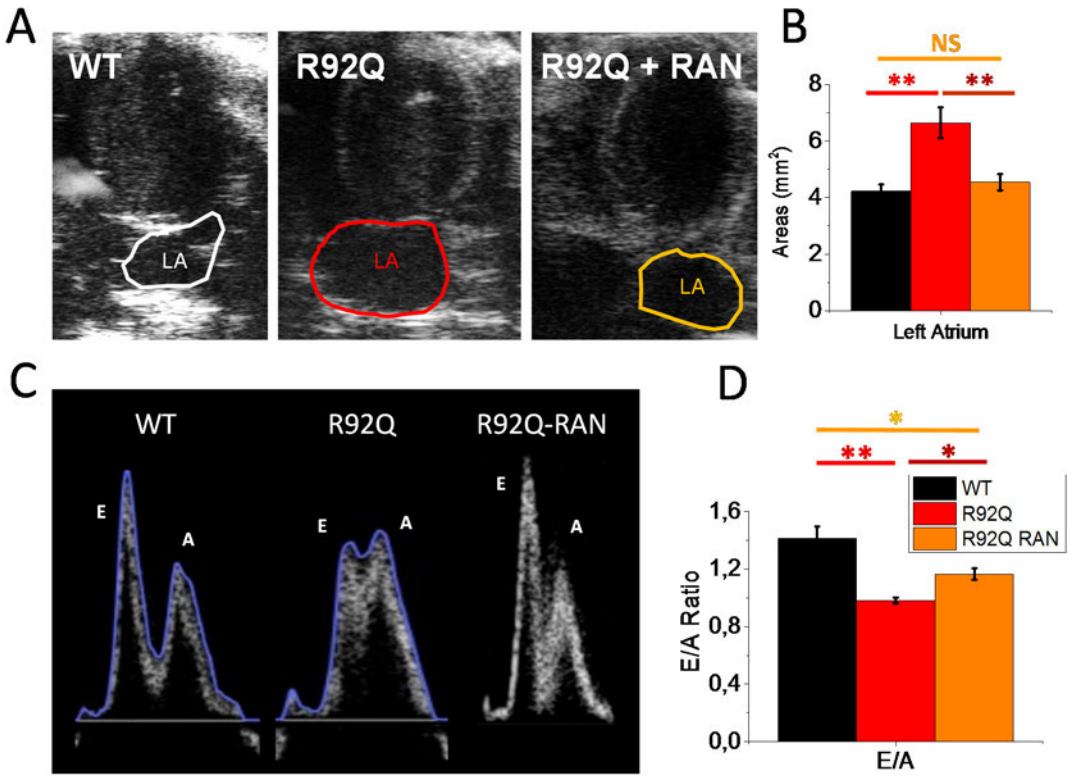

Figure 40: Transmitral blood flow and atrial dimension in R92Q mice during *in vivo* treatment: preventive effects of ranolazine in mutant mice. A) Representative images of atrial dimension of WT, R92Q untreated and treated mice. B) Left atrium areas. C) Representative images of mitral valve flow of WT, R92Q untreated and treated mice. D) E/A ratio of peaks E and A. *=p<0.05; **=p<0.01; NS=p>0.05, unpaired t-test.

4.3.3 - Magnetic Resonance (MRI) assessment

To deepen this field and increase the details on cardiac characterization beyond the ultrasound data, we performed a magnetic resonance imaging in about 24 mice, divided into three groups: WT, R92Q Keto (untreated) and R92Q Rano (treated). Data obtained, as in echocardiography, show the presence of morphological alteration and diastolic dysfunction in mutant mice, and the lifelong administration of ranolazine prevented the onset of these pathological features. In fact, R92Q Keto mice showed a significant reduction of LV cavity diastolic volume and tended to show a reduced volume of the right ventricle as well. Additionally R92Q Keto mice showed a reduction in global left ventricular mass, which is in apparent contrast with the increased septal thickness. However, the reduced mass is in line with the contractured LV that is typical of the restrictive presentation in this model. Finally, RI data confirmed the increase of ejection fraction. On the contrary R92Q Ran treated mice did not show any of the structural changes observed in untrated mice: there was not a reduction of left ventricular diastolic volume, while left ventricular mass was at the same level of WT mice (fig. 41-42).
These data confirm that the administration of ranolazine prevents the structural and morphological changes and significantly reduces the pathological phenotype in mutant mice.

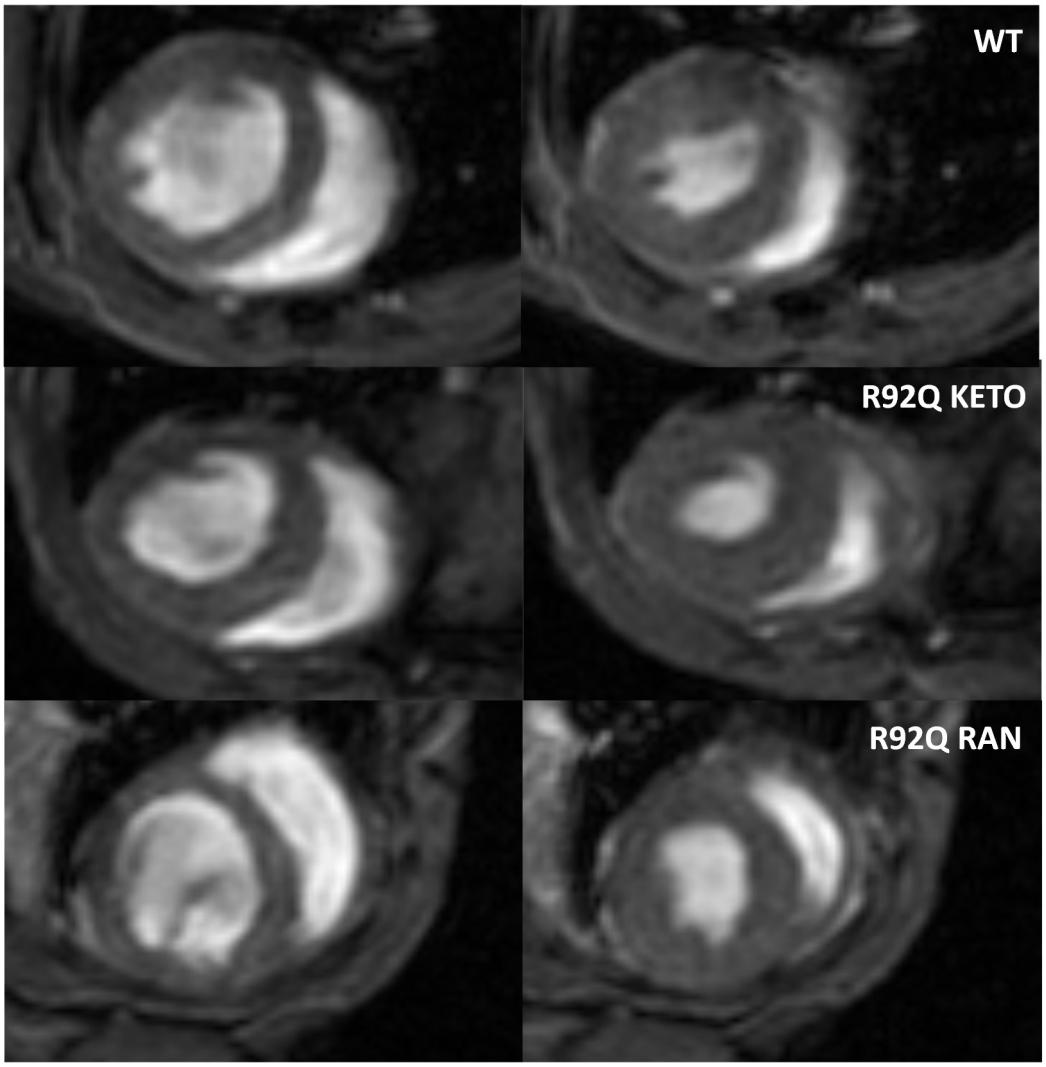

Figure 41: Magnetic Resonance in R92Q mice during *in vivo* treatment: representative images of whole heart through MRI acquisitions in diastole (right column) and systole (left column).

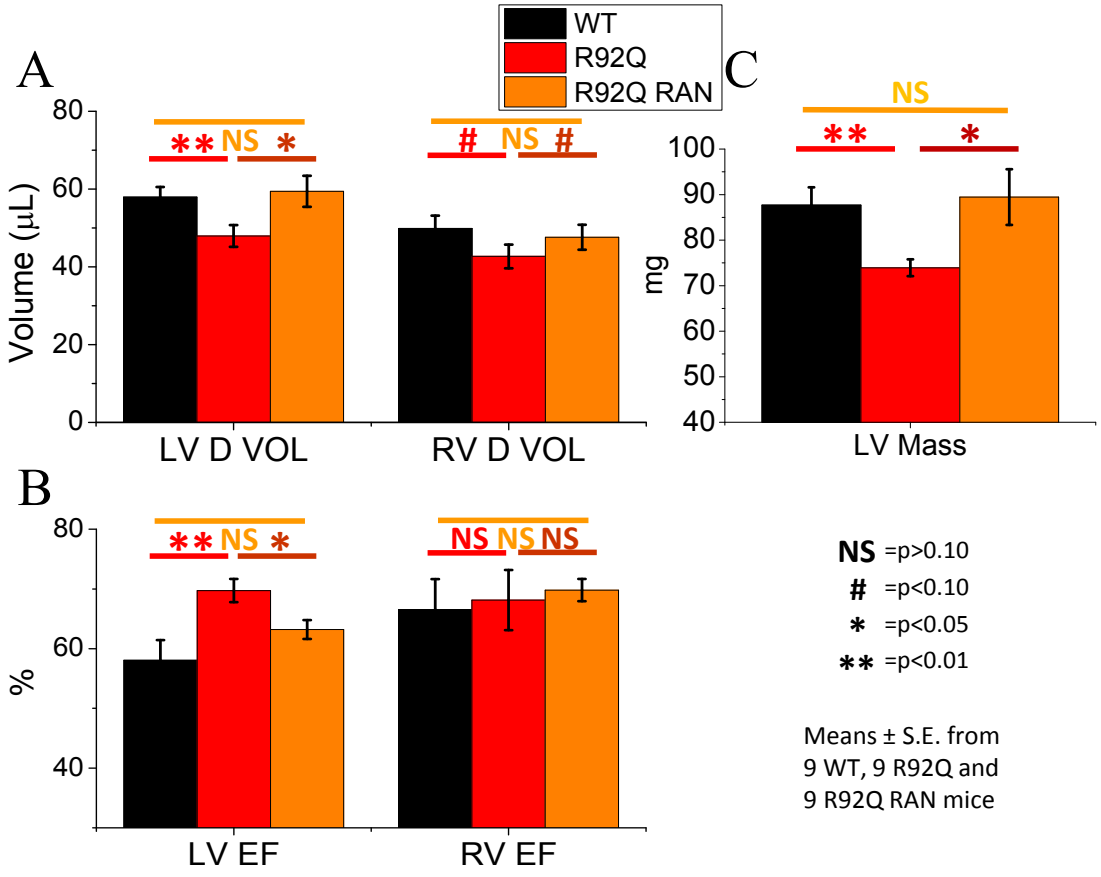

Figure 42: Magnetic Resonance, LV volumes and wall thickness in R92Q mice during *in vivo* treatment: representative graphs of left and right ventricles diastolic volume (A), ejection fraction (B) and left ventricular mass (C).

4.3.4 - Assessment of fibrosis: Gadolinium

The use of MRI has allowed the assessment of the degree of fibrosis in mutant mice with gadolinium diethylenetriaminepentacetic acid administration. Fibrosis was estimated by the fraction of extracellular volume. Data obtained showed that the amount of fibrosis was increased in mutant mice in comparison to WT. R92Q Keto mice, in fact, showed an elevated fraction of extracellular volume, when compared to WT, whereas R92Q Ran mice did not show any increase in the amount of fibrosis (fig. 43).
These results were correlated to the preventive effects of ranolazine that also reduced the formation of fibrosis alongside the other morphological abnormalities that are typical of HCM in R92Q mice.

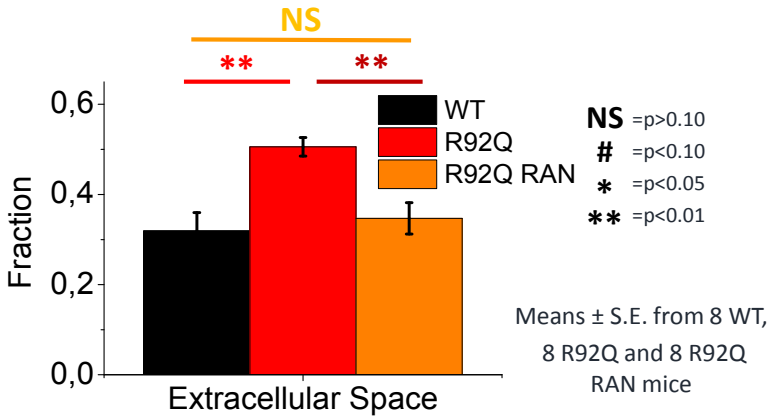

Figure 43: Magnetic Resonance and assessment of Gadolinium: representative graphs of assessment of fibrosis by the administration of Gadolinium.

4.3.5 - Assessment of structural alterations: confocal microscopy

To improve the data on the structural alterations we performed some confocal microscopy acquisitions. After cell isolation, the cells were incubated for 20 minutes with 5 µl/mL of [Di-4-AN(F)EPPTEA], a selective membrane dye. We used a similar method for imaging of intact cardiac tissue (10 µl/mL of dye and incubated for 30 minutes). By staining the membranes, the purpose of this analysis is to assess alterations of the organization of the t-tubule system within the myocytes. Cardiac diseases, including HCM in humans, have been associated with various degrees of t-tubular alterations.
Data obtained show that cells of mutant mice seem to be more affected compared to WT. The organization of the tubules was in fact altered: in particular the number of cells showing disorganized t-tubules that lost the regular spacing and transverse organization and rather appeared to be tangled and longitudinally extending. Although a proper quantitative analysis was not performed, qualitative analysis show that the incidence of damaged cells was higher in R92Q Keto samples compared to R92Q Rano samples. In fact, the number of cells showing a partial disruption of the t-tubular system was markedly lower in treated mice (fig. 44-45). Data from intact tissue confirmed this observation (Fig. 46)

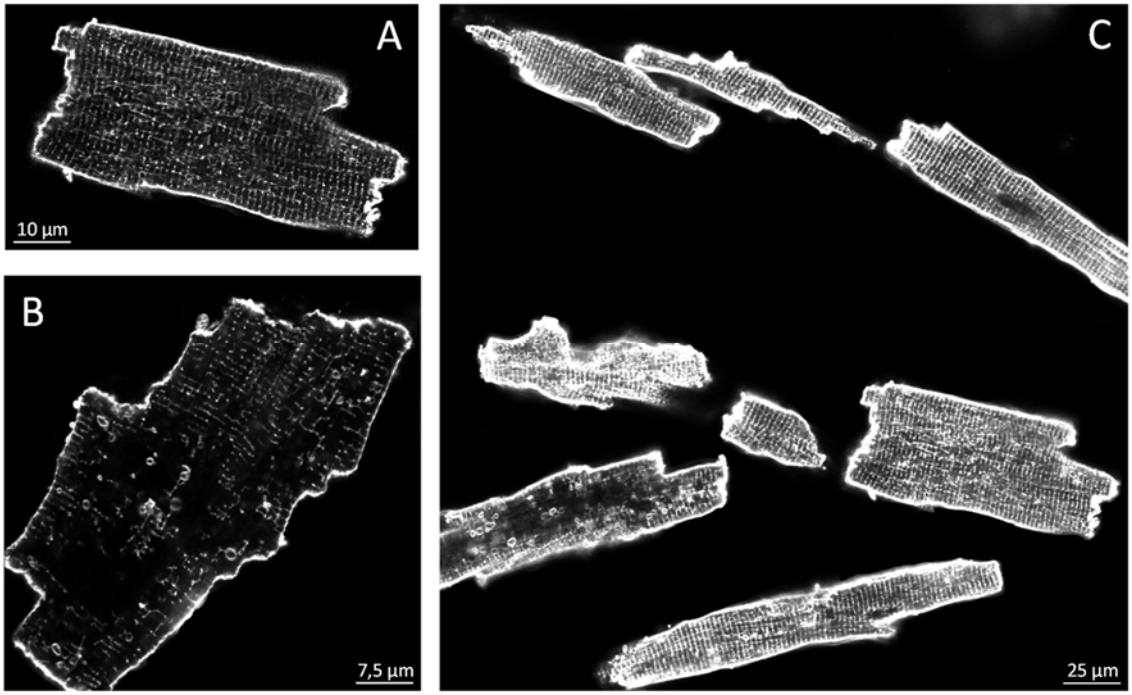

Figure 44: confocal microscopy: representative images of cardiomyocyte isolated from R92Q Keto mice. A-B) single cell; C) group of cells.

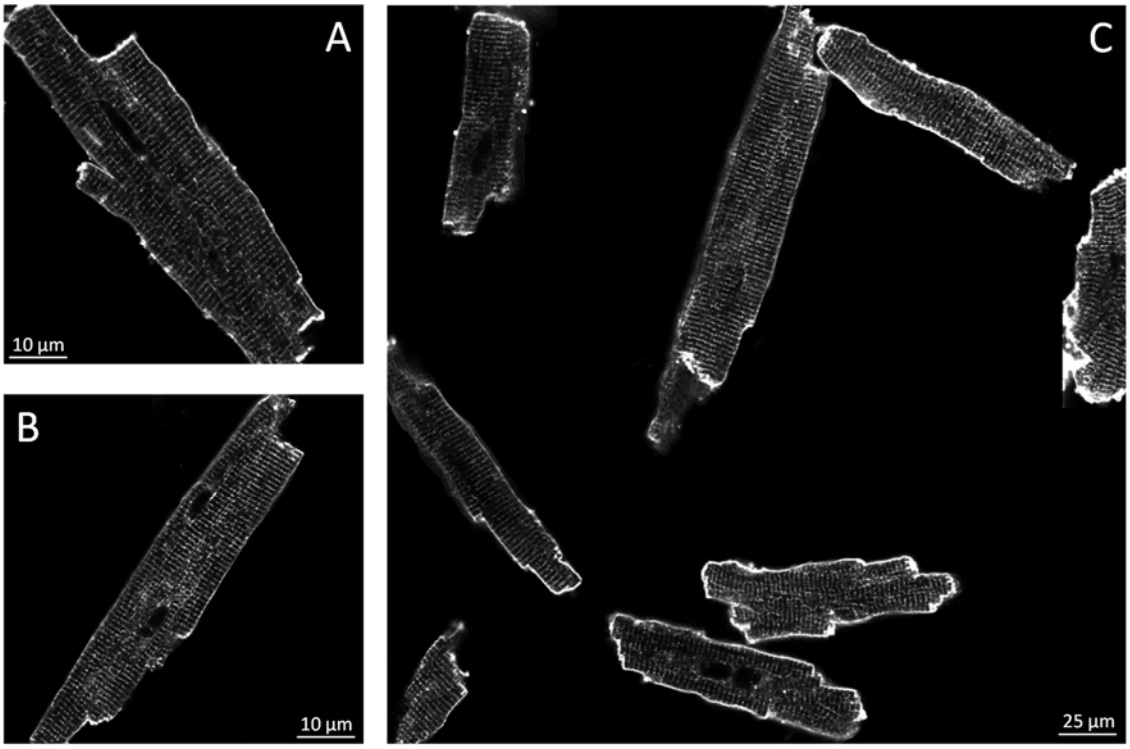

Figure 45: confocal microscopy: representative images of cardiomyocyte isolated from R92Q Rano mice. A-B) single cell; C) group of cells.

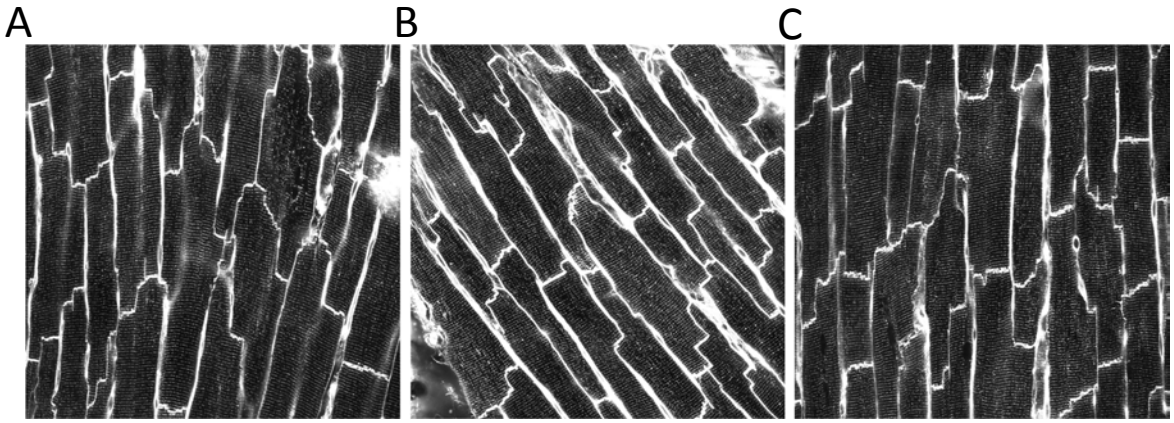

Figure 46: confocal microscopy: representative images of tissue from R92Q Keto (A-B) and Rano (C) mice.

4.3.6 - *In vivo* effect of ranolazine, kinetics and amplitude of Ca^{2+} transients

At the same time point (twelve months of age) mice were sacrificed and, after heart excision and cell isolation, cardiomyocytes were loaded with Fluoforte for intracellular Ca^{2+} measurements (see paragraph 4.2.2).
Data obtained confirm that R92Q Keto (untreated) mice, compared to WT, showed the presence of a slower rate of decay of calcium transients, lower transient amplitude and elevated diastolic calcium. Instead the administration of ranolazine in R92Q mice was able to prevent the alterations of the kinetics of calcium fluxes and of diastolic Ca concentration. In particular, data obtained shown on R92Q Ran (treated) cells show that the calcium transient kinetics was faster and diastolic calcium was lower, when compared with R92Q untreated mice (fig. 47A). Moreover, the amplitude of Ca transients was higher in treated mice than in untreated. Interestingly, the kinetics and amplitude of Ca fluxes in R92Q Ran mice did not show any differences from those of WT cells. The duration and the amplitude of calcium transient were similar to WT preparations, as was the diastolic Ca concentration (fig. 47B-C-D). The life-long administration of ranolazine prevented the development of the anomalies of calcium flow and thus reduced the progression of the disease. The ameliorated Ca transient decay kinetics and the lower diastolic Ca may play a role in the ameliorated diastolic function observed in treated mice.

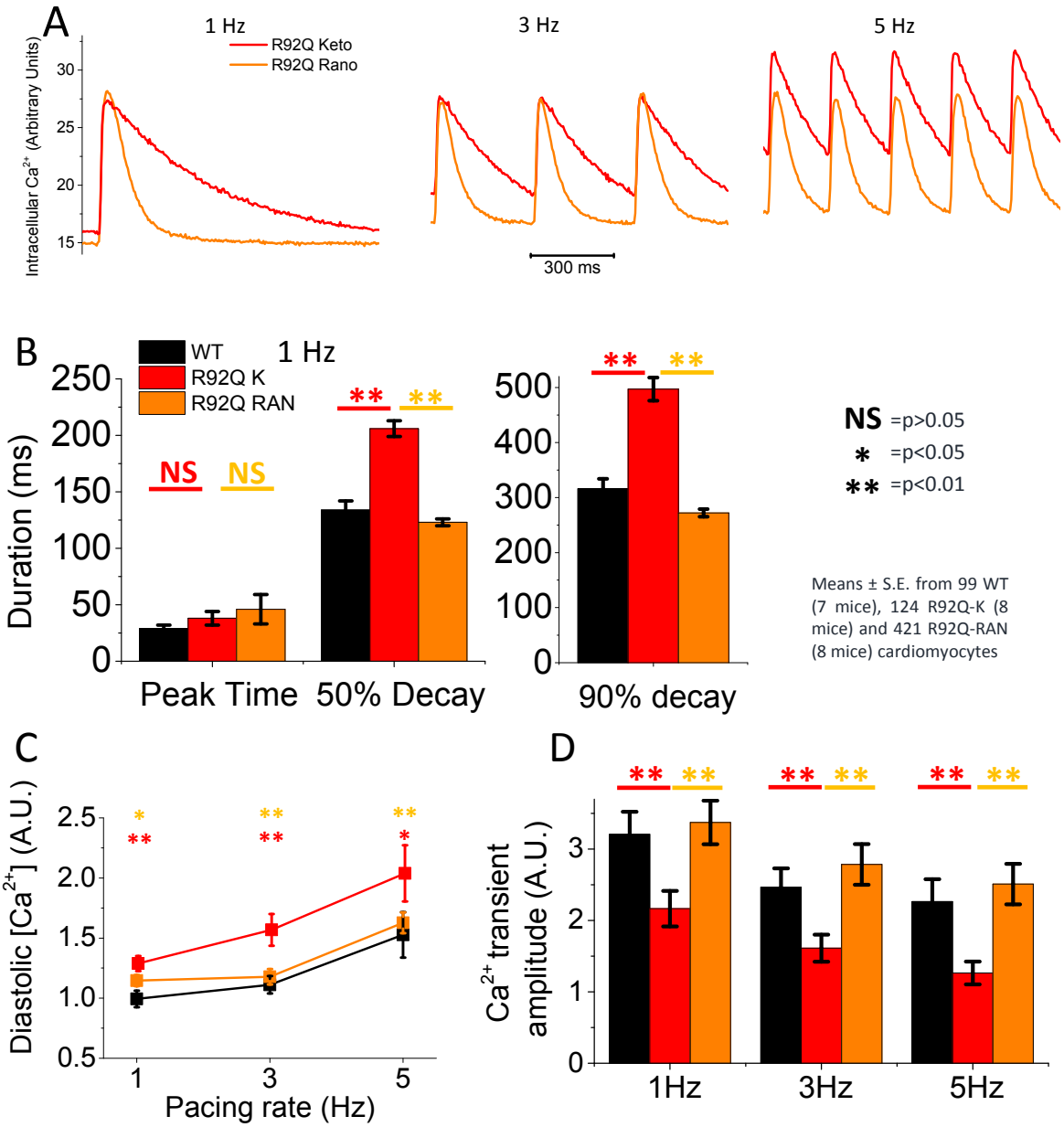

Figure 47: Effects of life-long treatment with ranolazine on calcium transient: A) Representative graphs of calcium transient of R92Q Keto mice compare to R92Q Rano mice. B) Duration of calcium transient (1 Hz) (Time to peak, 50% and 90% of decay). C) Diastolic calcium concentration (pacing rate 1, 3, 5 Hz). D) Calcium transient amplitude (1, 3, 5 Hz).

4.3.7 - Effects of life-long treatment with ranolazine on trabeculae

In figure 48**,** panel A shows superimposed representative twitches at 1Hz from WT, R92Q untreated and R92Q treated trabeculae. Panel B shows the relationship between isometric twitch tension and stimulation frequency in WT, R92Q and R92Q RAN trabeculae. In R92Q compared to WT we observed a significant reduction of twitch tension at high pacing rates (stimulation frequency > 4Hz). Long-term treatment with Ranolazine prevented the contractile impairment at high stimulation frequencies, restoring twitch tension to WT levels.

The kinetics of relaxation was prolonged in R92Q mice compared to control. Treatment with ranolazine did not prevent the prolongation of twitch relaxation time, which was found prolonged in treated mice, without any differences from the untreated group (Panel C).

Then we assessed the response to ionotropic stimuli, i.e. acute administration of Isoproterenol 10^{-7}M (Iso), and stimulation pauses (fig. 48**,** panel D). Twitch tension under Iso was significantly blunted in R92Q trabeculae compared to WT (tension was 30.1±9.6 vs 74.5± 5.7 mN/mm^2, respectively, $p<0.05$). Long-term treatment with Ranolazine restores the positive inotropic response to Iso (tension was 79.6±16.2 mN/mm^2 in R92Q RAN trabeculae, n.s. vs WT, $p<0.05$ vs R92Q).

In both WT, R92Q and R92Q RAN trabeculae mean isometric twitch tension increased in post-rest contractions, with no significant differences between the three groups. Notably, at variance with younger mice (Pioner et al. Biophysical Journal 2014, Abstract), active tension developed after 60s pause was not reduced in trabeculae from 1 year-old R92Q mice.

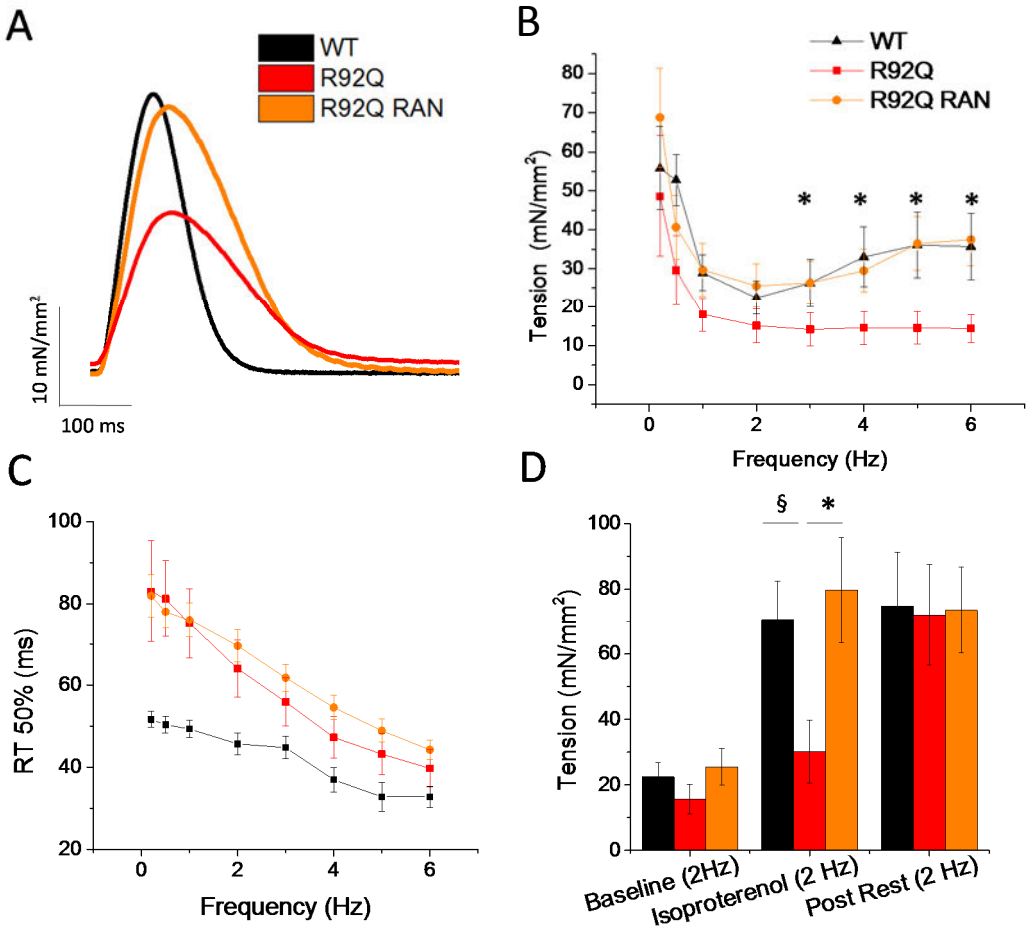

Figure 48: Effects of life-long treatment with ranolazine on isometric twitch tension. (A) Representative force traces recorded from intact trabeculae of WT, R92Q and R92Q treated with ranolazine (R92Q RAN) mice. (B) Relationship between steady state twitch amplitude and pacing frequency in intact trabeculae from WT (N=6, n=9), R92Q (N=8, n=11) and R92Q RAN (N=6, n=9) mice. N= number of animals, n=number of trabeculae. (C) Relationship between 50% relaxation time and pacing frequency from the same trabeculae as in (C). (D) Mean±SEM data of twitch tension under two inotropic stimuli: Isoproterenol 10^{-7} mM and resting pauses. Tension is expressed as a percentage of baseline steady state tension at 2 Hz. § indicates $p<0.05$ for R92Q vs WT, * indicates $p<0.05$ for R92Q RAN vs R92Q.

We then evaluated the occurrence of spontaneous beats during stimulation pauses at basal conditions and in presence of isoproterenol (fig. 49). Interestingly, the percentage of preparations showing spontaneous contractions during pauses in the presence of Iso was higher in R92Q untreated mice as compared with controls. The rate of spontaneous beats was instead in the same range as controls in R92Q treated mice. This shows that life-long ranolazine treatment is able to reduce the tendency to develop arrhythmias in the myocardium of affected mice.

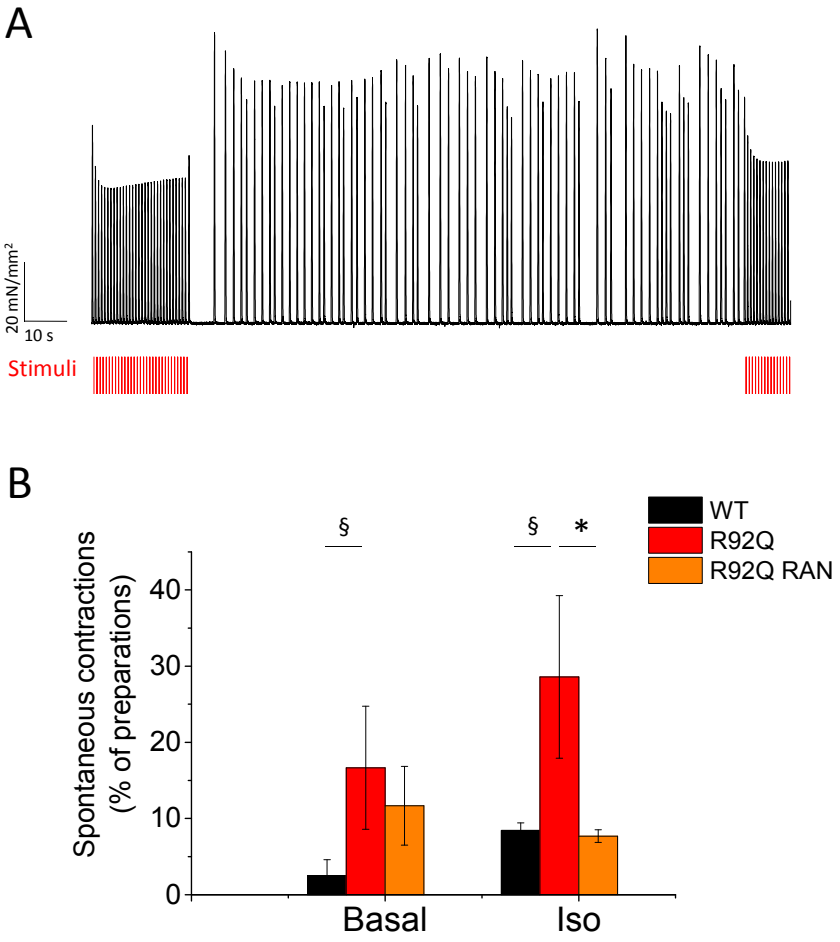

Figure 49: Effects of life-long treatment with ranolazine on isometric spontaneous activity.
(A) Representative traces from an R92Q trabecula showing an example of spontaneous activity during pauses. Short red lines indicate the times of stimuli. In this case the spontaneous activity is present in the form of multiple irregular premature contractions. (B) Mean±SE values of the global occurrence of spontaneous activity during pauses in in intact trabeculae from WT (N=6, n=9), R92Q (N=8, n=11) and R92Q RAN (N=6, n=9) mice. N= number of animals, n=number of trabeculae. § indicates $p<0.05$ for R92Q vs WT, * indicates $p<0.05$ for R92Q RAN vs R92Q.

4.3.8 – Spontaneous calcium release: effects of administration of ranolazine on arrhythmic events

For the assessment of spontaneous calcium release we used the same protocol of paragraph 4.2.2. After a rapid stimulation the stimulus is interrupted and so we can see the spontaneous beats. The data obtained confirms that R92Q Keto (untreated) mice have high spontaneous activity, in comparison to WT, both in singles cells and in trabeculae. Also, in presence of isoproterenol the rate of spontaneous events was even more increased. Instead the administration of ranolazine in R92Q mice was able to prevent the development of such arrhytmogenic potential. Indeed, cells from R92Q treated mice had a low frequency of spontaneous Ca transients and spontaneous calcium waves, in particular after β-adrenergic stimulation with isoproterenol. In fact, R92Q Ran (treated) mice showed a reduction of spontaneous calcium waves and the frequency of spontaneous transients was nearly abolish, showing a behavior that was not different from WT cells. Also the application of isoproterenol induced a smaller increase of spontaneous activity in R92Q treated cells, in line with WT cells (fig. 50).

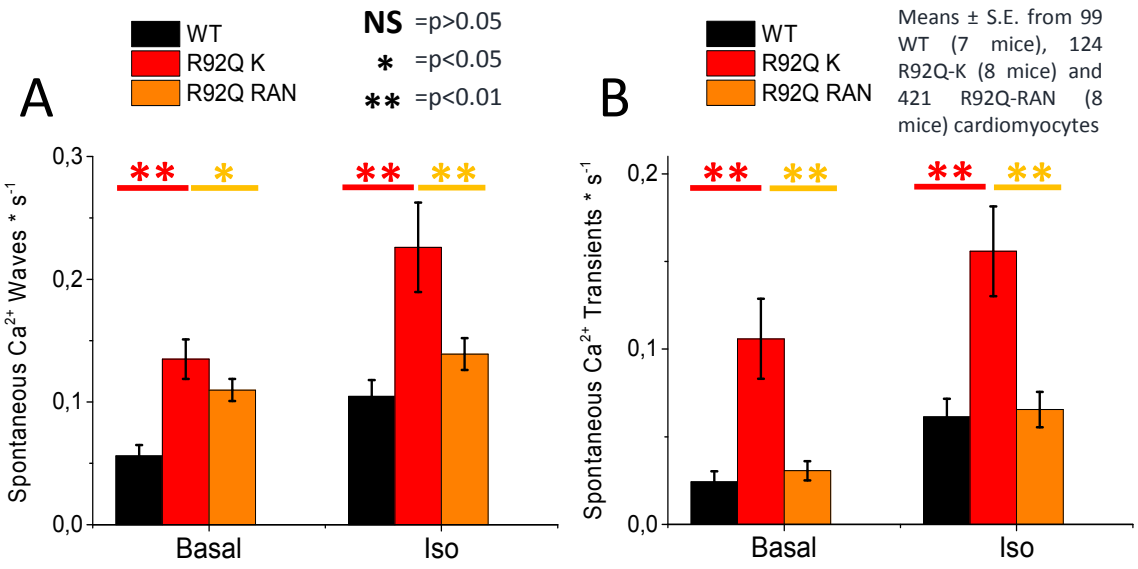

Figure 50: Effects of life-long treatment with ranolazine on spontaneous calcium release: representative graphs of spontaneous calcium waves (A) and peaks (B) of R92Q Keto and R92Q Rano mice compare to WT.

4.3.9 - Identification of the molecular substrate of the functional alterations: transcriptional modification of ion channels and ranolazine effects

On the basis of electrophysiological and mechanical data, experiments of RT-PCR were focused on investigating the possible alterations of genes that encode essential proteins in E-C coupling. We started with Serca (ATP2A2), the pump that mediates the transport of calcium from the cytoplasm to the sarcoplasmic reticulum, its regulator phospholamban (PLN), Sodium-calcium exchanger (NCX), the antiporter membrane protein that removes calcium from cells, and Ryanodine receptor (Ryr2), calcium channel that mediates the release of Ca^{2+} from the sarcoplasmic reticulum. Data obtained show a statistically significant reduction of the gene ATP2A2 and a tendency towards an increased PLN expression in R92Q Keto mice compared to WT. This was correlated to the progression of the disease and the alteration of calcium fluxes. The lifelong administration of ranolazine in R92Q Rano mice prevented the decrease of ATP2A2 gene, which was similar to WT (fig. 51A-B). Instead the expression of the gene NCX was not altered between WT and mutant mice and also the administration of ranolazine did not affect its expression (fig. 51C). Further, the expression of the gene RyR2 was not altered (fig. 51D).

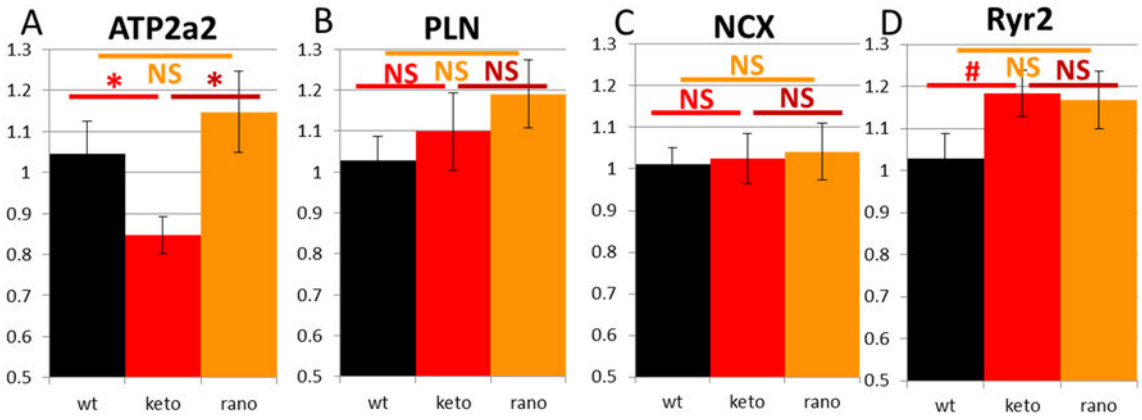

Figure 51: qRT-PCR: A) Serca (ATP2A2); B) phospholamban (PLN); C) Sodium-calcium exchanger (NCX); D) Ryanodine receptor (Ryr2).

Then we investigated ion channel genes likes Kchip2 and Kv4.3 genes, the main and auxiliary subunit, respectively, of the channels that mediate the transient outward potassium current, important determinant of the duration of the action potential, and Cacna1 (calcium channel, voltage-dependent, P/Q type, alpha 1A subunit) the voltage-dependent calcium channels that mediate the entry of calcium ions into the cell. Graphs showed an alteration of potassium channel, in fact, Kchip2 resulted decrease and Kv4.3 increased in R92Q Keto mice compared to WT. Conversely, R92Q Rano mice showed that the expression levels of Kchip2 and Kv4.3 remained comparable to WT (fig. 52A-B). Besides, the expression of the gene Cacna1 was unchanged in both R92Q Keto and R92Q Rano mice (fig.52C).

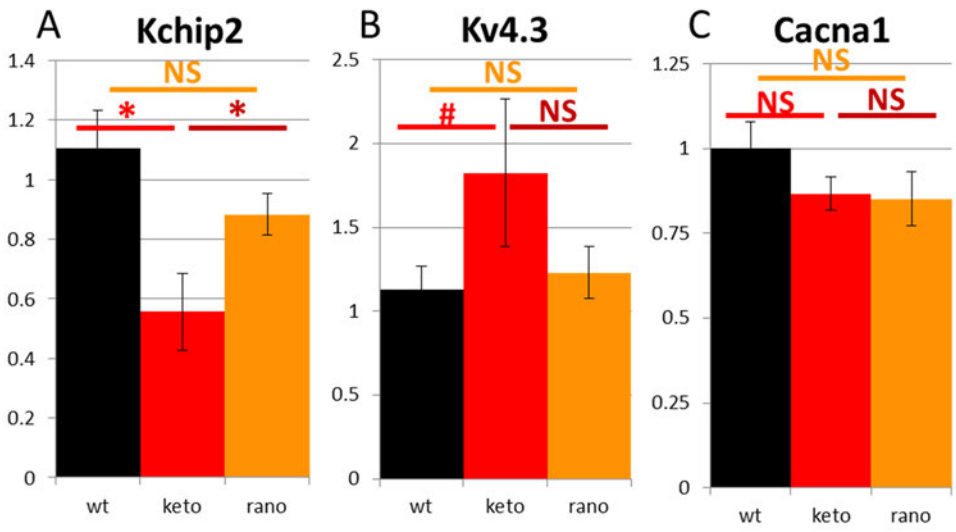

Figure 52: qRT-PCR: A) Kchip2, the main subunit of potassium channel; B) Kv4.3 the auxiliary subunit of potassium channel; C) Cacna1 (calcium channel, voltage-dependent, P/Q type, alpha 1A subunit).

After we analyzed Brain Natriuretic Peptide (BNP), a member of the natriuretic peptide family and encode a protein that functions as a cardiac hormone, and Atrial Natriuretic Peptide (ANP), implicated in the control of extracellular fluid volume and electrolyte homeostasis. Compare to WT, in R92Q Keto mice these genes were significantly increased, while the administration of ranolazine reduce these increases. In fact, R92Q Rano mice showed did not show any increase of BNP and showed a mild increase of ANP in comparison to WT; however, the expression of both genes was much lower than in R92Q untreated mice (fig. 53A-B).

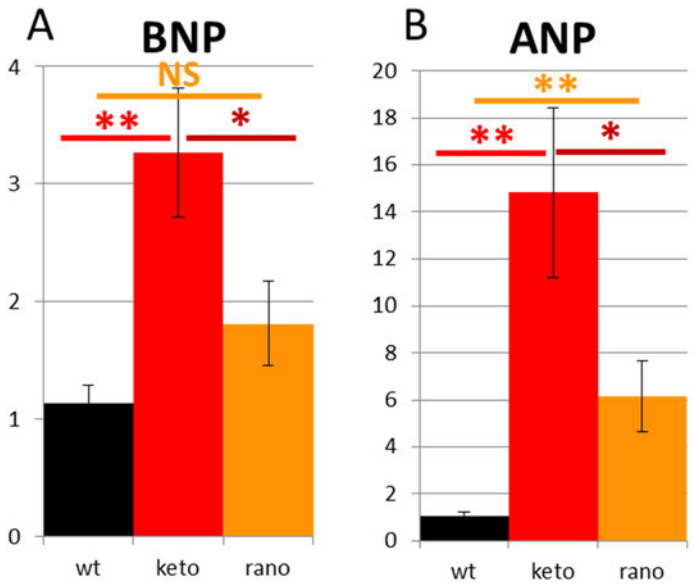

Figure 53: qRT-PCR: A) Brain Natriuretic Peptide (BNP); B) Atrial Natriuretic Peptide (ANP).

Furthermore, we investigated the expression of the genes Myh6, gene that gene encodes the alpha heavy chain subunit of cardiac myosin, and Myh7, gene encoding a myosin heavy chain beta (MHC-β) isoform. Myh7 genes resulted significantly increased in both R92Q Keto and R92Q Rano mice, compared to WT. MyH6 gene was mildly increased in R92Q treated mice. The administration of ranolazine did not inhibit the increase in expression of Myh6 during the progression of the disease (fig. 54A-B). Notably, alpha myosin is the prevailing isoform in mouse ventricles and is faster. Beta myosin is slower but uses less ATP. The persistent of beta myosin overexpression in treated mice may explain the persistence of a slower twitch relaxation in treated trabeculae, despite the faster calcium transient.
As a last thing we evaluated the expression levels of TGF-β gene, a marker of inflammation and fibrosis. In R92Q Keto mice, compare to WT, this gene resulted significantly increase. Instead, in R92Q Rano mice this gene result increased in comparison to WT, and tended to be decreased in comparison with R92Q Keto mice (fig. 54C). This result was correlated to the efficacy of ranolazine to prevent the main features of the disease and thus reduce the onset of fibrosis.

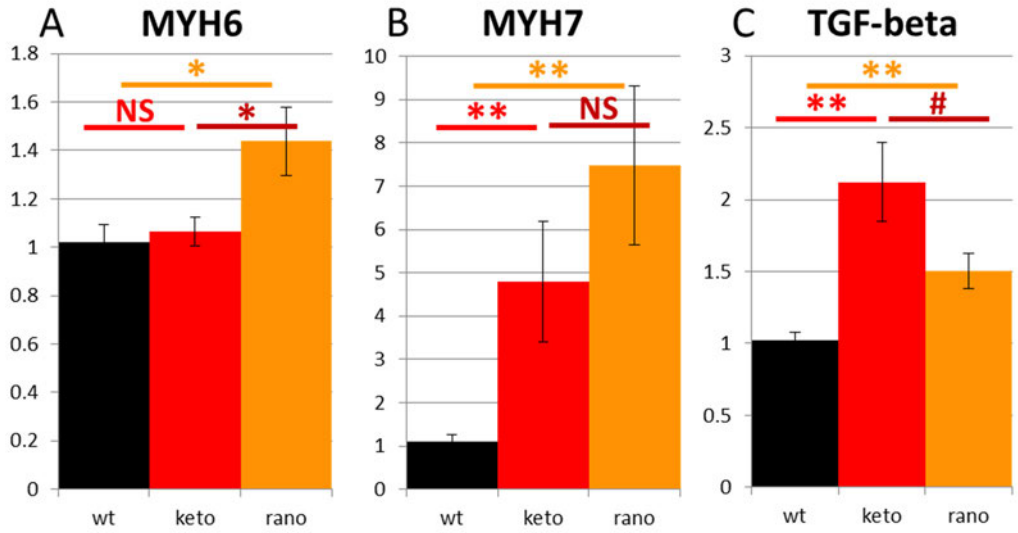

Figure 54: qRT-PCR: A) myosin heavy chain alpha (Myh6); B) myosin heavy chain beta (Myh7); C) Tissue grow factor beta (TGF-β).

4.3.9 - Conclusion part III

Ranolazine, administered since birth in R92Q, leads to a significant reduction of phenotype expression in mice. Treated mice show less hyper-contractility, reduced LV wall thickness and less diastolic dysfunction, as compared with age-matched untreated mice. Also correct calcium flow was maintained, in fact, in R92Q Ran mice, ranolazine hastened calcium transient kinetics and reduce diastolic calcium. In addition, arrhythmic events were nearly abolished.
In conclusion, data obtained demonstrate that the administration of ranolazine reduce the progression of the disease and prevent pathological phenotype in mutant mice.
Ranolazine, thanks to its remarkable safety profile, may be a candidate drug to be employed in HCM mutation carriers to prevent phenotype onset and/or disease progression.

Chapter 5: SUMMARY AND DISCUSSION

In HCM, primary functional alterations at sarcomere level (Belus et al, 2008) are associated with secondary modifications in Ca^{2+} handling and E-C coupling, leading to remodelling of the cardiomyocyte (Coppini et al, 2013). The relative contribution of primary vs secondary alterations is still unknown and the molecular bases of this adaptive/maladaptive remodeling are still poorly understood. However we do know that the secondary changes occurring in diseased HCM myocardium cause electrophysiological remodelling and alterations of calcium and sodium fluxes that ultimately are responsible for diastolic dysfunction and ventricular arrhythmias in HCM patients.

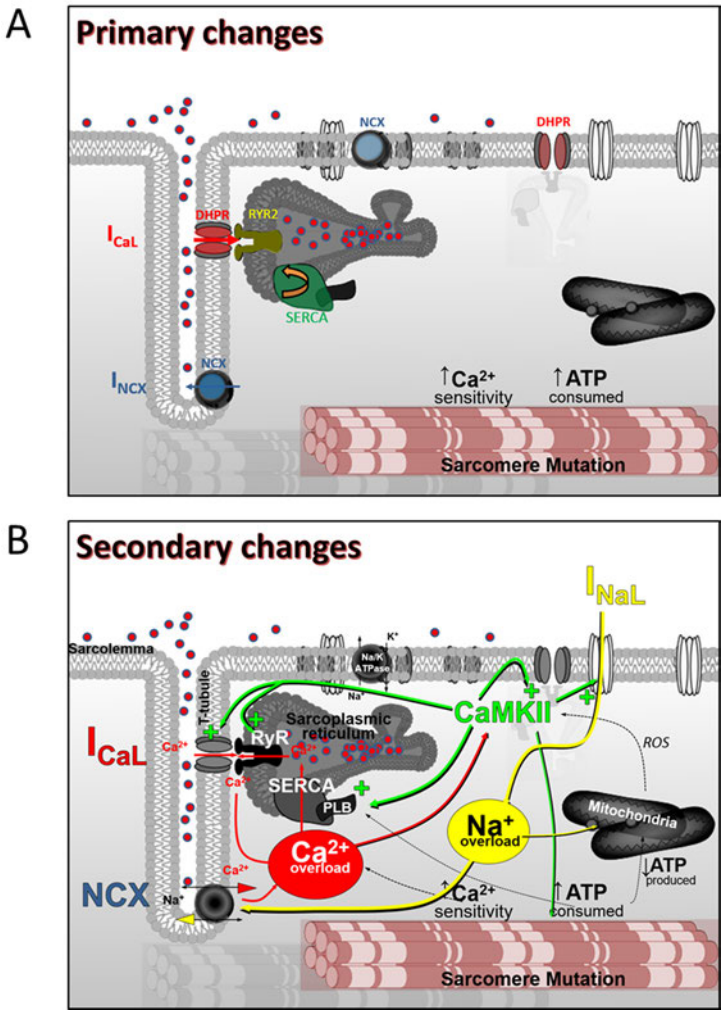

Fig : Primary and secondary changes in HCM myocardium. (A) Sarcomeric mutations may cause direct alterations in sarcomeric function: increased sarcomeric ATP consumption and enhanced myofilament Ca^{2+} sensitivity could together trigger a secondary adaptive/ maladaptive cellular remodeling. (B) The energy depletion at sarcomeres levels may lead to SERCA (and mitochondria) dysfunction and impaired Ca^{2+} removal; plus, the enhanced myofilament Ca^{2+} sensitivity slows Ca^{2+} dissociation from the myofilaments and contributes to increased Ca^{2+} levels during diastole. Intracellular Ca^{2+} overload could be responsible for triggering the secondary remodeling in cardiomyocytes.

Very limited information is available on the cellular basis of arrhythmias and diastolic dysfunction in HCM myocardium. Studies on myocardial samples from patients with HCM are made extremely difficult by the scarce availability of material and the intrinsic variability among patients. The use of animal models of HCM can overcome these limitations and allow us a more complete characterization of the pathways determining the cellular pathophysiology of HCM without confounding effects of unpredictable contributors.
The aim of this thesis is to study and characterize the phenotypic and biophysical alteration of TnT mutant mouse models of HCM. In addition we tested the efficacy of ranolazine, a selective late sodium current blocker, first on single cells and trabeculae (*in vitro*) and then on mice (*in vivo*). We studied HCM-related functional abnormalities in single cells and trabeculae from the ventricles of transgenic mouse models aged 6/12 months carrying HCM-related mutations of cTnT (R92Q and E163R).

5.2 – Cardiomyopathy associated R92Q and E163R cardiac troponin T mutation causes specific E-C coupling alterations and pro-arrhythmogenic changes

The assessment of the phenotypic characteristics, comprising heart size and chambers dimensions, of our mouse model E163R was particularly important given the limited availability of clinical information in literature on this mutation (Koga et al, 1996). Through the use of echocardiography and MRI we were able to characterize the complete morphology of both mutant mouse lines (R92Q and E163R). Mutant mice showed a marked increase of LV wall thickness compared to WT. Moreover, R92Q mice show a significant decrease of diastolic and systolic LV volumes compared to WT, while E163R mice did not show any difference in LV chamber size. The left atrial size was larger in both mutant mice than in WT and the presence of diastolic dysfunction was confirmed by analysis of mitral valve flow.
Analyzing the alterations in the kinetics and amplitude of Ca^{2+} transients, R92Q mouse cardiomyocytes displayed a slower rate of decay of calcium transients and elevated diastolic calcium, with regards to WT. This resulted in a slower muscle contraction and relaxation. Conversely, in E163R mice the kinetics of force development and relaxation was still prolonged, despite calcium transient was not slower than WT.
A common feature observed in both R92Q and E163R was a marked pro-arrhythmogenic phenotype. Compared to WT both groups showed spontaneous activity during pauses, as observed in trabeculae, in the form of either irregular premature contractions or run of regular spontaneous beating. In single cardiomyocytes, the occurrence of spontaneous calcium transients was significantly higher in both R92Q and in E163R cells when compared to WT and significantly augmented under administration of Iso. Of note, R92Q mice show an increased frequency of spontaneous Ca transients compare to E163R, while the occurrence of Ca^{2+} waves was higher in E163R compared to R92Q. This result could indicate that the likelihood of Ca^{2+} waves to propagate and generate a global calcium transient is lower in E163R than in R92Q.
We can hypothesize that the presence of sarcolemma remodeling in R92Q, but not in E163R, could promote generation of delayed after depolarization and premature action potentials following a Ca wave, inducing a global Ca^{2+} release.

5.2 – *In vitro* effect of ranolazine on electrophysiological properties of ventricular myocytes

We tested the potential reversal of these alterations in contractile function and intracellular calcium handling observed single cardiomyocytes and in intact trabeculae by the selective inhibitor of late Na^+ current (I_{NaL}), Ranolazine. In R92Q preparations, the application of ranolazine induced a significant reduction of the duration of the action potential; this result is compatible with the inhibition of the inward I_{NaL}. Moreover, the application of ranolazine (10 μM) on cells from mutant mice improved the kinetics of calcium fluxes and reduced diastolic dysfunction. In R92Q preparations ranolazine hastened calcium transient kinetics and reduced diastolic calcium. Instead, in E163R preparation ranolazine did not affect the kinetics of calcium transients even if it reduced the level of diastolic calcium. In mutant mouse cardiomyocytes the treatment with ranolazine was able to reduce the frequency of spontaneous transients and spontaneous calcium waves in both mutant mouse samples; this happens even after β-adrenergic stimulation with isoproterenol. In both R92Q and E163R trabeculae ranolazine applied on top of Iso significantly reduced the occurrence of aftercontractions and premature beats below basal levels. The application of ranolazine reversed the enhancement of spontaneous Ca^{2+} waves induced by Iso to basal levels in both R92Q and E163R, with a quantitatively larger effect in R92Q, milder in E163R. Furthermore, Ranolazine almost completely reversed the higher occurrence of spontaneous calcium transients under Iso administration in both mutants, exerting negligible effect on WT. These results may be related to the efficacy of ranolazine to restore the proper flow of calcium.

5.3 – *In vivo* effect of ranolazine on mouse models, preventive effects on disease progression

Afterwards the characterizations of TnT mutant mouse models and the assessment of ranolazine *in vitro* effects, we tested the potential reversal or preventive effects of ranolazine *in vivo* on R92Q mice. To this aim we decided to treat mutant R92Q mice since birth, aiming to expose mutation carriers to the beneficial effect of the drug when the disease is developing (1 to 6 months of age). Our objective was to counteract the remodeling process and stop disease onset and progression, effectively preventing the most deleterious consequences of HCM.
Echocardiography and MRI analysis confirms a severe alteration of heart structure and function in the untreated mutant mice. In contrast, R92Q treated mice did not show the typical morphological alteration of mutant mice. There were no increased ejection fraction and septal dimension, also LV volume was at the same levels of WT mice. Also, left atrial size was similar to WT and the analysis of mitral valve flow showed a reduction of diastolic dysfunction in treated vs. untreated mice. These morphological data showed how the administration of ranolazine since birth reduced pathological phenotype in mutant mice. Administration of ranolazine seems to prevent, or mitigate, the structural and morphological changes typical of the disease. Other important data was the assessment of fibrosis with gadolinium administration. The amount of fibrosis resulted increase in mutant mice in comparison to WT, whereas R92Q Ran mice did not show any increase of fibrosis. This may be related to the preventive effects of ranolazine that also reduces the proliferation of fibroblasts and collagen deposition.
At cardiomyocyte level, analyzing the alterations in the kinetics and amplitude of Ca^{2+} transients, R92Q Keto mice, compared to WT showed a slow rate of decay of calcium transient

and elevated diastolic calcium. Instead ranolazine-treated R92Q mice showed normal calcium fluxes and reduced diastolic calcium. Even the pro-arrhythmogenic phenotype was prevented in treated R92Q mice. R92Q Ran mice showed less spontaneous calcium waves than untreated mice and the frequency of spontaneous transients was nearly abolished; this was evident even after β-adrenergic stimulation with isoproterenol.
Further, the qRT-PCR analysis provided many indications about the preventive effects of ranolazine administration. In R92Q Rano mice the expression levels of Serca, Kchip2 and Kv4.3 remains at the same levels of WT, while all three genes were altered in untreated R92Q mice. Also the expression of BNP and ANP was reduced in treated mice as compared to R92Q Keto mice. Plus, TGF-β expression, in line with the reduced fibrosis, was also significantly reduced in R92Q Rano mice. Only the expression of the genes MYH6 and MYH7 remained increased in both R92Q Keto and R92Q Rano mice compared to WT.
These results may be related to the direct effects of ranolazine on calcium/ions fluxes.

REFERENCES:

Belus, A., Piroddi, N., Scellini, B., Tesi, C., Amati, G.D., Girolami, F., Yacoub, M., Cecchi, F., Olivotto, I., and Poggesi, C. (2008). The familial hypertrophic cardiomyopathy-associated myosin mutation R403Q accelerates tension generation and relaxation of human cardiac myofibrils. The Journal of physiology 586, 3639-3644.

Coppini R, Ferrantini C, Yao L et al. Late sodium current inhibition reverses electromechanical dysfunction in human hypertrophic cardiomyopathy. Circulation 2013;127:575-84.

Koga Y, Toshima H, Kimura A, Harada H, Koyanagi T, Nishi H, Nakata M, Imaizumi T (1996) Clinical manifestations of hypertrophic cardiomyopathy with mutations in the cardiac beta-myosin heavy chain gene or cardiac troponin T gene. *Journal of cardiac failure* 2: S97-103.

Chapter 6: CONCLUSION

In conclusion, in this thesis, we investigated the role of ranolazine in preventing the symptoms of hypertrophic cardiomyopathy on TnT mutant mouse models. In particular, we focused on R92Q and E163R mutation because these two models summarize different possible disease phenotypes in patients and, taken together, they represent an optimal test bench for drugs aimed at reducing the burden of HCM. In brief, R92Q mice show a restrictive-like disease presentation with fibrosis and severe diastolic dysfunction; E163R mice show an early onset disease with scarce hypertrophy and fibrosis but high risk of arrhythmias.

Data obtained confirm that transgenic mutant mice are a good experimental model and reflect the main features of human disease. Besides some advantages such as availability of tissue, reproducibility of the model and exposure to drugs after the onset of the disease, mutant mice showed left ventricular hypertrophy, interstitial fibrosis and disorganization of cardiomiocytes, also diastolic dysfunction and arrhythmias. Although some phenotypic similarities exist between E163R and R92Q, including diastolic dysfunction, a lack of overt cardiac hypertrophy, increased Ca^{2+} sensitivity and cardiomyocyte disarray, the mutations cause disease via distinct molecular mechanisms. In fact, the two mutations are localized at opposite ends of the TNT1 tail domain, and are supposed to cause different effect on TNT1flexibility.

Administration of ranolazine, a selective late sodium current blocker, improved symptoms of HCM. Acute administration of ranolazine in preparations from adult R92Q mice leads to hastened calcium transients, reduced diastolic calcium and abolishes arrhythmic spontaneous activity. As in human HCM, the beneficial effects of ranolazine on R92Q myocardium are likely mediated by the consequences of late sodium current inhibition.

In E163R preparations, myocardial arrhythmogeneicity is not accompanied by remodeling of ion currents and thus appear to be a direct consequence of increased myofilaments calcium sensitivity or anomalies of RyR2 function. The beneficial effects of ranolazine on Ca^{2+} mediated spontaneous activity in E163R myocardium supports the hypothesis that the anti-arrhythmic effect of ranolazine can also be mediated by mechanisms other that INaL inhibition (i.e. reduction of myofilaments Ca^{2+} sensitivity or RyR2 inhibition).

For *in vivo* treatment we focused on R92Q mutant mice because, in contrast to E163R, showed a marked hypertrophy, calcium fluxes alterations and other main features of HCM. Furthermore, the effects of ranolazine were more marked in R92Q mice than in E163R.

Ranolazine, administered since birth in R92Q mice, leads to a significant reduction of phenotype expression. In fact, treated mice show less hyper-contractility, reduced LV wall thickness and less diastolic dysfunction, as compared with age-matched untreated mice.

Also correct calcium flow was maintained and arrhythmic events were nearly abolished, in fact, in R92Q Ran mice, ranolazine hastened calcium transient kinetics and reduce diastolic calcium.

To conclude, data obtained demonstrate that the administration of ranolazine reduce the progression of the disease and prevent pathological phenotype in mutant mice.

Ranolazine, thanks to its remarkable safety profile, may be a candidate drug to be employed in HCM mutation carriers to prevent phenotype onset.

List of abbreviations

AMP 5’ adenosine monophosphate
AMPK AMP-activated protein kinase
ANP Atrial Natriuretic Peptide
AP: Action potential
APD: Action Potential duration
APD90%: Action potential duration at 90% repolarization
ATP adenosine triphosphate
bMHCbeta myosin heavy chain
BNP Brain Natriuretic Peptide
cMyBP-Ccardiac myosin binding protein-C
CMR cardiac magnetic resonance
cTnI cardiac troponin **I**
cTnT cardiac troponin **T**
ECC: Excitation contraction coupling
ELC essential myosin light chain
Gd Gadolinium
HCM hypertrophic cardiomyopathy
KI knock-in
KO knockout
$\mathbf{I_{Ca\text{-}L}}$: L-Type calcium current
$\mathbf{I_{to}}$: transient outward potassium current
$\mathbf{I_K}$: delayed rectifier potassium current
$\mathbf{I_{K1}}$: inward rectifier potassium current
LGE late gadolinium enhancement
LV Left ventricle
LVAD Left ventricular assist device
LVH left ventricular hypertrophy
Myh6 Myosin heavy chain alpha
Myh7 Myosin heavy chain beta
MRI Magnetic resonance imaging
NCX Sodium-calcium exchanger
PCR polymerase chain reaction
PCr Phosphocreatine
PET positron emission tomography
PLN phospholamban
Ryr2 Ryanodine Receptor
RLC regulatory myosin light chain
RT-PCR Reverse transcription-PCR
SERCA Sarcoplasmic reticulum calcium pump
SR Sarcoplasmic reticulum
TDI Doppler imaging
TG Transgenic
TGF-β Tissue grow factor beta
Tm Tropomyosin